UNITED KINGDOM · CHINA · MALAYSIA

# Increasing the Road Safety of E-bike: Design of Protective Shells Based on Stability Criteria

Lele Zhang, BEng

*Thesis submitted to The University of Nottingham*

*for the degree of Doctor of Philosophy*

January 2017

# ABSTRACT

China currently occupies the world's leading Electric bicycle (e-bike) market. However, the popularity of e-bikes is accompanied by massive numbers of injuries and deaths due to accidents involving e-bikes. As a result, the safety of e-bikes has recently received much attention from the public and the government and researchers have concentrated on improving the safety features of e-bikes with innovative technologies. It has been shown that well-designed protective shells can protect a driver involved in an e-bike accident. However, there is a lack of criteria on which to base the design of an effective protective shell for e-bikes. Therefore, this research focuses on the development of a design criterion based on the specific case of Roly-Poly stability. This stability criterion can be formulated for one curved surface as $r > h$, which is in a stable stability configuration - one of a number of static stability configurations. In this study, static stabilities are configured based on knowledge of potential energy (PE). In order to verify the design criteria, three types of protective shells are designed with different stability conditions. The first type follows the design criterion ($r > h$), while the remaining two do not ($r = h$ and $r < h$). A finite element model of an e-bike is constructed with key components, such as the main frame, CoM (the position of which is obtained by a plumb line experiment), and the designed protective shells. The meshed models are produced and employed to determine the contact

parameters using the frictionless penalty method. The corresponding results of sideways falling simulation successfully demonstrate the validity of the design criterion.

# ACKNOWLEDGEMENTS

I would like to recognise my initial main supervisor - the late Professor Nabil Gindy - who funded my full scholarship and assigned my research subject.

Many thanks to my supervisors, in particular Dr. Hui Leng Choo, who steadily worked with me on my PhD research over the last two years.

As one of my Co-supervisors, Dr Alexander Konyukhov provided me with the original ideas and the guidance of my research direction.

Prof. Shuguang Li, my second Co-supervisor, offered me valuable technical advice in addition to financial support.

Dr. Yanwang recruited me to the University of Nottingham Ningbo China.

I greatly appreciate Dr. Edwin Mok's comments on my research, and Jane Hao's funding for conference attendance.

# TABLE OF CONTENTS

# ABBREVIATIONS

| | |
|---|---|
| ABS | antilock braking system |
| BSEB | bicycle style electric bike |
| CAD | computer-aided design |
| CoG | centre of gravity |
| CoM | centre of mass |
| DOF | degree of freedom |
| DSM | direct stiffness matrix |
| EB | electric bike |
| EPAC | electric power-assisted cycle |
| EPoDB | electric power-on-demand bicycle |
| EPoDS | electric power-on-demand scooter |
| FE | finite element |
| FEA | finite element analysis |
| FEM | finite element method |
| ISS | Injury Severity Score |
| MPE | Minimum Potential Energy |
| PE | Potential Energy |
| Pedelec | Pedal Electric Cycle |

| | |
|---|---|
| PTW | Powered two-wheeler |
| SSEB | scooter style electric bike |
| TWV | two-wheel vehicle |

# CHAPTER 1. INTRODUCTION

## 1.1. Introduction to the E-bike

E-bike, an abbreviation for 'electric bike', is a general term for a two-wheeled vehicle (TWV) which is either motorized or pedal-assisted by electrical power. The frames of e-bikes are similar to those of bicycles, scooters, or even heavier types of vehicles, such as motorcycles.

### 1.1.1. The Classification of E-bikes

E-bikes are categorized according to the power of the electric motor (e-motor) installed. They are classified as an:

1) electric pedal-assisted cycle (EPAC) with low powered e-motor;
2) electric power-on-demand bicycle (EPoDB) with normal powered e-motor;
3) electric power-on-demand scooter (EPoDS) with high-power e-motor.

#### *Electric pedal-assisted cycle (EPAC)*

EPAC is also known as Pedelec (Pedal electric cycle) according to the EU directive (EN15194 standard) [1]. This type of e-bike comprises a standard bicycle frame with the addition of an electric powertrain installation. The electric powertrain system comprises a central drive unit with an electric motor, the battery of which provides electric power, and a control system with sensors and computer controls on the handlebars, as seen in Figure 1.1. EPAC has a sensor to detect the pedalling speed and/or the pedalling force. In fact, under the control of the central smart system, the e-motor of EPAC only augments the efforts of the riders when they are actually pedalling [1, 2]. Therefore, EPAC is environmentally superior to other motorized modes of transport [3, 4]. Experimental testings of EPAC performance are described in articles [2, 5, 6].

*Figure 1.1 EPAC and its electrical powertrain (Photo: Björn Gerteis)*

### *Electric power-on-demand bicycle (EPoDB)*

Different from EPAC where the electric power is as an assistant to the motive power, the other two types of e-bike are driven by a power-on-demand e-motor, which requires more power compared to the EPAC. EPoDB resembles a regular bicycle [7, 8], but it is almost solely propelled by electricity. Pedals are chosen only when the electric power runs out. Figure 1.2 shows the common structure of an EPoDB.


***Figure 1.2 EPoDB consists of power-on-demand e-motor and pedals (Hosted @ Lelong Picture Services)***

### *Electric power-on-demand scooter (EPoDS)*

EPoDS has an e-motor that operates on a power-on-demand basis only, and is typically heavier and bigger than the motors used in the EPAC and the EPoDB (see Figure 1.3). It contains a high-powered motor and multiple sets of batteries in series, this allows for high voltage and results in high power, high speed, and, relatively high weightage. Consequently, this type of e-bike is involved in the majority of e-bike accidents. This research focuses on the safety features of e-bikes based on the prototype of an EPoDS.

*Figure 1.3 EPoDS is heavier and bigger than EPAC and EPoDC (Photographs: ekovehicle.com).*

### 1.1.2. The E-bike Market

The market for e-bikes has been increasing worldwide, especially in China, Europe, the United States, and East Asia (excluding China). The major reasons for this increase are:

1) "Zero Pollution". The traction of e-bikes is provided by electric power, which is a type of zero-pollution power. The reduction of environmental impacts meets that which public administrations vigorously advocate [9].
2) Cost-effectiveness [10, 11]. The price of an e-bike is much less than that of a private car, as a result, for a short commute (within 20km), people are willing to choose an e-bike rather than a car.
3) Reduced impact of traffic congestion in city areas which results in improved transport efficiency. Their small size, compared with that

of a car, allows users to move with agility and to park with ease in narrow urban streets. [11, 12]

4) Additional benefits, including, amongst others: reducing the use of non-renewable energy, i.e., the more popular the use of e-bikes, the less demand on non-renewable energy, such as petrol and diesel; maximising accessibility; and mobility benefits [13].

### *E-bikes in China*

China is currently the world's largest producer and distributor of e-bikes, which are replacing gasoline-powered motorcycles and public transit vehicles [14, 15]. Due to their low cost, simple technology, and efficiency in terms of personal mobility, e-bike sales have grown far faster than the sales of any other mode of transportation in China [16]. Compared with the ordinary bicycle, e-bikes allow people to commute longer distances and to carry more cargo within a relatively short period of time. In addition, triggered by Chinese local governments' efforts to restrict motorcycles in city centres, e-bikes are fast becoming the most optimistic solution for the substitution of motorcycles [17, 18]. The cost of an e-bike is typically around RMB 2,000, less than one tenth that of a car [19], making it affordable to most Chinese people. Figure 1.4 shows the growth in e-bike sales from 2005 to 2010 [20]. The sales of e-bikes increased approximately three-fold from 2005, reaching 27 million units in 2010. The total number of e-bikes on the road in China is now estimated to be over 120 million [21].

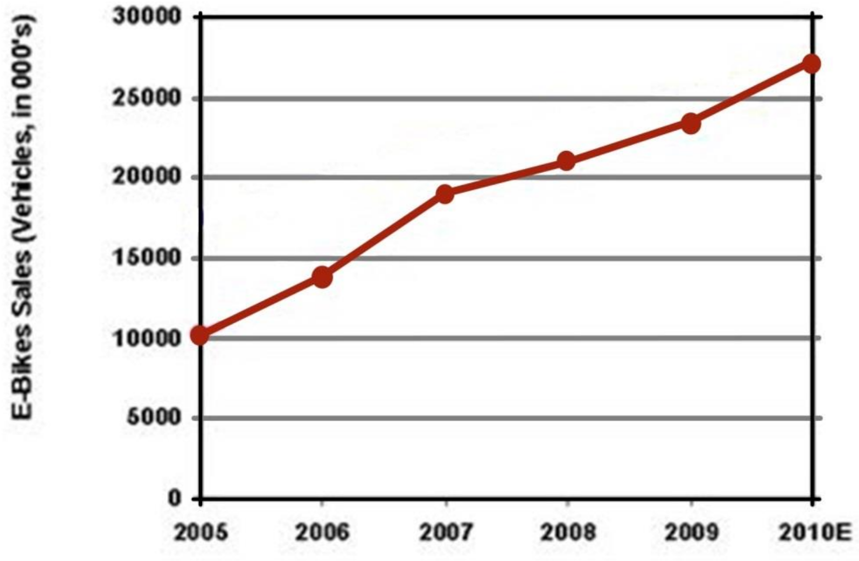


***Figure 1.4 Historical e-bike sales growth, China: 2005-2010 (Source: Pike Research)***

## *E-bikes in Europe*

In Europe, the most common type of e-bike is the EPAC, which is rapidly becoming popular. The annual sales of e-bikes in Europe grew from just under 100,000 units to more than 1.1 million units from 2006 to 2014 [1, 22], as shown in Figure 1.5. Most of these e-bikes are manufactured in Germany, the Netherlands, and Belgium. [22].

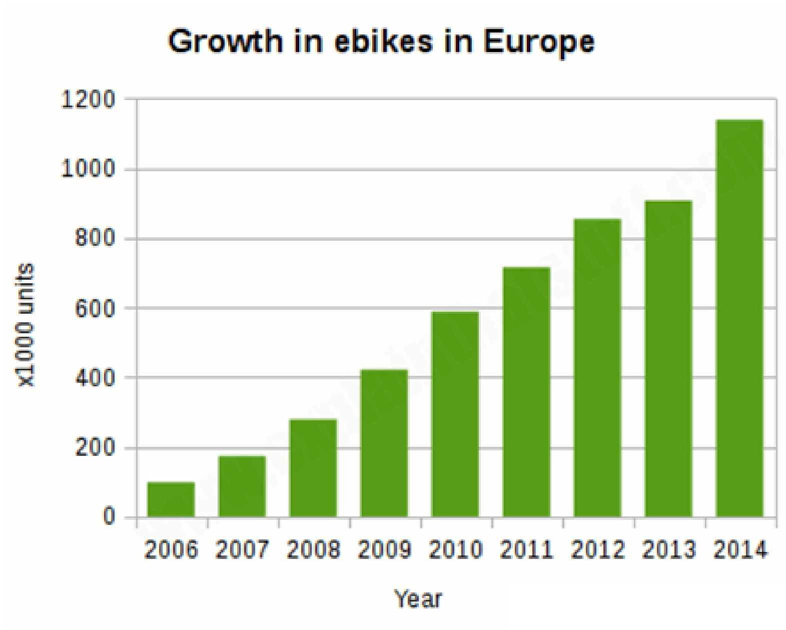


***Figure 1.5 Annual sales of e-bikes in Europe from 2006 to 2014 [22].***

*E-bikes in the United States*

With regards to the United States, from 2012 to 2014 the e-bike market was positive and grew steadily with the volume estimated at 193,000 units in 2014 [23]. Although the majority of e-bikes are imported from Mainland China or Taiwan, and it is not a large market when compared with the other countries mentioned, the US e-bike market is steadily emerging [23, 24].

*E-bikes in East Asia (excluding China)*

In Japan, annual e-bikes sales have remained steady, at around 300,000 units, for a number of years [25]. Meanwhile, the market continues to grow in Korea and other East Asian countries [25].

### 1.1.3. Accidents Associated with E-bikes in China

Market investigation shows that e-bike use is growing rapidly in China. However, the increasing number of e-bikes on the road has resulted in rising numbers of injuries and deaths among e-bike drivers. A review of the literature reveals three major causes of severe e-bike accidents: 1) Violation of traffic rules. In China, over 60% of fatal crashes involving TWV result from violation of traffic rules, such as red-light running [26]; 2) Travelling at speed. It is known that speeding will increase the risk involved and the severity of a crash [27]; 3) Carrying excess weight. When the vehicle is overloaded, the risk of severe injury or fatality during an accident is increased [28]. In China Zhuhai, Shenzhen, and Xiamen have all passed laws which ban e-bikes in main downtown areas, and Guangzhou has banned motorized TWVs completely in order to reduce related traffic accidents [15]. According to China's Electric Bike General Technical Qualification GB17761-1999 [29], e-bikes may not exceed 20 km/h and may not be heavier than 40 kg. Due to some drivers failing to follow technical instructions, traffic rules and laws, deaths as a result of e-bikes accidents have increased more than four-fold across the nation, from 1340 cases in 2005 to 5752 cases in 2013, as shown in Figure. 1.6 [30].

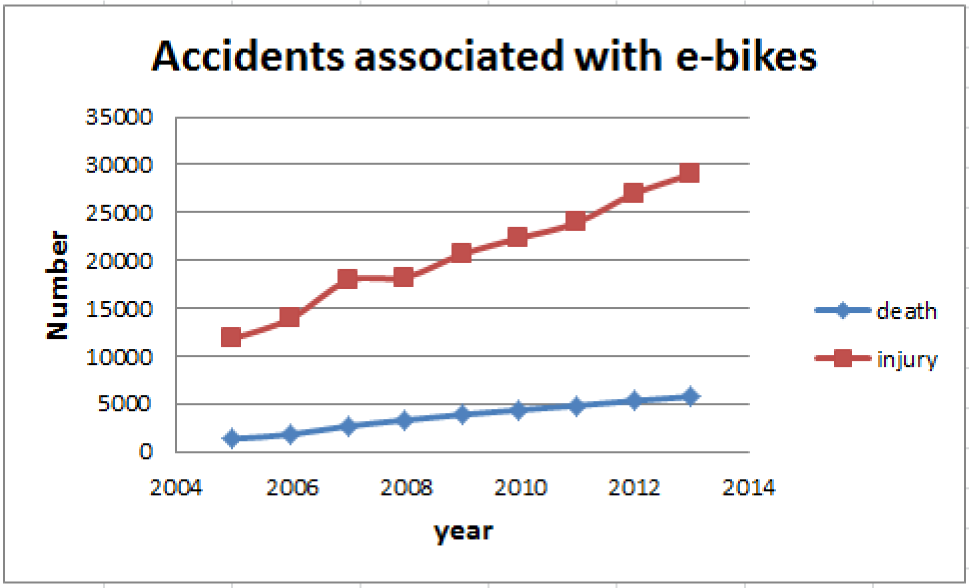


***Figure 1.6 Deaths associated with e-bike accidents from 2005 to 2013 in China***

Figure 1.7 shows the percentage of all type of injuries which have occurred as a result of e-bike accidents and the ISS (Injury Severity Score) group comparison for 205 patients who are victims of such accidents. The most common are axial skeletal injuries. The number of injuries to extremities is 99, which is 48% of those 205 injuries.

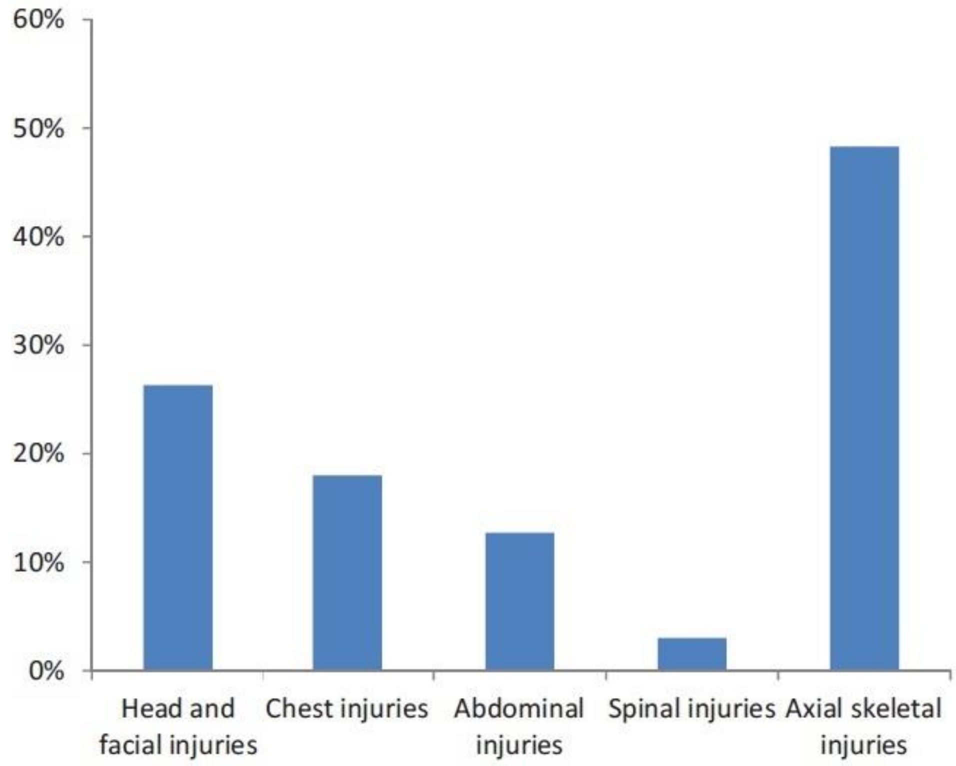


***Figure 1.7 The percentages of a number of injuries which occur in e-bike accidents [31].***

This section has provided the research background for the topic under investigation from which aims and objectives of the research are set accordingly.

## 1.2. Aims and Objectives

China leads world e-bike market. However, in recent decades, with the increasingly widespread use of e-bikes, road traffic safety has attracted the growing attention of the Chinese public. The aim of this PhD research is to propose the employment of stability criteria based on principles of passive road safety applied to e-bikes. This stability criteria is to be formulated for the case of severe road accidents which occur during the sideways falling of an e-bike. Safety shells protecting the driver during sideways falling can be designed based on this criteria. The full sequence of the proposed safety design approach involves the following steps:

1) Formulation of the "Roly-Poly" stability criteria used as the design criterion for the protective shells.
2) Collection of data about the centre of mass (CoM) of the e-bike product. This is the critical parameter for the simplification of the FE model.
3) Presentation of the basic knowledge of the shell element and the beam element (which are selected to construct the FE model), and their stiffness matrix. This is the preliminary stage of the modelling.
4) The design of the protective shells. The protective shells are designed in different stability configurations.
5) The modelling and simulation of the e-bike with the different shell designs. The corresponding results will be used to verify the design criteria.

## 1.3. Thesis Outline

This thesis consists of seven chapters.

Following this first chapter, Chapter 2 provides the Literature Review which introduces current safety technologies for both e-bikes and motorcycles by dividing these into active and passive safeties. The existing methodologies on e-bike structure design and optimization are presented.

In Chapter 3, stability criteria and stable equilibrium, as one of the configurations of static stability, are discussed. The geometric design of the protective shells is developed in the circumstance of the stable stability theory and the case of Roly-Poly.

Chapter 4 presents the experimental study. CoM data are collected as the essential factor to be applied in simplification of the modelling.

Chapter 5 shows the Relevance of the Finite Element Method to the Present Project. Beam element and shell element are adopted to model the prototype of the e-bike. Basic knowledge about these two types of elements and their matrices is illustrated. In addition, the Direct Stiffness Method is introduced by a simple beam-shell element case, which is the principle behind the solution to the complicated formulas.

In Chapter 6, the modelling and simulation of the e-bike is conducted. A CAD model is constructed as a dimensional presentation. Static calculations are carried out for the verified FE model in ANSYS, and transient analysis is conducted to determine the contact parameters during the straight falling testing. The static and transient simulations are preliminary to the sideways falling case in LS-DYNA. The simulation results with different shell designs are compared and used to validate the design criterion.

Chapter 7 features conclusions and suggestions for future work. The key results of this project and suggestions for further research are presented.

# CHAPTER 2. LITERATURE REVIEW

## 2.1. Introduction

E-bike use in China has experienced an enormous increase in the last decade. As a result, traffic safety for e-bike riders has become an issue attracting public attention because of the rapid increase in the number of deaths and injuries. In an effort to reduce the number of accidents attributed to e-bikes, measures which focus on their safety have been considered both by researchers and the government. One of the standard approaches in Europe (ISO 26262) [32] and the US (FMVSS 108) [33, 34] is to increase the passive road safety of the vehicle.

Little research has been undertaken into the structure of e-bikes. However, research which focuses on two wheel vehicles (TWVs), including motorcycles and bicycles, is well-established. As e-bikes have been developed based on motorcycles and bicycles, their structure is patterned directly on those two types of TWV, e.g., a bicycle style e-bike (BSEB), and a scooter style e-bike (SSEB) [35]. In this chapter, research areas include all types of TWV (e-bike, motorcycle, bicycle etc.).

A review of the literature and current technologies is provided in this chapter.

## 2.2. Current and Proposed Safety Technology for TWVs

Active safety and passive safety are two significant aspects of road safety [36]. Active safety concerns features which aim to assist drivers to avoid accidents and so result in decreasing the probability of an accident occurring [37, 38]. Passive safety, as opposed to the concept "active safety", refers to the technology used to decrease the injury levels and their severity when accidents take place, rather than direct avoidance of accidents occurring [39, 40].

### 2.2.1. Active Road Safety Technology

In active safety features, a number of factors can contribute to reducing the risk of an accident occurring. These measures include: 1) an enhanced infrastructure designed to minimise conflict between users; 2) an effective braking system; 3) management of speed through measures which focus on the technology of the rider [41].

#### *Infrastructure Design*

Analysis shows that road camber is one element of transportation infrastructure which influences the stability and safety of motorcycles [42, 43]. A well designed geometry of roadways (e.g., intersections [44, 45], horizontal and vertical curvature [46], and roadside barriers [47]) can significantly reduce the frequency of motorcycle accidents [48-50].

### *Auxiliary brake - ABS*

It has been concluded that antilock brake system (ABS) technologies should be mandatory on powered two-wheelers to ensure a safer urban transportation system [51]. This is because ABS installed in a motorcycle or e-bike has the effect of controlling the stopping distance under various conditions [52-54]. Experiments conducted in [55] also substantiate that compared to those without ABS, crashes and their severity were clearly reduced in ABS-equipped powered TWVs [56, 57].

### *Speed Limitation*

Driving a TWV at high speeds results in a high risk of accident occurrence and increases the severity in the event of an accident [58], thus, it is necessary to fix a maximal safe speed for TWVs [59, 60]. Such limitations to the speed of e-bikes is compulsory and mandatory by law [61]. On roads the speed hump is one infrastructure used to lower traffic speed [62, 63]. The fitting of a control centre to e-bikes can ensure that they are operated under the maximum legal speed [61].

## 2.2.2. Passive Road Safety Technology

### *The over-head shell as a safety measure on e-bikes.*

In 1996, BMW launched a new class of e-bike, the C1, which is equipped with an overhead aluminium space-frame.

*Figure 2.1 C1 safety frame[64]*

The conceptual TWV with fully covered frame was first proposed by Daswick and Landry in 1981 [65]. These conceptual protective shells were experimentally demonstrated to protect drivers in various types of collision. However, the criteria for their design have not been clarified.

### *Prototype Airbag for motorcycles*

A number of researchers have raised the idea of installing an airbag system into a motorcycle [66, 67]. The airbag system in a passenger car absorbs a considerable amount of impact energy and reduces injury in a collision [68]. For the proposed airbag system attached to a motorcycle, the experimental results show that while it may provide a measure of protection, such protection is not significant due to limitations in the structure of the motorcycle to support an airbag [69].

### *Helmet efficacy for TWVs*

Fatal injuries are nearly always the result of injury to the brain. Wearing a helmet reduces any impact to the head and limits the incidence and severity of head injuries in the event of a collision [70-73]. Helmet use is mandatory under legislation for all types of TWV user [74-81]. Such laws are supported by surveys which show helmet use is 17 times more likely to save a driver from death by head injury than is likely for non-helmet users [82].

### *Motorcycle Crash Bars*

It is necessary to consider improvements to the crashworthiness of motorcycle frames for the safety of the riders [83]. Data show crash bars, designed to protect against deformation in a collision, reduce the injury to a driver's leg, at a certain level, in the case a motorcycle falling laterally [84]. The weakness of such a crash bar is that it focuses only on protection of the leg and overlooks other areas which require critical injury protection.

## 2.3. The Proposal for Structural Design and Optimization

The design and improvement of e-bike structure is the major focus of this PhD project. The techniques of design and optimization focus on the aspect of the structure of TWVs in the following section.

### 2.3.1. Light Weight

Any increase in the weight of an e-bike has three major, negative effects. 1) There is a higher request for motion power when the weight of the vehicle is heavier, which lowers power efficiency. 2) The heavy weight makes it more difficult to propel the e-bike when power is running low [85]. 3) The added weight increases the extent of property damage or injury in the event of a crash due to the increased inertia, a direct result of the heavier weight of the bike while driving [61, 86]. Thus, many researchers focus on lightweight motorcycles [87], with some studies aiming to optimize design and minimise the frame mass by the application of evolutionary algorithm methodology. [88].

### 2.3.2. Improvement in Riding Comfort

To improve the performance of ride comfort, close attention has been paid to the design and optimization of the frame of the bicycle [89] and its suspension system [90, 91]. The suspension system basically consists of the spring, the shock absorber, and the mechanism system which sustains the vehicle's main body and transmits impact between the machine and the road. In year 2014, a model was established by Stefano Barone andGiovanni Lo Iacono involved in the interaction between the rider and the motorcycle in terms of comfort [92]. Comfort performance is also linked to safety characteristics [93, 94].

### 2.3.3. Drag Reduction

Any road vehicle has to work against a force produced by air resistance, also known as aerodynamic resistance [95]. The impact of air resistance is influenced by air density, relative speed of the vehicle, and the vehicle geometrical design such as the size of frontal area of the vehicle etc. [96, 97]. The benefit of aerodynamic drag reduction is in terms of power saving, which is even greater for a heavy vehicle [98]. Figure 2.2 shows the air resistance forces on an e-bike.


*Figure 2.2 Force on an e-bike [99]*

Drag force caused by the air is regarded as one of critical resistance. In this circumstance, the reduction of the air drag force is an essential design point in the analysis of the propulsion system of e-bikes.

### 2.3.4. Stability

It is necessary for stability to be taken into account in the design of the structure of an e-bike because it is directly associated with the safety element of the vehicle [100, 101]. The phenomenon of weave instability when driving at high speed has been researched in a combined analytical and experimental program [102]. The driver's passive steering impedance was considered as a factor which influences the stability of the motorcycle (V. Cossalter, A. Doria etc.) [103]. The front fork has been shown to have a significant effect on motorcycle stability [104].

## 2.4. Summary

This chapter provides a review of the literature on current and proposed safety technologies for TWVs. The current technologies which concern structural design and optimization, such as being light weight, improving ride comfort, reducing drag, and improving stability, have been considered as research directions. Combined with safety features and structural design, structural stability is highlighted in this PhD project. The attachment of protective shells to improve the stability of the structural system of an e-bike is one approach to achieve the goal of stability .

Well-designed protective shells have been demonstrated as able to increase the stability of the whole e-bike structure, which helps protect the driver during an e-bike accident [64]. However, not all shells attached to e-bikes have sufficient safety functions. For example, the overhead half covered shell cannot absorb the energy of a side collision. An e-bike, as a TWV with an axial structure, suffers from instability and can easily fall sideways if it suddenly locks or is involved in a collision. Thus, well-designed protective shells which can efficiently isolate shock from the side during a severe e-bike accident are essential. However, according to author reviews, there is no clear standard theory about how to design effective safety shells for an e-bike. Therefore, this study pays attention to developing a design criterion for shells which provide protection in the event of falling sideways.

# CHAPTER 3. STABILITY CRITERIA

## 3.1. Introduction

This chapter introduces the stability criterion employed in the design of e-bike protective shells for safety in sideways falling incidents. The stability criterion is formulated according to the Roly-Poly stability system, which is stable due to its self-righting characteristic designed based on the stabilities theory. The content of this chapter is presented in the following sections: 1) derivation of the fundamentals of Roly-Poly stability; 2) static stability as illustrated by a pendulum system; 3) a simple example to determine if conditions are satisfied to realize the building of a safe stability system; 4) a proposal for the geometry of protective shells to be constructed as a stable equilibrium system.

## 3.2. Roly-Poly Stability

In this study, Roly-Poly stability is used to develop a design criterion for protective shells for e-bikes.

The motivation originates in the famous property of the "Roly-Poly" toy which allows it to right itself when pushed over. Its simple prototype consists of a hollow shape with a curved bottom and a weight at its lowest point (Figure 3.1).

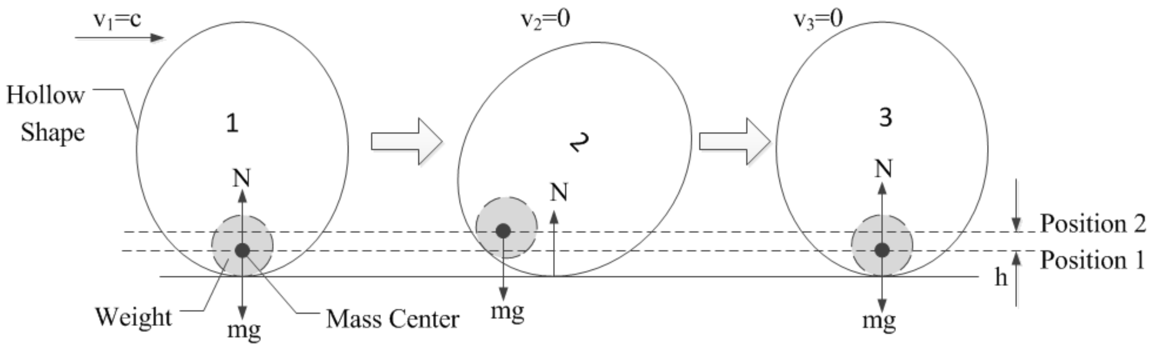


*Figure 3.1 The stability scheme of the Roly-Poly prototype.*

There are three stages in the process of how the Roly-Poly toy rights itself: toy with initial velocity, *c*; toy with maximum angle with respect to its vertical symmetric axis; and toy in static status. When the toy gains an initial velocity, it starts to roll to one side. The bottom of the toy, with specific curvature contacting the surface, makes the CoM rise from the original height (position 1) to its highest position (position 2). In stage 2, the CoM is no longer in the same axis as the normal reaction force, *N*. An unstable equilibrium moment arises and seeks the upright orientation. The potential energy (PE), $\eta$, in stage 2 is:

$$\eta = mgh \tag{3.1}$$

As an effect of inertia and friction force, the toy will keep wobbling until all the kinematic energy is fully converted and it finally stays motionless in stage 3.

## 3.3. Static Stability Theorem

Static stability is fundamental to Roly-Poly stability, and is an element which must be clarified before deriving the design criterion for protective shells. There are three static stabilities: stable equilibrium; unstable equilibrium; and neutral equilibrium. In order to better understand static stabilities, they are introduced via the case of a simple pendulum system and configured by the limiting conditions of potential energy (PE). Stable equilibrium, which is the principle of Roly-Poly stability, is emphasized.

### 3.3.1. Pendulum System

A specific pendulum system is shown in Figure 3.2. A mass point, $m$, suspended on a cable with a length, $l$, is oscillating within a plane. Unit vectors $\tau$ and $e_{\varphi}$ are tangential to the motion trajectory of which the circumference is $s$. Vector $\upsilon$ and $e_r$ are along the normal direction of the trajectory. $\varphi$ is the angle between the cable and the vertical axis, a function which depends on time.

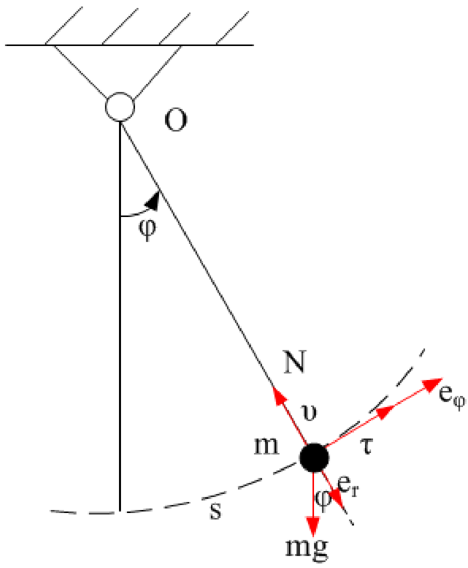


*Figure 3.2 Pendulum system with mass point m.*

The simple pendulum system can be described by mathematical formulae as follows:

The motion equation based on Newton's second law is,

$$m\vec{a} = m\vec{g} + \vec{N} \tag{3.2}$$

Equation (3.2) when expressed in polar coordinate system becomes,

$$m\ddot{s} = -mg \cdot sin\,\varphi \tag{3.3}$$

where the acceleration vector is the result of components in tangent and normal directions respectively,

$$\vec{a} = \ddot{s}\vec{\tau} + \frac{\dot{s}^2}{l}\vec{v} \tag{3.4}$$

Force in normal direction is determined by,

$$\frac{m\dot{s}^2}{l} = mg\,cos\,\varphi - N \tag{3.5}$$

Circumference of the trajectory is calculated by,

$$s = l\varphi \tag{3.6}$$

The second derivative of equation (3.6) is,

$$\ddot{s} = l\ddot{\varphi} \tag{3.7}$$

Combining (3.3) and (3.7), obtains,

$$\ddot{\varphi} + \frac{g}{l} sin\,\varphi = 0 \tag{3.8}$$

Equation (3.8) is a non-linear equation. Its solution process is via elementary functions.

Sine φ is written in the format of a Taylor series,

$$sin\,\varphi = \varphi - \frac{\varphi^3}{3!} + \frac{\varphi^5}{5!} - \cdots \quad -1 \leq \varphi \leq 1 \tag{3.9}$$

When $\varphi$ is very small, the values of high-order components are extremely close to zero. Therefore, those high-order components can be ignored. Thus, the expression (3.9) can be given in the form,

$$\varphi = sin\,\varphi \tag{3.10}$$

Substituting equation (3.10) into (3.8), it is formatted as,

$$\ddot{\varphi} + \frac{g}{l}\varphi = 0 \tag{3.11}$$

Since coefficient $\frac{g}{l}$ could be regarded as a constant, a new parameter $\omega = \sqrt{\frac{g}{l}}$ has been introduced in equation (3.11). This is the angular frequency of this pendulum system, $\omega = \frac{2\pi}{T}$. [105] Therefore, it contains the dimension of time$^{-1}$.

$$\ddot{\varphi} + \omega^2\varphi = 0 \tag{3.12}$$

The solution to Equation (3.12) is,

$$\varphi = A\,cos\,\omega t + B\,sin\,\omega t \tag{3.13}$$

Expression (3.13) is the function of angular, $\varphi$, and its unique variable, angular velocity, $\omega$. It describes the motion of this simple pendulum system during the whole period.

### 3.3.2. Potential Energy (PE) of the Pendulum System

The stabilities have been configured based on the limitations of PE, the knowledge of which is introduced by means of the pendulum system. Still considering the case of the simple pendulum system, as in Figure 2, the mass point is oscillating at a particular point at angle, $\varphi$.

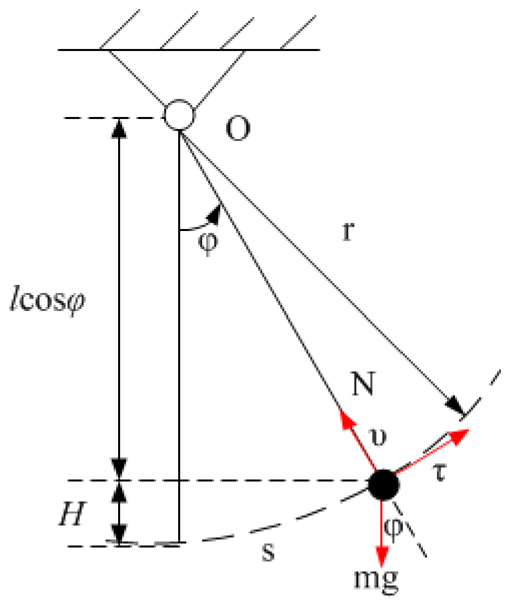


*Figure 3.3 Introduction of PE by the pendulum system.*

The mechanics of the pendulum in Figure 3.3 are analysed as follows.

Resultant force at this moment is,

$$\vec{F} = m\vec{g} + \vec{N} \tag{3.14}$$

The useful path vector $\vec{r}$ corresponding to the resultant force is normal to the trajectory all the time, of which the differential is,

$$d\vec{r} = ds \cdot \vec{\tau} \tag{3.15}$$

Useful elementary work done by the force, F, in its path is,

$$dW = \vec{F} \cdot d\vec{r} \tag{3.16}$$

Work function is evaluated by,

$$W = \int \vec{F} \cdot d\vec{r} = \int m\vec{g} \cdot \vec{\tau} ds + \int \vec{N} \cdot \vec{\tau} ds \tag{3.17}$$

Because normal vector, *N,* and tangential vector, *τ,* are orthogonal, which causes virtual work, the result of $\int \vec{N} \cdot \vec{\tau} ds$ is zero.

Therefore, equation (3.17) is simplified to,

$$W = \int m\vec{g} \cdot \vec{\tau} ds = (l\cos\varphi - l)mg \tag{3.18}$$

The distance between the new and the original positions along the vertical direction is *H*,

$$H = l - l\cos\varphi \tag{3.19}$$

With (3.18) and (3.19), the work done by the mass point oscillating is,

$$W = -mgH \tag{3.20}$$

For a conservation system, the decrease in work of a force is equal to the increase of PE [106], which is independent of the path and depends only on the initial and final positions. The PE is described in mathematical function as,

$$\eta = -W = mgH = mg(l - l\cos\varphi) \tag{3.21}$$

The expression of PE has been obtained. The relationship between static stabilities and PE is explained in the following section.

### 3.3.3. Static Stabilities

Static stability is generally used to describe the initial tendency of an object. There are three types of static stabilities: positive static stability; negative static stability; and neutral static stability. Positive static stability is the status of one system which has the tendency to return to its equilibrium position when reacting to a small disturbance. Conversely, if the initial tendency of the system due to any small disturbance causes the deflection to become worse, the system is a negative static stability system. Neutral static stability is the tendency for the deflection to remain in place, as shown in Figure 3.4 [107].

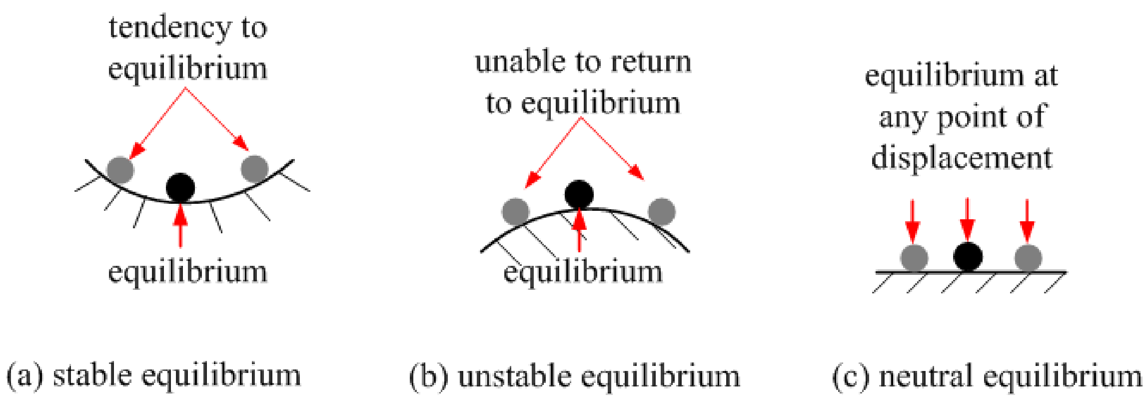


***Figure 3.4 Position of mass point: (a) Positive static stability (stable equilibrium); (b) Negative static stability (unstable equilibrium); (c) Neutral static stability (neutral equilibrium) [107] [108]***

As an example, see Figure 3.5(a), if the ball is placed on one side of the bowl, the initial tendency of this ball is to eventually return to its original position (equilibrium). This is called positive static stability. On the contrary, Figure 3.5(b) shows negative static stability. The ball is located at the top of an upside-down bowl and deflected in one direction, the initial tendency will not be where it started. Figure 3.5(c) indicates that the neutral static stability means that no matter where the ball is placed, it will stay exactly where it is. It will not move closer to its original position and it will not move further away.

In this example, the initial position of the ball is on the equilibrium points. The definition and the configuration of equilibriums are introduced in the following section.

**Equilibrium** is defined as a condition when all the forces and moments acting on the whole system are balanced [109] and all the torques and forces at a particular point in the system are zero [110]. The equilibrium system can be determined where the condition of the first derivation of PE of the whole system is zero [107]. In the equilibrium system, if the object has zero velocity, it is exactly in static equilibrium [111].

The limitation of PE is expressed as,

$$\eta(\varphi) = mgl(1 - cos\,\varphi) \rightarrow limit \tag{3.22}$$

In order to determine the limitation of PE, its first derivation fixed to zero is given by,

$$\eta'^{(\varphi)} = mgl\,sin\,\varphi = 0 \tag{3.23}$$

Solutions of equation (3.23) are,

$$\begin{cases} \varphi = 0 \\ \varphi = \pi \end{cases}$$

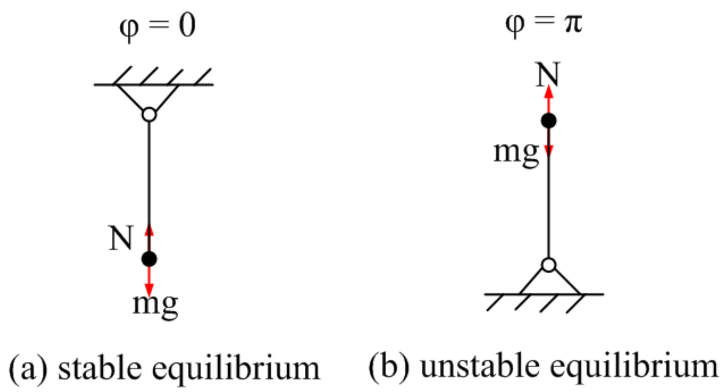


***Figure 3.5 Two equilibriums***

The two equilibrium configurations shown in Figure 3.4 are:

1) when the CoM is at the lowest position, $\varphi = 0$, $\vec{N} + m\vec{g} = 0$; and

2) when the CoM is at the highest position, $\varphi = \pi$, $\vec{N} + m\vec{g} = 0$.

In order to validate equilibrium configurations, unstable equilibrium is introduced. The condition of the unstable stability system is shown in Figure 3.5(b), when $\varphi_{eq} = \pi$, the system is subject to a small disturbance $\hat{\varphi}$. The angle of the particular point described by a math expression is,

$$\varphi = \varphi_{eq} + \hat{\varphi} = \pi + \hat{\varphi} \quad (\hat{\varphi}\ is\ small) \tag{3.24}$$

When the Sine function $\varphi$ is presented in the format of a Tayler formula [112, 113], the solution is obtained,

$$Sin\,\varphi = sin(\pi + \hat{\varphi}) = -\hat{\varphi} \tag{3.25}$$

where, $x \equiv \varphi - \pi \equiv \hat{\varphi}$

the second derivation of (3.25) is,

$$\ddot{\varphi} = \ddot{\hat{\varphi}} \tag{3.26}$$

Substitution of (3.25) and (3.26) into formula (3.8) gives,

$$\ddot{\hat{\varphi}} - \frac{g}{l}\hat{\varphi} = 0 \tag{3.27}$$

Solution of equation (3.27) is,

$$\hat{\varphi} = Ae^{-wt} + Be^{wt} \tag{3.28}$$

When $t \to \infty$, the value of $\hat{\varphi}$ tends to be unstable ($\hat{\varphi} \to \infty$,). Thus far, the unstable equilibrium configuration has been demonstrated.

**Minimum potential energy** (MPE) is applied to determine the particular points of the system where the system is located in stable equilibrium [114, 115]. Equilibrium configurations occur in three groups: stable equilibrium; unstable equilibrium; and neutral equilibrium, which can be classified by the sine of the second differential of PE.

The expression of second variation of PE is,

$$\eta''(\varphi) = mgl\,cos\,\varphi \tag{3.29}$$

When this pendulum system is in its two equilibrium positions, shown in Figure 3.5, the sine of the equation (3.29) is,

$$\varphi = 0: \quad \eta''(0) = mgl > 0 \ \to min \to stable\ equilibrium$$

$$\varphi = \pi: \quad \eta''(\pi) = -mgl < 0 \to max \to unstable\ equilibrium$$

Stable equilibrium is a stationary position, i.e., minimum potential energy (MPE). In such position, an infinitesimal variation involves no change in energy [116]. Unstable equilibrium means that any small disturbance immediately leads to different values for the PE of the system.

### 3.3.4. Stable Stability Realization of a Given System

To design the protective shells of the e-bike, it is important to determine the stable stability condition. Figure 3.5 shows how a satisfactory condition of stable stability may be determined. In order to make analysis easier, the system is divided into two sub-systems, the spring motion system and mass point with a connecting bar system.

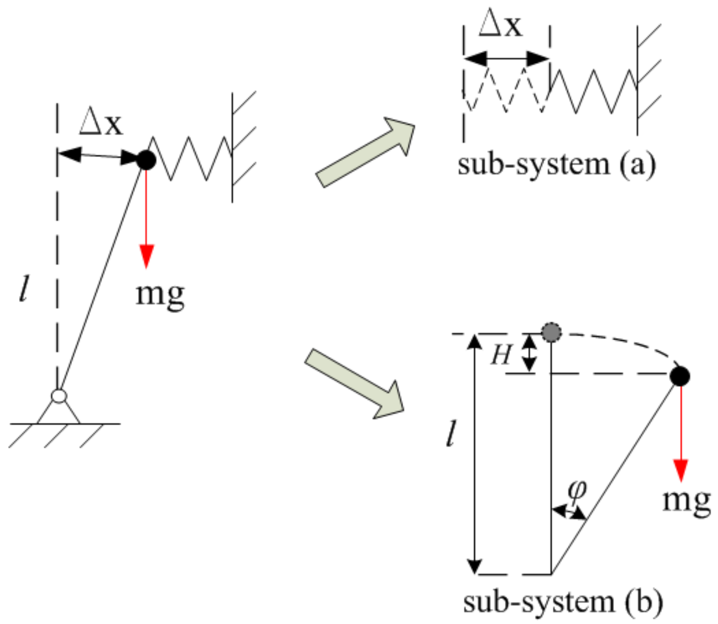


***Figure 3.6 Spring-mass system with a rotating mass point and a spring with stiffness c.***

1) Spring system

The force giving rise to the deformation of the spring is,

$$F_{spring} = -cx \tag{3.30}$$

Work done by the external force is,

$$W_{spring} = \int \vec{F} d\vec{r} = -\int cxdx = -\frac{c(\Delta x)^2}{2} \tag{3.31}$$

As a conservative system, an increase in PE equates to the same magnitude of decrease of work done. PE of the spring is,

$$\eta = -W = \frac{c(\Delta x)^2}{2} \tag{3.32}$$

2) Mass system

From the pendulum system demonstrated, PE caused by gravity is,

$$\eta(m\vec{g}) = -mgH = -mg(l - l\cos\varphi) \tag{3.33}$$

3) The whole spring-mass system

The total PE of the system is the sum of that which is loaded by the spring and gravity.

$$\eta = \eta(m\vec{g}) + \eta(spring) = -mgl(1 - \cos\varphi) + \frac{c(\Delta x)^2}{2} \tag{3.34}$$

When φ → small, $\Delta \boldsymbol{x} \approx \boldsymbol{l\varphi}$ , thus,

$$\eta = -mgl(1 - \cos\varphi) + \frac{(l\varphi)^2}{2}c \tag{3.35}$$

The equilibrium configuration is determined when the first derivation of the whole system equates to zero,

$$\frac{d\eta}{d\varphi} = -mgl\sin\varphi + l^2\varphi \cdot c = 0 \tag{3.36}$$

The solution of (3.37) is,

$$\varphi = 0 \quad equilibrium \tag{3.37}$$

The stable stability position, which is also the location at which the PE tends to be at its minimum, is obtained when the second variation of the system is positive at the position of equilibrium,

$$\frac{d^2\eta}{d\varphi^2} = -mgl\cos\varphi + l^2c > 0 \quad at\ \varphi = 0$$

$$-mgl \cdot 1 + l^2c > 0 \tag{3.38}$$

The solution to equation (3.38) is,

$$c > \frac{mg}{l} \tag{3.39}$$

The solution to equation (3.39) is exactly the condition of the stable stability of the system in Figure 3.6. That is, when the stiffness of the spring, c, is larger than the value of $\frac{mg}{l}$, the system, in this example, is in positive static stability.

## 3.4. A Brief Introduction to Dynamic Stability

As seen in section 3.3 above, static stability is the tendency an object has to return to its equilibrium position when it is moved. However, dynamic stability refers to the movement of an object with respect to time [117]. Static stability should be taken into account in the categorization of dynamic stability. Positive static stability will cause oscillatory motion, which is the only motion considered in this project. Negative and neutral static stability result in non-oscillatory motion because neither of these stabilities tend to move back to their equilibrium position [118]. There are three dynamic stabilities with oscillatory motion: positive static and positive dynamic stability; positive static and neutral dynamic stability; and positive static and negative dynamic stability [119].

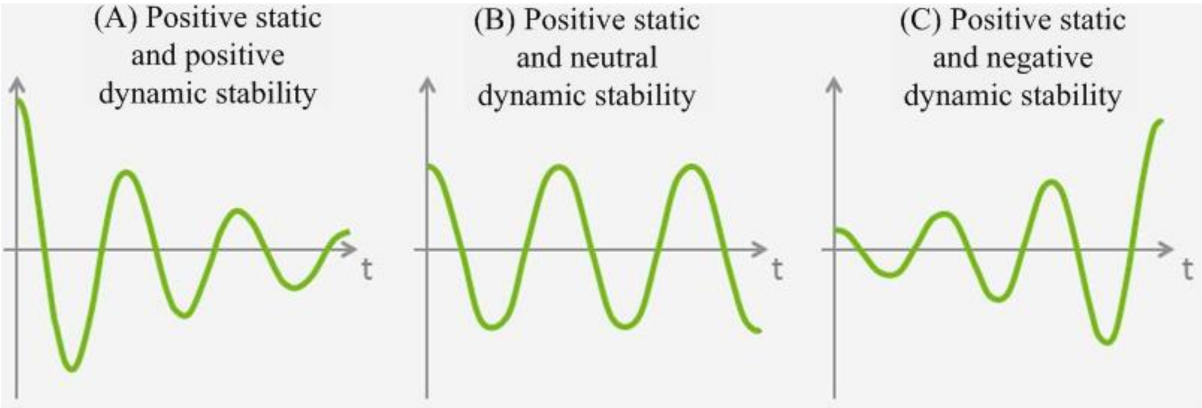


*Figure 3.7 Dynamic stabilities with oscillatory motion[120]*

Figure 3.7(A) describes an oscillation which, because of positive static stability, wants to come back down and this means it will overshoot the equilibrium position and make it want to go back up. Eventually, the amplitude of oscillations will even out and almost come to rest on the static stability equilibrium. This is positive dynamic stability because over time the oscillations get smaller and end up right at the point of equilibrium. Neutral dynamic stability with elapsed time, seen in Figure 3.7(B), is similar. However, the oscillations do not get better as time passes because the neutral amplitude means they remain the same and never diminish. An increasing amplitude over time indicates an oscillation with negative dynamic stability which will become worse (i.e., divergent), as shown in Figure 3.7 (C).

This section has provided a summary of dynamic stability. In the next section, the design of the protective shells, which depends on these stability theorem, is illustrated.

## 3.5. Protective Shells Design

This section presents the development of the strategy used to increase e-bike road safety by designing a special shell protecting the driver during a sideways falling road accident. The design criterion is based on "Roly-Poly" stability criteria for stable rolling vibration.

### 3.5.1. Stable Side Rolling

Considering a general statement of problems in terms of stability of the equilibrium, the rigid body – for simplicity taken in 2D - is shaped from below with a curve y(x).

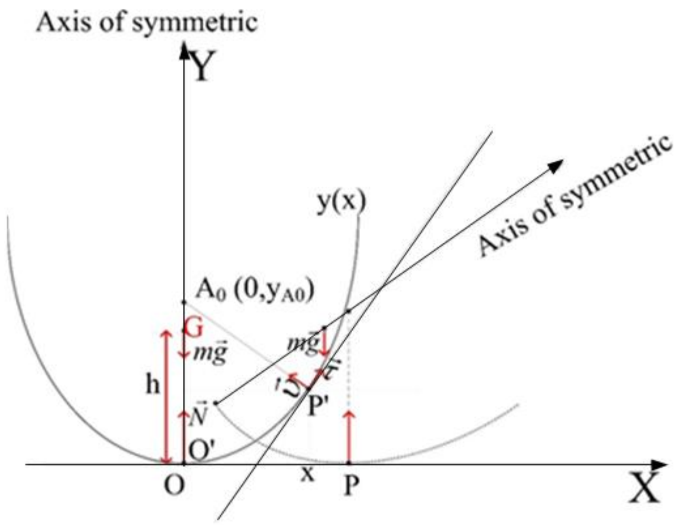


*Figure 3.8 Curve rolling to the side.*

The body has a mass, *m*. The CoM is at point G, situated at height y(x), for the equilibrium situation. A geometrically exact formulation of contact conditions is necessary to describe the rolling action [121].

The curve y(x) is unknown. Thus, the task to find y(x) is based on the following conditions:

1. The height of the centre of gravity is known;
2. Curve y(x) is symmetric with regard to the OY-axis;
3. Assumption of pure rolling during all procedures
4. During rolling motion length OP = length OP’
5. Such that, point (0,0) equilibrium is stable

The equilibrium formula of the rolling system can be described by the two equivalent expressions below:

1) The equation for equilibrium of force,

$$N = mg \tag{3.40}$$

2) PE of this system

$$\eta = mgY_G \tag{3.41}$$

The parameters are defined below:

1. The intersection of normal vector $\bar{\boldsymbol{N}}$ with the axis of symmetry is at point $A_0$, which is also the centre of the geometry;
2. $\bar{\boldsymbol{\nu}}$ is a unit normal vector to the curve at the x axis;
3. $\bar{\boldsymbol{\tau}}$ is a unit tangent vector.

### 3.5.2. Stability Criteria - Geometric

Now consider the situation of rolling contact for the profile *O'P'* – the profile is rolled into the line *OP*. A CoM is moved to a new point. One can see that the point with coordinates (0,0) is stable during the rolling motion if, when rolling to the right (left), the direction of the gravity force vector $\boldsymbol{m\vec{g}}$ remains from the left (right) side with respect to the normal reaction vector $\vec{\boldsymbol{N}}$. This stability criterion, at the initial position (shown in Figure 3.7), can be formulated geometrically as,

$$y_{A_o} \geq h \tag{3.42}$$

The following shows how to derive the stability criteria mathematically. The main goal is to find *y(x)* such that the stability criteria is fulfilled. Some knowledge of the differential geometry of curves should be applied to formulate this criterion in the form of ordinary differential equations.

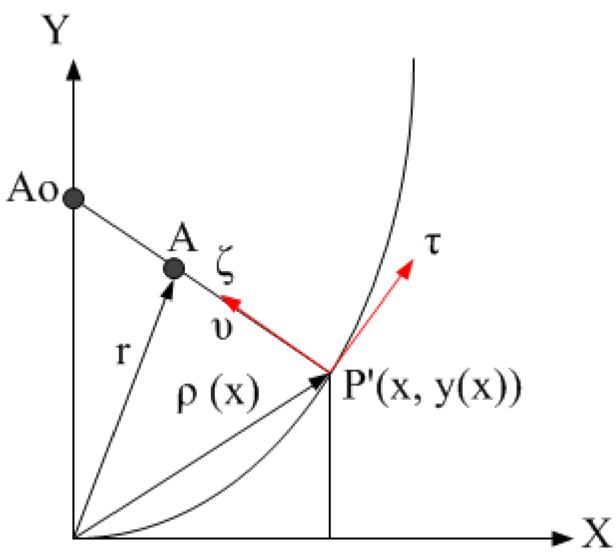


*Figure 3.9 Coordinate system of the curve*

In Figure 3.9, the profile *O′P′* is given in a 2D Cartesian system as,

$$\vec{\rho}(x) = \begin{Bmatrix} x \\ y(x) \end{Bmatrix} \tag{3.43}$$

With the differential in respect of the x-axis,

$$\frac{d\vec{\rho}}{dx} = \begin{Bmatrix} 1 \\ \frac{dy}{dx} \end{Bmatrix} \tag{3.44}$$

The unit tangent vector to this profile is,

$$\tau = \frac{\frac{d\vec{\rho}}{dx}}{\left|\frac{d\rho}{dx}\right|} = \begin{Bmatrix} 1 \\ \frac{dy}{dx} \end{Bmatrix} \frac{1}{\left|\frac{d\rho}{dx}\right|} \tag{3.45}$$

For convenience, the derivative $\frac{dy}{dx}$ is abbreviated as $y'$. The length of the vector $\left|\frac{d\rho}{dx}\right|$ is calculated by,

$$\left|\frac{d\rho}{dx}\right| = \sqrt{1 + (y')^2} \tag{3.46}$$

Thus,

$$\vec{\tau} = \begin{Bmatrix} 1 \\ y' \end{Bmatrix} \frac{1}{\sqrt{1+(y')^2}} \tag{3.47}$$

Due to vector υ being orthogonal to vector τ, the scalar product is,

$$\vec{\tau} \cdot \vec{\upsilon} = 0 \tag{3.48}$$

Another format of the equation can be expressed by coordinates as,

$$\tau_x \upsilon_x + \tau_y \upsilon_y = 0 \tag{3.49}$$

This allows the equation for the unit normal vector to be written based on the condition of orthogonality as,

$$\vec{v} = \begin{Bmatrix} -y' \\ 1 \end{Bmatrix} \frac{1}{\sqrt{1+(y')^2}} \tag{3.50}$$

So far, all the parameters are clarified. Then the curve is described in terms of these parameters.

An equation of the line P'A$_0$ is then written as,

$$\vec{r} = \vec{\rho} + \vec{v} \cdot \zeta = \begin{Bmatrix} x \\ y(x) \end{Bmatrix} + \zeta \begin{Bmatrix} -y' \\ 1 \end{Bmatrix} \frac{1}{\sqrt{1+(y')^2}} = \begin{Bmatrix} x - \frac{\zeta \cdot y\prime}{\sqrt{1+(y')^2}} \\ y(x) + \frac{\zeta}{\sqrt{1+(y')^2}} \end{Bmatrix} \tag{3.51}$$

In the equation above, the scalar $\zeta$, which denotes the length of line *P'A*, is unknown. The goal, from now on, is to determine the parameter $\zeta$. The distance $\zeta$ is found by,

$$(\vec{r})_x = 0 \tag{3.52}$$

$$x - \frac{\zeta \cdot y'}{\sqrt{1+(y')^2}} = 0 \tag{3.53}$$

$$\Rightarrow \zeta = \frac{x\sqrt{1+(y')^2}}{y'} \tag{3.54}$$

After some transformation the coordinate of point *A* can be found as,

$$(\vec{r})_y = y_{Ao} = y(x) + \frac{\zeta}{\sqrt{1+(y')^2}} \tag{3.55}$$

Substitution of $\zeta = \frac{x\sqrt{1+(y')^2}}{y'}$ into this equation, gives,

$$y(x) + \frac{x\sqrt{1+(y')^2}}{y\prime\sqrt{1+(y')^2}} = y(x) + \frac{x}{y\prime} \tag{3.56}$$

The differential equation for the curve y(x), the position when “y'=0”, is absolutely stable during the rolling of a curve. From Roly-poly stability criteria, when the CoM is not above the centre of curvature at the contact point, the system is stable. The last equation gives us the following differential equation for the limit case curve,

$$y(x) + \frac{x}{y'} \geq h$$

$$\Rightarrow y(x) \cdot y' + x \geq h \cdot y'$$

$$\Rightarrow y(x) \cdot y' - h \cdot y' \geq -x$$

$$\Rightarrow y'^{(y-h)} \geq -x$$

$$\Rightarrow \frac{dy}{dx} \cdot (y - h) \geq -x$$

$$\Rightarrow \frac{d(y - h)}{dx} \cdot (y - h) \geq -x$$

$$\Rightarrow \frac{(y-h)^2}{2} \geq -\frac{x^2}{2} + c \qquad (3.57)$$

The solution of this ordinary differential equation is,

$$(y - h)^2 + x^2 \geq 2c = r^2 \qquad (3.58)$$

Equation (3.58) describes a circle as the limit case curve which gives us stable rolling. All smooth curves lying below this curve give us the rolling profile which will cause stable vibrations at the equilibrium point (0,0) in the given coordinate system, as seen in Figure. 3.10.

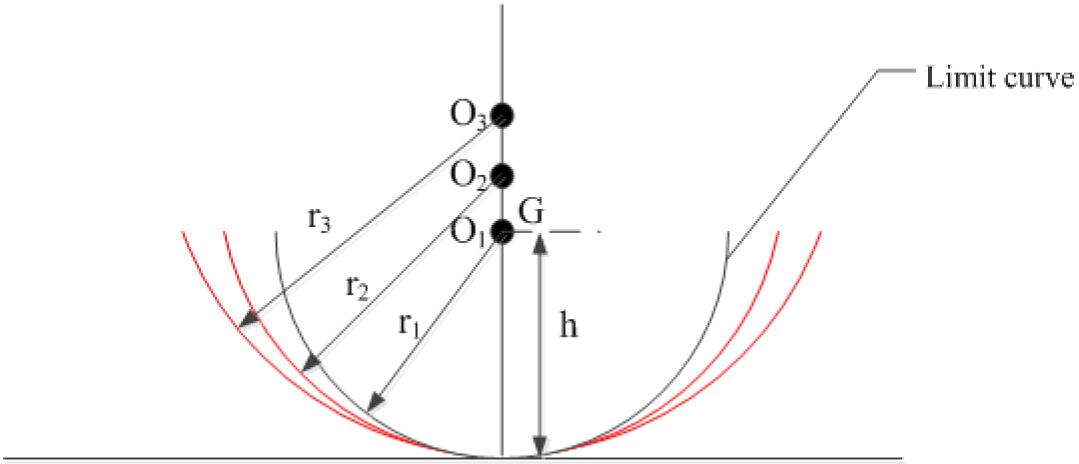


*Figure 3.10 Curves are leading to stable rolling*

It is shown that in this case, the rolling profile should satisfy the corresponding differential equation. In the simplest 2D case, it is proved that all smooth curves lying below the limit stability curve (a circle) lead to stable rolling vibration profiles.

### 3.5.3. Design Criteria for the Protecting Shells – No Overturning During Sideways Falling

From the stability of the Roly-Poly toy, the formula for stable stability is derived as $r > h$. This indicates that the ratio of the protective shell should be larger than the distance between the CoM and the contact point, *p*, on the ground at any instance of contact. The principle of Roly-Poly stability fulfils the condition of static stable stability. If the structure of an e-bike is required to be totally stable during the whole period of sideways falling, it is anticipated that this would result in the need for dramatically large shells. The requirement is that the sideways falling should not lead to overturning. In this case, the curve is not starting at zero point of contact, but at a certain point, *O*, of possible side contact, see Figure 3.11.

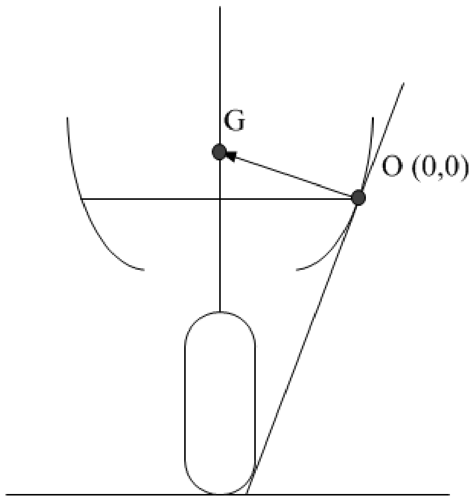


***Figure 3.11  Initial position of the curve***

Hence, the height of CoM, *h*, is in fact a changing distance between the point of CoM and the contact point *O*, in real time.

All smooth curves delivering a stable rolling vibration at point zero are satisfying the condition,

$$r > h \quad stable\ stability \tag{3.59}$$

The neutral position is where the curve goes through the original point O,

$$r = h \quad neutral\ stability \tag{3.60}$$

And the unstable conditions of the curves are proposed as,

$$r < h \quad unstable\ stability \tag{3.61}$$

Referring to equation (3.58), expression (3.59) is exactly the condition of the design criterion.

## 3.6. Summary

This chapter has introduced the Roly-Poly stability system. From the geometry of the Roly-Poly toy, the design criterion for the protective shells of the e-bike has been developed. The condition of a stable stability system is $r > h$. The foundation and formulation of the Roly-Poly system is derived from static stability theorem. The three types of equilibrium configurations of stability systems have been illustrated and derived from a simple pendulum system. One example, the spring-mass system, has been given to denote the procedure of how to realize a stable stability condition. The essential procedure of protective shell design has been proposed.

# CHAPTER 4. EXPERIMENTAL STUDY - MASS CENTRE COLLECTION

## 4.1. Introduction

CoM (centre of mass) is an imaginary point. It is the position of resultant torque, caused by gravity force, and is equal to zero. Therefore, the CoM is also called the centre of gravity (CoG) [122]. In order to determine the CoM of an e-bike, two experiments have been designed according to two different methods. They are the proportional method and plumb line method. Once the CoG, or CoM, is determined for the e-bike, it can be treated as a single mass resting at that point.

CoM is one of the critical parameters and is warranted for use in future modelling. Two experimental approaches have been designed to determine the CoM of an e-bike.

## 4.2. Experiment 1 - Proportional Method

As it is difficult to know the mass distribution of the whole e-bike, the data concerning two wheels are considered. On this point, experiment No.1 is designed as: percentages of the reaction force on two wheels to calculate the CoM. The operation process of Experiment No.1 is to measure weights instead of reaction forces on both wheels at various heights, as shown in Figures 4.1 and 4.2.

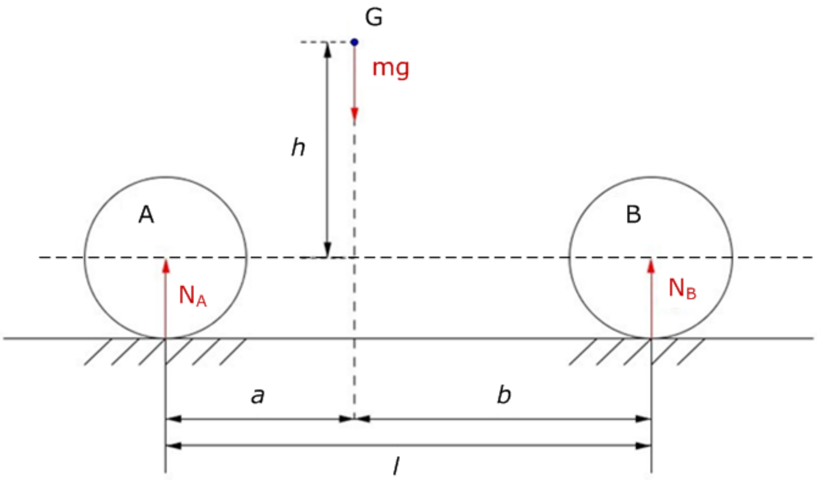


*Figure 4.1 E-bike situated on a horizontal floor.*

Figure 4.1 shows an e-bike situated on a horizontal floor. Circles A and B, front wheel (rear wheel) and rear wheel (front wheel), contact the ground at points A and B respectively. $N_A$ and $N_B$ are two reaction forces and point $G$ is the CoM. The horizontal range from the wheels to the CoM are at "$a$" and "$b$". The wheelbase is at "$l$".

Here, equilibrium equations are,

$$N_A + N_B = mg \tag{4.1}$$

The resultant torque at point $A$ is zero. Assuming the clock-wise direction is positive, it is expressed as,

$$+mga - N_B(a + b) = 0 \tag{4.2}$$

Analogously, the resultant torque at point $B$ is zero,

$$-mgb + N_A l = 0 \tag{4.3}$$

The solution to the horizontal distances between the two wheels and the CoM can be acquired from equation (4.2) and (4.3),

$$a = \frac{N_B}{N_A+N_B} \cdot l \tag{4.4}$$

$$b = \frac{N_A}{N_A+N_B} \cdot l \tag{4.5}$$

Wheelbase *l* is calculated as,

$$l = a + b \tag{4.6}$$

Where, reaction forces $N_A$, $N_B$ are known as measured data, distances *a*, *b* are determined by applying equations (4.4) and (4.5) respectively.

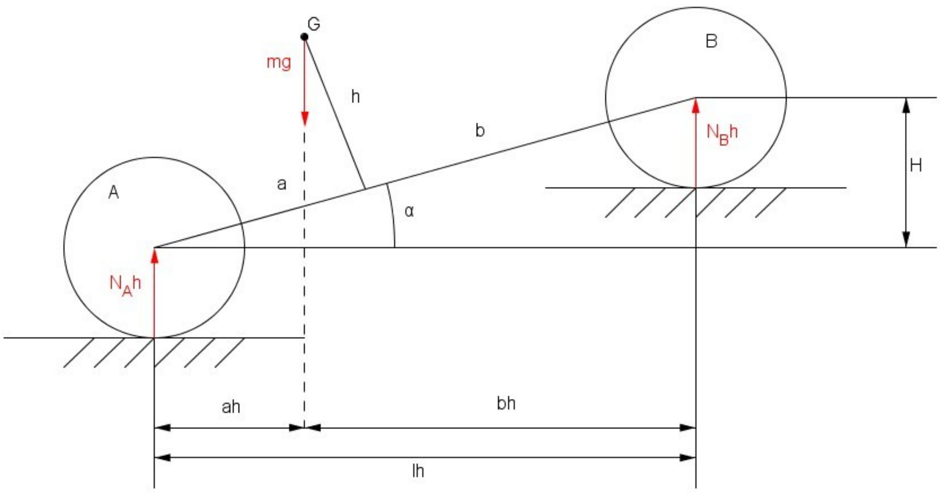


*Figure 4.2 E-bike put on slant*

In Figure 4.2, α is the angle between the wheelbases and the horizontal plane; "*h*" is the perpendicular distance from CoM to the wheelbases.

Accordingly, both resultant torques at point *A* and *B* vanish, so that the lengths of $a^h$, $b^h$ expressed by $N_A^h$, $N_B^h$ are,

$$a^h = \frac{N_B^h}{N_A^h + N_B^h} \cdot l^h \tag{4.7}$$

$$b^h = \frac{N_A^h}{N_A^h + N_B^h} \cdot l^h \tag{4.8}$$

The wheelbase projected on the horizontal plane is,

$$l^h = l \cos \alpha \tag{4.9}$$

In order to determine angle *α*, the trigonometric functions are expressed as,

$$\cos \alpha = \frac{l^h}{l} = \frac{\sqrt{l^2 - H^2}}{l} \tag{4.10}$$

$$\sin \alpha = \frac{H}{l} \tag{4.11}$$

Parameter $a^h$ can also be expressed as,

$$a^h = a \cos \alpha - h \sin \alpha \tag{4.12}$$

The value of $a^h$ is known in equation (4.7). Thus, the unique unknown "*h*" is determined by,

$$h = \frac{a \cos \alpha - a^h}{\sin \alpha} \tag{4.13}$$

From the derivation above, all the parameters of CoM, which are *a*, *b,* and *h*, can be determined by collecting experimental data to apply the theory.

### 4.2.1. Experiment Procedure

The sequence of the experiment is as follows:

1) The e-bike is placed on the horizontal floor.
2) The weight of the e-bike is tested.

3) The length of the wheelbase is measured.
4) The data for the weight of the front and rear wheels are recorded.
5) The front wheel of the e-bike is placed on a forklift and the rear wheel on the ground.
6) The front wheel is raised to several specific heights by adjustment of the forklift.
7) The weight data for front and rear wheels are collected.

### 4.2.2. Experiment Results

The data of $H$, $Na$, $N_b$, and wheelbase measured in the experiment are shown in Table 4.1.

*Table 4.1 Weights of the two wheels at different slope levels*

| $H$ | value of H | Wheelbase | $N_A$ | $N_B$ | sin $a$ | cos $a$ | $a$ | $l_h$ | $A^h$ | $b^h$ | $h$ |
|---|---|---|---|---|---|---|---|---|---|---|---|
| H1 | 0 | 153 | 67 | 47 | 0 | 1 | 0 | 153 | 63.08 | 89.92 | none |
| H2 | 35.7 | 153 | 62.5 | 45.5 | 0.23 | 0.97 | 0.24 | 148.78 | 62.68 | 86.10 | -5.75 |
| H3 | 45.7 | 153 | 71 | 47.5 | 0.30 | 0.95 | 0.30 | 146.02 | 58.53 | 87.49 | 5.59 |
| H4 | 55.7 | 153 | 66 | 47.5 | 0.36 | .093 | 0.37 | 142.50 | 59.64 | 82.86 | -2.44 |
| H5 | 70.2 | 153 | 65 | 46 | 0.46 | 0.89 | 0.48 | 135.94 | 56.34 | 79.61 | -0.63 |
| H6 | 35.7 | 153 | 71.5 | 51 | 0.23 | 0.97 | 0.24 | 148.78 | 61.94 | 86.84 | -2.58 |
| H7 | 45.7 | 153 | 68 | 52 | 0.30 | 0.95 | 0.30 | 146.02 | 63.27 | 82.74 | -10.29 |
| H8 | 55.7 | 153 | 66 | 53 | 0.36 | 0.93 | 0.37 | 142.50 | 63.47 | 79.03 | -12.96 |
| H9 | 70.2 | 153 | 65 | 54 | 0.46 | 0.89 | 0.48 | 135.90 | 61.69 | 74.26 | -12.30 |

The other values, such as $\sin\alpha$, $\cos\alpha$, $\alpha$, $l_h$, $a^h$,$b^h$ and $h$, are calculated by substituting the measured data into the equations above. In terms of analysing the value of parameters $a^h$, $b^{h,}$ and h above, there are considerable errors between each set of data.

## 4.3. Reasons for the Failure to Obtain MoC in Experiment 1

The failure to obtain the exact position of CoM may be attributed to the overlooking of the spring components, i.e., the shock-absorbers, in the e-bike structure [123-126], see Figure 4.3.

*Figure 4.3 Spring components in the e-bike*

Due to the unacceptable error in the result of Experiment 1, a second experimental method is applied to determine the CoM of the e-bike.

## 4.4. Experiment 2 - Plumb Line Method

In order to avoid interference from the spring structure when locating the CoM, the plumb line method is employed to design Experiment No.2. In general, for a symmetrical body, the CoM is an anchoring point on its symmetrical plane [127]. In this sense, 3D symmetrical geometry can be regarded as a 2D shape, which is suitable for an e-bike as it is an axial structure.

As demonstration objects, two suspensions are chosen, one is longitudinal hanging at location A, and the other is vertical hanging at location B. Figure 4.4 shows the starting points: extending the ends of the plumb lines (suspension points on hooks) and making the extended lines parallel to the vertical edge of the wall. The intersection point of the two plumb lines is the exact location of the CoM [128].

### 4.4.1. Experiment Procedure

This experimental process combined the plumb line method and the photographic overlap method, as follows:

1) The e-bike is hung from the crane at suspension points A and B and photographed as shown in Figure 4.4.

*Figure 4.4 E-bike suspension at locations A and B*

2) To calculate the scale of each graph, a photo of the e-bike including a ruler is taken as a reference (datum photo), see Figure 4.5.

*Figure 4.5 The datum for the e-bike scale*

3) The plumb line is drawn, starting from the hook, by referring to the vertical edge of the wall.
4) The photos (in Figure 4.4) are enlarged to the same scale and overlapped to determine the cross point which is the CoM.

A local coordinate is created on the graph and the location of the CoM in that is determined. The calculation procedure is shown in Figures 4.6 and 4.7.

## 4.4.2. Experiment Results

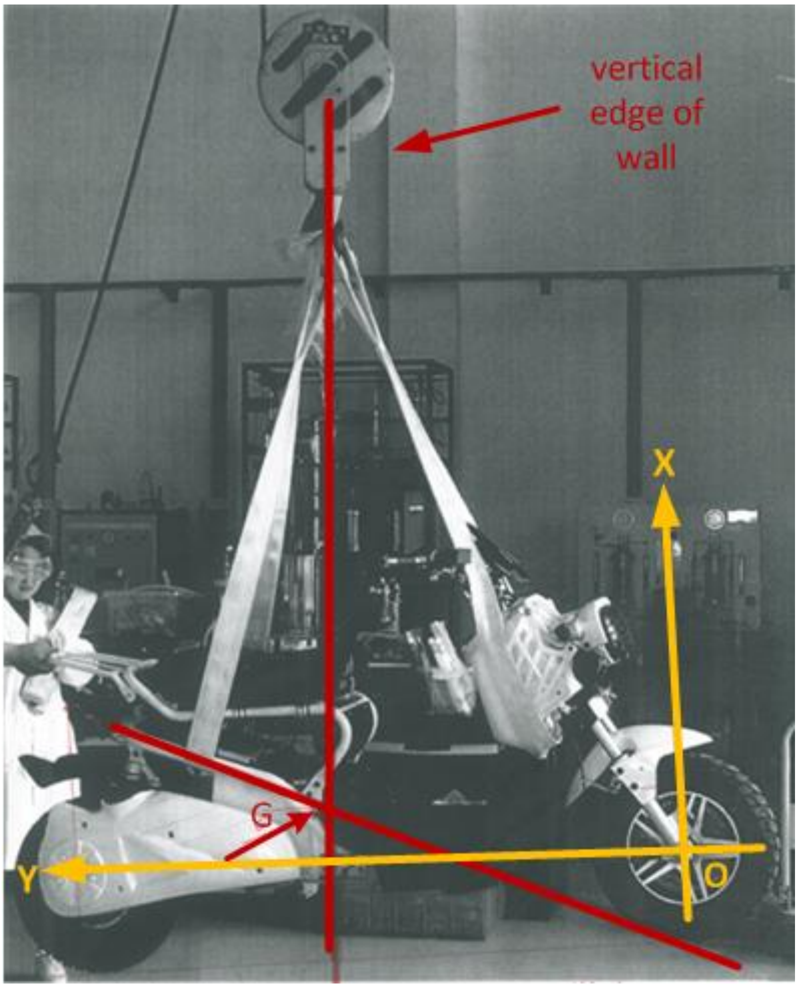


Figure 4.6 E-bike suspension A

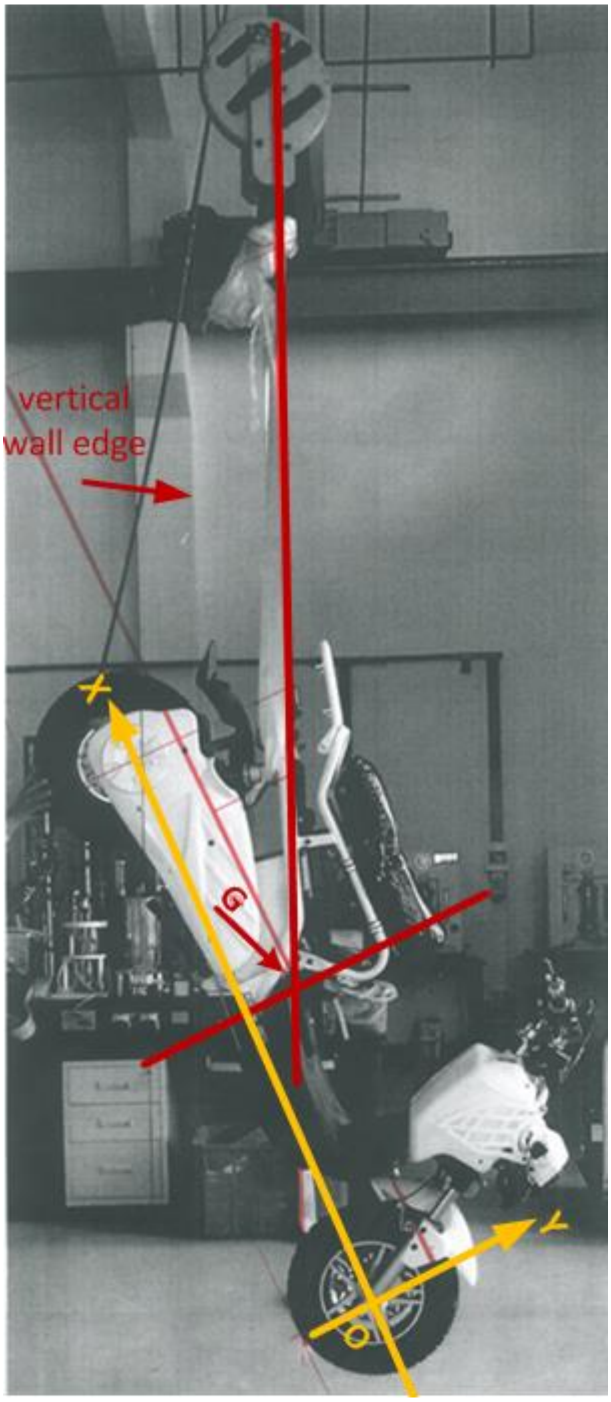


*Figure 4.7 E-bike suspension B*

The CoM occurs at the intersection of the two red lines. In the datum scale photo (Figure 4.5), the wheelbase shown on the ruler is 156.5 cm, and the wheelbase of the datum photo itself is 32.09 cm. Therefore, the scale of the datum photo is,

$$scale = \frac{32.09\text{cm}}{156.5\text{cm}} = 0.205 \tag{4.14}$$

In the picture of suspension A, the wheelbase is 21.5 cm. Substituting it in equation (4.14), the scale is 0.137. In the same way, the scale in the picture of suspension B is 0.109.

A local coordinate is settled as follows:

1) The centre of the front wheel is set as the original point
2) The X-axis coincides with the centre line of the two wheels, and the positive direction points towards the rear wheel.
3) The Y-axis is vertical to the X-axis and they cross at the original point, *O*, thus, the positive direction is upward.

It is determined that the location of the CoM in the local coordinate in Figure 4.5 is (12.3 cm, 5.47 cm). When dividing the scale by 0.137, as determined in Figure 4.5, the realistic position of the CoM in the local coordinate is (89.5 cm, 39.8 cm).

## 4.5. Summary

CoM is a significant element, not only in original design, but also during the stages of modelling and simulation of the protective shells. The data for the CoM have been collected and calculated from the experiment, this is applied in the following section about the model construction.

# CHAPTER 5. FE MODEL CONSTRUCTION - 3D GEOMETRIC MODELLING MESHES GENERATION AND MODAL ANALYSIS

The Finite Element Method (FEM) is a numerical method which solves a problem by discretizing a physical model into small finite elements, describing these elements and their relationships by series of formulae, and determining the results of these complicated formulae. It is a numerical method to allow approximate solutions with preconfigured precision. The basic idea of FEM can be summarized into two aspects, discretization, and shape (interpolation) function. Discretization is a technique employed to generate sub-domains to show a physical model by a finite number of elements, which are also known as meshes. Shape function, also known as interpolation function, is a mathematical function which evaluates corresponding elements with partial differential equations within boundary conditions. It uses a trial function on every element to solve the whole domain problem [129-131].

## 5.1. Introduction

In this chapter, an FE model of the e-bike is constructed. FE modelling is pre-processed to find a solution for the simulation. In order to build the e-bike FE model, steps of 3D geometric modelling, model meshing, and model validation (modal analysis) should be taken sequentially.

Three-dimensional modelling (3D modelling) represents the database of the physical body of an object [132]. The database of the geometry of the model has to be presented and its output, i.e., the basic data of the whole modelling step, established. In order to construct an e-bike FE model, preliminary modelling by CAD is used to obtain the geometric data of the e-bike. Thus, a 3D model of the e-bike is produced.

Meshing is the downstream step of 3D geometric modelling during FE model composition. Mesh generation is considered the most critical aspect during the engineering simulation and it takes up most of the simulation time. The quality of meshes has a direct influence on the accuracy, the running time, and even the convergences of the simulation results [133]. Very fine mesh (where the cells of the finite elements are too small) would ensure the precision of the results, but it would take a long time to run the solution. Conversely, very coarse mesh (where the cells of the finite elements are too large) saves time, but could lead to inaccurate results [134]. Meshes can be generated in ANSYS, Hyper Mesh, or in other FE software. In this project, the meshes were created directly in ANSYS rather than in other software in order to avoid the inconvenience of communication between different environments.

Modal analysis is employed to verify the FE model. Since the quality of the meshes are counted in the accuracy of the solution, it is necessary to modify the shape of the meshes previously created in the meshing step [135]. Thus, a series of modal analyses using the FEM are carried out to investigate the correctness of the meshes in the original FE model.

The following sub-sections illustrate in detail the steps taken for the construction of the FE model of the e-bike.

## 5.2. A 3D Geometric Model of the E-bike

The 3D geometric attributes of the e-bike are presented by CAD modelling in the computer system. CAD, or computer-aided design, is built for the purpose of the creation, modification, analysis, and optimization of a model using CAD software [136].

PTC Creo is one of a number of CAD software available and is widely used in 3D modelling. The attribute of the model in Creo is represented based on particular parameters [137]. The parametric modelling approach is a useful computational method as it provides a convenient mode of communication between a computer and its users. The method uses parameters to define the models in terms such as their dimension, features, material property, and particularly the relationship between the parts or assemblies. [138]. When one parameter is modified, the reflected modification of the model will update automatically [139]. Consequently, Creo is adopted to construct the CAD geometric model of the e-bike.

The database for the e-bike is collected from a real product - Zuma, shown in Figure 5.1. The Zuma e-bike is, in fact, a type of e-scooter. The features of the Zuma are: a heavy frame, with a total weight of 114 kilograms; a speed of 60 kilometres per hour at its fastest: and an e-motor with power of more than 1000 watts.

*Figure 5.1 Zuma e-scooter -a type of heavy e-bike.*

The general geometric parameters of this Zuma e-bike are: 1970mm length, 1130mm height, and 450mm width. The CAD model was created in Creo. The proposed modelling steps are illustrated based on this e-bike. For many questions which arise in the structural design, e.g., properties concerning stability, it is not necessary to build each detail of the e-bike. Thus, the simplified model is both warranted and sufficient.

The performance of this simplified step in the CAD model followed the sequence: 1) modelling of essential parts responsible for transmitting all loads – namely all frames; 2) modelling of essential parts for contact during sideways falling – wheels, handlebar, and side frames. The intrinsic geometric parameters are presented in Figure 5.2.

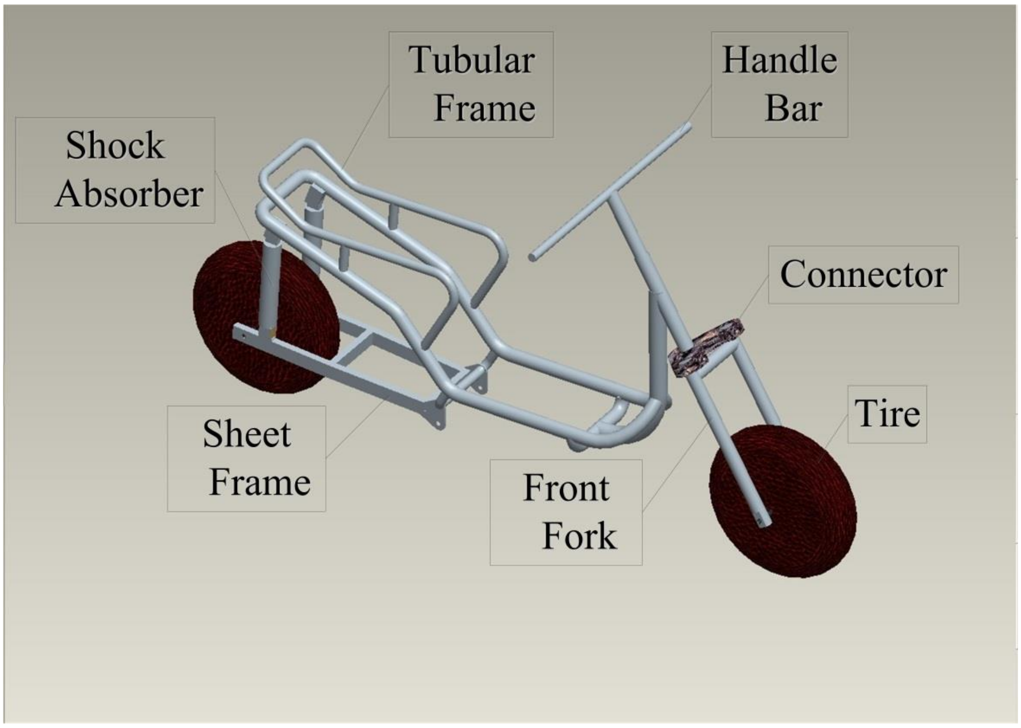


***Figure 5.2 The simplified CAD model consists of frames, front fork, shock absorber, axles, tires, and some connectors. Pro-Engineer CAD-software.***

This CAD geometric model of the e-bike is a representation designed to show the machine's predominant components and functions. This simplified structure can be categorized into three rigid, laterally symmetric, and ideally hinged components: two wheel assemblies and the frame assembly.

Now the geometric model is constructed in Creo. However, it is necessary to establish the geometric model in the ANSYS environment, which is in preparation for meshing in ANSYS. There are two approaches to realize the proposed model construction in ANSYS, the importing model method and the direct modelling method.

### 5.2.1. Importing Model Method

In the context of this project, the importing model method means that the 3D geometric model created using CAD software is imported into the FE software environment.

The steps taken are as follows: 1) the e-bike model created in Creo, shown in Figure 5.2, is output in a general format, such as STP or IGES, which maintains the curves, surfaces and solids of the geometric shapes of the e-bike. 2) The STP or IGES file is then imported into ANSYS. The corresponding geometric model is shown in Figure 5.3.

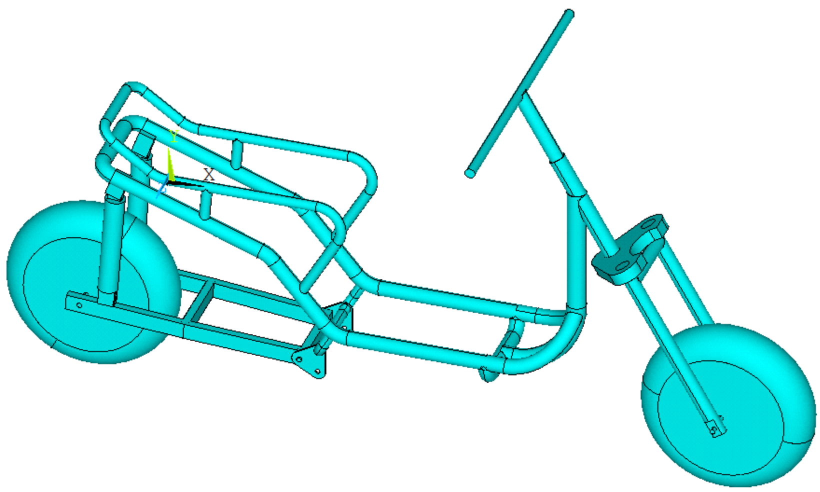

***Figure 5.3 The geometric model imported from IGES to ANSYS software***

However, this geometric model imported from Creo has its weaknesses. Errors are easily identified, for example, some surfaces are lost, some points are duplicated, and some parts are given the wrong shape. This phenomenon is caused by the way the different software communicate with each other, thus, it took some time to repair the geometry until the model seen in Figure 5.3 was eventually generated. Additionally, the size of the model created in this way is too large (more than a billion bits) so that further simulation steps based on this model would become prohibitively costly. Since the importing method can introduce errors and result in expensive simulation time, it is expected that the direct modelling method will remedy those problems.

### 5.2.2. Direct Modelling Method

The direct modelling method is a way of generating a 3D model directly in ANSYS. For simplification, and in order to avoid the added computing and programming time and effort, the parameters of the model created in Cero (i.e., dimensions such as width, length, thickness of the parts etc., shapes, coordination, and so on) are referred to and the e-bike geometry intensified. The 3D model of the e-bike created in ANSYS by this direct modelling method is shown in Figure 5.4.

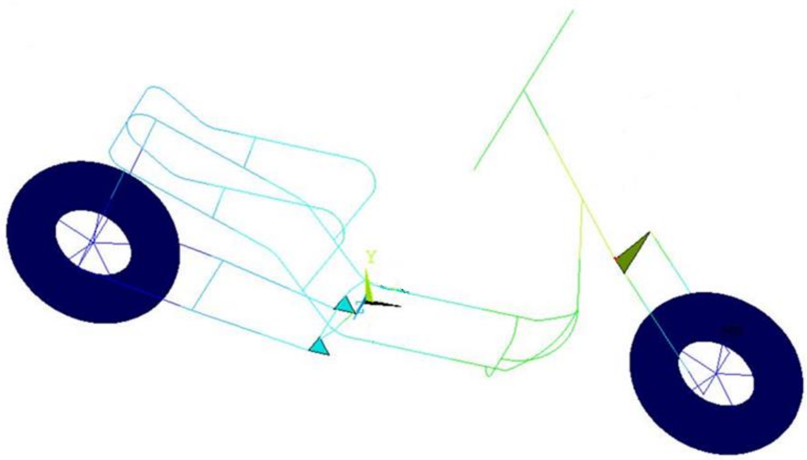

*Figure 5.4 E-bike geometric model created and simplified directly in ANSYS*

According to the Finite Element Method, it is necessary to discretize the model of the e-bike into a finite number of elements, which is the meshing step.

## 5.3. Mesh Generating in ANSYS

In general, it is necessary to produce meshes prior to applying computational analysis in order to find a solution to a problem[140], even though there are very few implementations of meshfree methods [141, 142].

In computational analysis, meshing is a technique for approximately discretizing the complex geometry by finite small domains (meshes) with polygonal or polyhedral shapes [143]. The basic idea of discretization in FEM is to divide a physical body into an assemblage of elements. These elements are discrete, they are interconnected by the common nodes located at the boundaries of elements [144]. In a physical system (i.e., the structure of the e-bike in this project), elements represent different properties in respect of predefined attributes [145].

ANSYS pre-processor was chosen for the creation of the model, as well as for mesh generation, in order to avoid the need for communication between different codes. ANSYS contains abundant elements, such as beam element, shell element, solid element, link, combine, pipe, etc. The first three of these elements are the most common for use in the structural construction of a model in finite elements analysis (FEA). The geometric model of the e-bike was mainly meshed by beam and shell elements. The following formulations explain the characteristics and nuances of these two types of elements.

### 5.3.1. Formulae of the Shell and Beam Elements - Interpolation Method

Interpolation, in the mathematical aspect of numerical analysis, is a method of constructing a database of a new point based on the data of known points.

The interpolation formulae of both shell and beam elements are derived from those of solid elements. In essence, their geometry is simplified from that of the solid element. For the purpose of calculation, and time-saving during simulation, only the characters which could lead to critical impact are considered. The dimensions which are insufficient to the solution can be ignored. Normally, those dimensions are idealized as given-by constants.

The interpolation functions and their parametric coordinates of the solid element are illustrated as the foundation of the shell and beam elements.

Parametric coordinates are also known as curvilinear coordinates, a coordinate system which can consist of curved coordinate lines [146]. Figure 5.5 introduces an example of the parametric coordinate of an 8-node solid element.

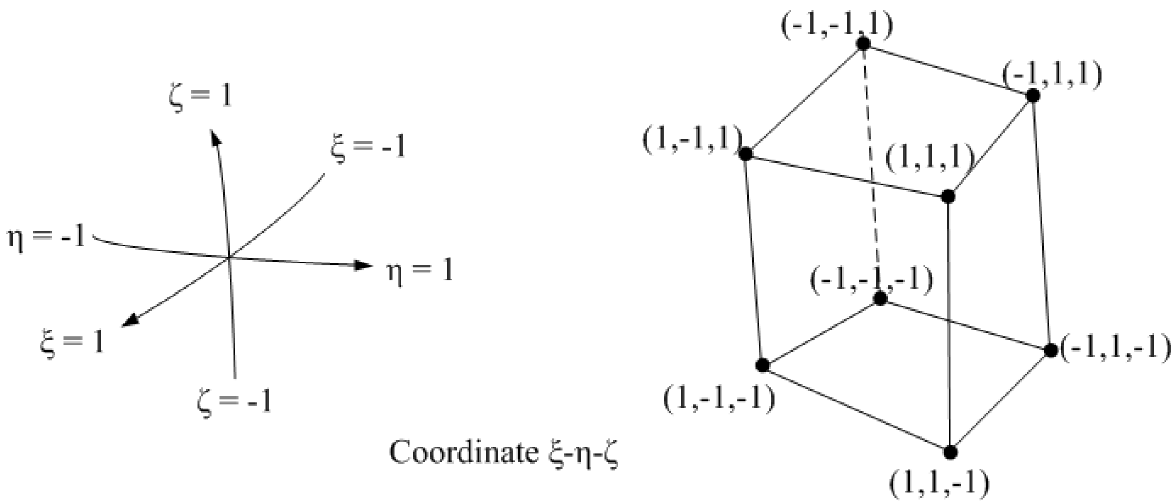


***Figure 5.5 Parametric Coordinate ξ-η-ζ [147]***

In Figure 5.5, the parametric coordinate $\xi$-$\eta$-$\zeta$ is defined. The positive directions of $\xi$-$\eta$-$\zeta$ coordinate curves are out-of-plane, right-hand-side, and upward respectively. The coordinates of each node of this solid element are shown in Figure 5.5 (right).

The parametric coordinates and corresponding shape functions serve as the interpolation formula.

For the displacement of any node of the 8-node solid element, the vector of displacement in the space expressed as parametric coordinate is,

$$\begin{Bmatrix} X \\ Y \\ Z \end{Bmatrix} = \sum_{i=1}^{8} N^i\,(\xi,\eta,\zeta) \begin{Bmatrix} X^i \\ Y^i \\ Z^i \end{Bmatrix} \quad (-1 \le \xi,\eta,\zeta \le 1) \tag{5.1}$$

Where, the shape function $N^i$ is given as,

$$N^i{}_{(\xi,\eta,\zeta)} = \frac{(1+\xi)(1+\eta)(1+\zeta)}{8} \tag{5.2}$$

Where *ξ, η, ζ* are evaluated at each node, refer to Figure 5.5.

The formulae of the 8-node solid element were introduced prior to those of the beam and shell elements, to which they are fundamental.

### *Formulation of the Shell Element*

The shell element is usually chosen in the instance of the thickness being far smaller than the length and width. Figure 5.6 shows the process of an 8-node solid element transformed into a 4-node shell element. This implies that the shell element can be regarded as the simplified solid element by ignoring the influence caused by the minimal thickness in this instance [148].

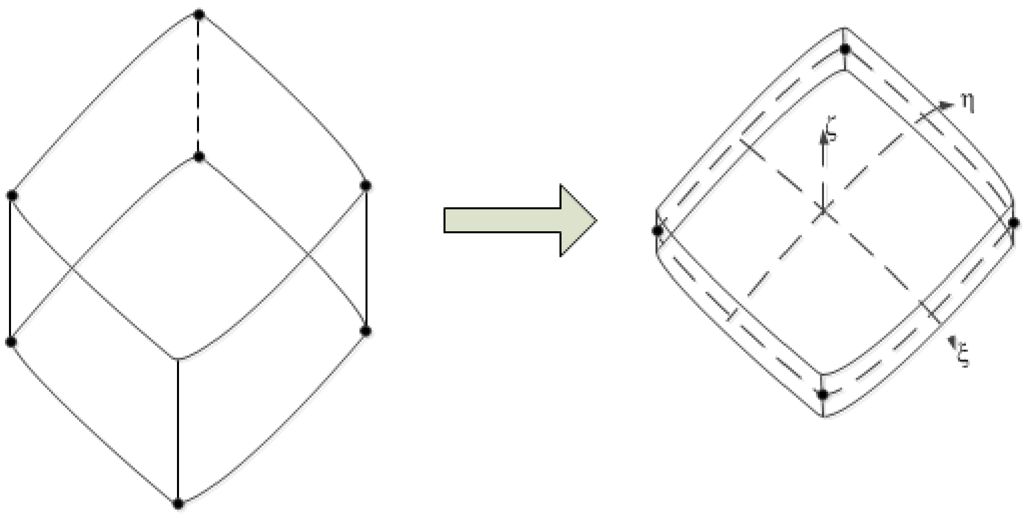


*Figure 5.6 The solid element is transformed to a shell element [149]*

The schematic diagram, shown in Figure 5.7, denotes the formulation of the shell element. In global coordination, the coordinate of each node is along the z-axis. Assuming the z axis is normal to the shell, the corresponding magnitude is constant, "z". Consequently, all nodes of the shell can be analysed in 2D.

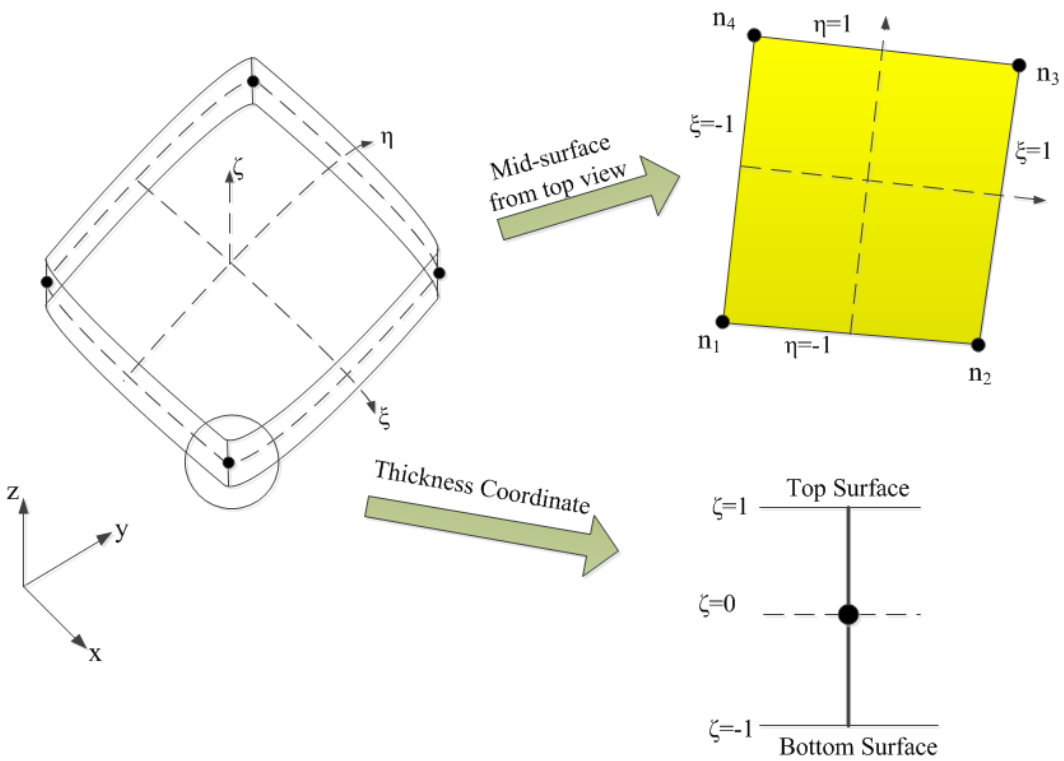


*Figure 5.7 Analysis of the 4-node shell element. [147, 150]*

The geometric varieties of the shell elements are referred to the 2D surface-Mid-surface, shown in the top right corner of Figure 5.7.

The coordinate of each node is shown in Figure 5.5. Approximation of the geometry of the shell expressed in a mathematical equation is,

$$\bar{x} = \bar{x}^{(1)} N^{(1)}{}_{(\xi,\eta)} + \bar{x}^{(2)} N^{(2)}{}_{(\xi,\eta)} + \bar{x}^{(3)} N^{(3)}{}_{(\xi,\eta)} + \bar{x}^{(4)} N^{(4)}{}_{(\xi,\eta)}$$

$$= \sum_{i=1}^{4} \bar{x}^{(i)} N^{(i)}{}_{(\xi,\eta)} \tag{5.3}$$

Referring to Lagrangian approximation, the shape functions, N, evaluated at all the nodes are,

$$
\begin{aligned}
N^{(1)} &= \frac{(1-\xi)(1-\eta)}{4} \\
N^{(2)} &= \frac{(1+\xi)(1-\eta)}{4} \quad -1 \le \xi \le 1 \\
N^{(3)} &= \frac{(1+\xi)(1+\eta)}{4} \quad -1 \le \eta \le 1 \\
N^{(4)} &= \frac{(1-\xi)(1+\eta)}{4}
\end{aligned}
\tag{5.4}
$$

The value of the thickness along $\zeta$ axis is specified as $h$. The geometric expression of this 4-node shell is given by [151],

$$
\begin{Bmatrix} X \\ Y \\ Z \end{Bmatrix} = \underbrace{\sum_{i=1}^{4} N^i(\xi,\eta) \begin{Bmatrix} X^i \\ Y^i \\ Z^i \end{Bmatrix}}_{①} + \underbrace{\sum_{i=1}^{4} N^i(\xi,\eta) \frac{h^i}{2} \zeta \vec{e}_3^{\,i}}_{②} \quad (-1 \le \xi, \eta, \zeta \le 1) \tag{5.5}
$$

Where the shape function, N, determines the position of the point on the mid-surface, $h^i$ is the value of the shell thickness, and $\vec{e_3}$ is the union vector which is normal to mid-surface. In equation (5.5), part ① is the vector of an arbitrary point on the mid-surface, which is calculated by the positon of the four corner nodes. Part ② denotes the vector starting from a point on the mid-surface in the direction of the thickness. Thus, the position of any point of the shell can be determined by this equation.

### *Formulation of the Beam Element*

A 2-node beam element is intensified for simplification from the shell element. It is also the simplest element in a three-dimensional model. When the ratio of the section dimensions to the length reduces to a small value, i.e., more than 5:1, the impact on the cross section is as that on a point. The schematic diagram in Figure 5.8 shows the process of an 8-node solid element transmitted to a 2-node beam element [148].

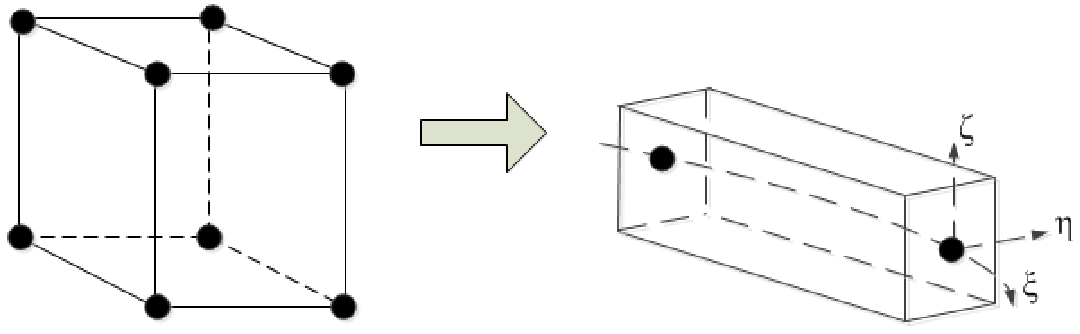


*Figure 5.8 Solid element is transferred to beam element*

The detailed information of the geometry of a 2-node beam element is shown in Figure 5.9.

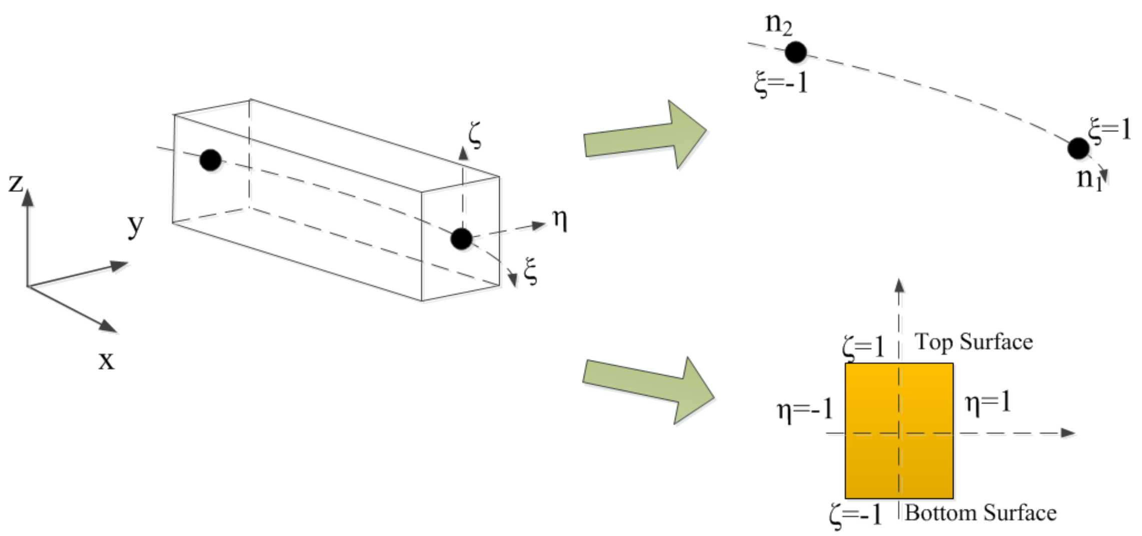


*Figure 5.9 Analysis of 2-node beam element*

The two nodes of the beam element, see Figure 5.9, are located on the reference axis which, generally, is predefined because the curves always pass through the geometric centre of cross sections. The coordinate, in Figure 5.9, consists of only one dimension axis curve $\xi$. To form a Lagrange approximate, the value of $\xi$ varies from -1 at the end position of the beam to +1 at the other end position.

The geometry of this beam element is described by equation (5.6) [151, 152],

$$\begin{Bmatrix} X \\ Y \\ Z \end{Bmatrix} = \underbrace{\sum_{i=1}^{2} N^i(\xi) \begin{Bmatrix} X^i \\ Y^i \\ Z^i \end{Bmatrix}}_{①} + \underbrace{\sum_{i=1}^{2} N^i(\xi) \frac{h_2^i}{2} \eta \vec{e}_2^{\,i}}_{②} + \underbrace{\sum_{i=1}^{2} N^i(\xi) \frac{h_3^i}{2} \zeta \vec{e}_3^{\,i}}_{③}$$

$$(-1 \le \xi, \eta, \zeta \le 1) \tag{5.6}$$

where *N* is the shape function, which determines the position of the point on the reference axis. Constants $h_2$ and $h_3$ are the magnitudes of the thickness of the cross section in two orthogonal directions. Vectors $e_2$ and $e_3$ create the union vector along axis $\eta$ and axis $\zeta$ respectively. Back to the formula, part ① denotes the position vector point to reference axis $n_1$ and $n_2$. Based on the point on the reference axis, parts ② and ③ are the vectors which determine the position of a point on the corresponding cross section.

The formulae of the shell and beam elements have been introduced in this section. The implementation of these formulas are now mapped into the model meshing.

### 5.3.2. Model Meshed by the Shell and Beam Elements

In ANSYS, various types of finite elements can be used directly to create a model comprising the most important mechanical properties. The beam and shell elements make up the main structure of the e-bike. The frame of the e-bike was modelled using beam elements with various predefined sections; two wheels and some connectors were modelled depending on the geometry of the shell elements. All parts or components are connected by common nodes. The FE model of the e-bike is shown in Figure 5.10.

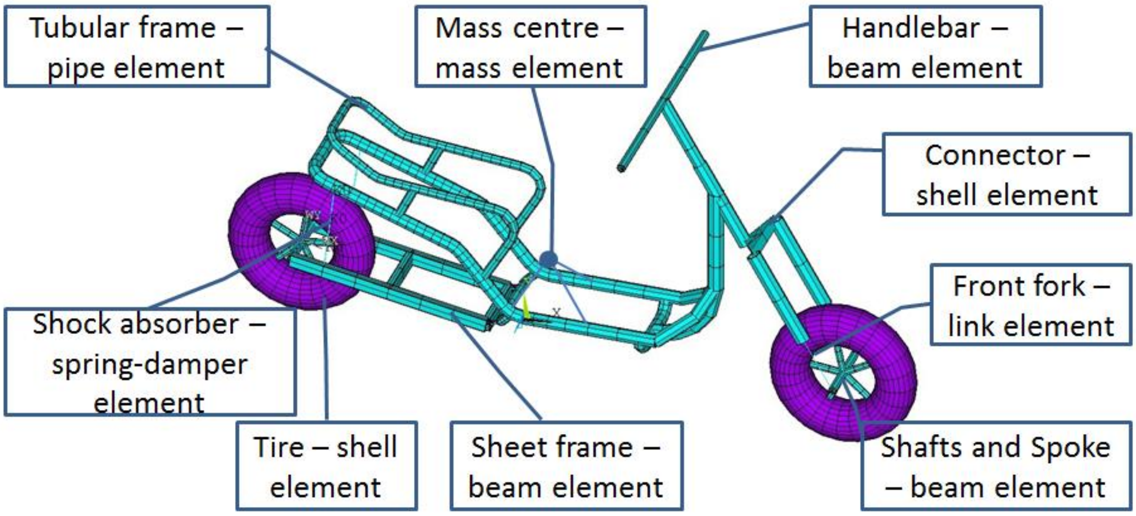


*Figure 5.10 Finite Element Model of Zuma e-bike.*

This type of the FE model requires specification of the total mass of the e-bike which can be modelled as MASS element in ANSYS. The location of the CoM point of the e-bike structure has been obtained in the experimental study (refer to Chapter 4). The mass element is connected to the main frame by the use of artificial beam elements, shown in Figure 5.10.

So far, the FE model of the e-bike has been meshed in the ANSYS environment.

## 5.4. Modal Analysis - Model Validation

Modal analysis can be applied for non-destructive inspection of a structure [153]. The most common utilization of modal analysis is to determine the natural modal shape and the various orders of frequencies of a mechanical structure during free vibration by testing the object using FEM or an experimental method [154, 155]. Nevertheless, by checking the degrees of freedom of the global model and the mesh connectivity, modal analysis is employed to determine the mesh quality of the FE model.

### 5.4.1. Formula of Modal Analysis

The formulae of modal analysis are taken into account to give a clear interpretation of its output results. The general equation of dynamic motion is well known, it is a linear elastic spring mass system expressed as [156],

$$[M]\{\ddot{u}\} + [C]\{\dot{u}\} + [K]\{u\} = \{F\} \tag{5.7}$$

Where $[M]$ is the mass matrix [157], $[C]$ is the damping matrix, and $[K]$ is the stiffness matrix, while $\{u\}$ is the displacement vector. Its first time derivation, $\{\dot{u}\}$, is the velocity, and its second time derivation, $\{\ddot{u}\}$, is the acceleration. Vector $\{F\}$ is the global external force.

For modal analysis, it is assumed that the damping of the system is ignored and there is no external force. The structure is free of vibration. Thus, equation (5.7) reduces to,

$$[M]\{\ddot{u}\} + [K]\{u\} = 0 \tag{5.8}$$

When applying modal analysis using FEM, substituting a time harmonic solution for the displacement $\{u\}$ in equation (5.8), then $\{\ddot{u}\}$ is the variable based on $\{u\}$, which is taken into $-\omega^2\{u\}$ [158]. $\omega$ is the natural circular frequency and is given by,

$$(-\omega^2[M] + [K])\{u\} = \{0\} \tag{5.9}$$

Considering the foundation of modal analysis in equation (5.9), the solution is to calculate the determinant of,

$$|[K] - \omega^2[M]| = 0 \tag{5.10}$$

The number of roots equal the number of DOFs. Due to the complicated stiffness matrix, $[K]$, and the mass matrix, $[M]$, of this e-bike FE model, it might be difficult to solve equation (5.10) using a mathematical approach. Modal analysis using FEM is a good way to solve this complication and is discussed in the following section.

### 5.4.2. Modal Analysis

Modal analysis is the approach which reveals whether the meshed components of the model are properly connected to, or disconnected from, each other. The connecting situation of the model can be checked directly on the basis of the results animation (when the structure is vibrating independently). For example, if there is a gap between two elements, the location of the breaking nodes belonging to those two elements can be found. This requires the connection between the nodes of neighbouring domains. In this case, the modelling needs to return to the meshing step to be modified. The flow chart in Figure 5.11 shows the detailed process used to determine the model according to modal analysis and correction of the meshing in FEM.

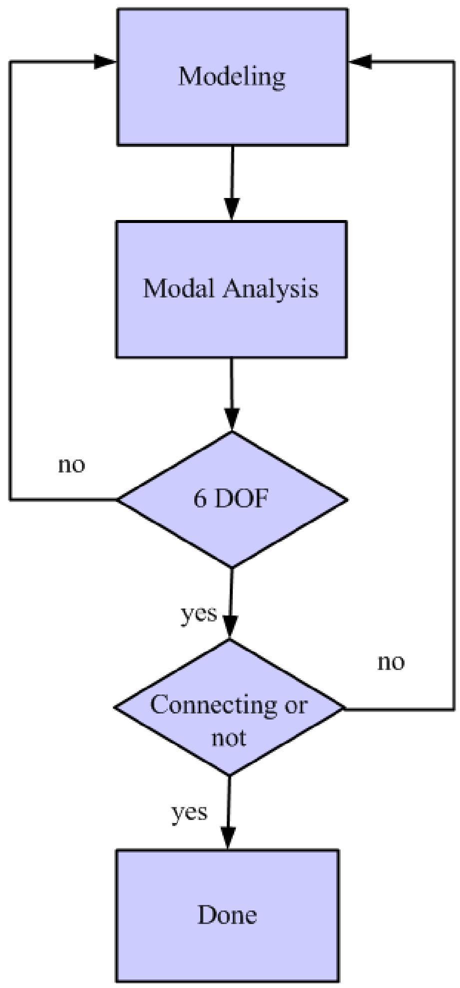


*Figure 5.11 Flow chat to show the process of model verification*

The results of the modified model in modal analysis are revealed in Table 5.1.

*Table 5.1 The Results Summary of modal analysis of e-bike with mass*

| SET | 1 | 2 | 3 | 4 | 5 | 6 | 7 | 8 | 9 | 10 |
|---|---|---|---|---|---|---|---|---|---|---|
| TIME | 0 | 0 | 0 | 0 | 0 | 0 | 0.45 | 0.16 | 0.53 | 0.14 |

In general, during free vibration, a 3D physical body has six DOFs - three translation DOFs and three rotation DOFs. In this sense, as an entirety, the value in the first six sets should be zero, otherwise, dis-connectivity exists.

A screen shot of the animation of the modified model is shown in Figure 5.12.

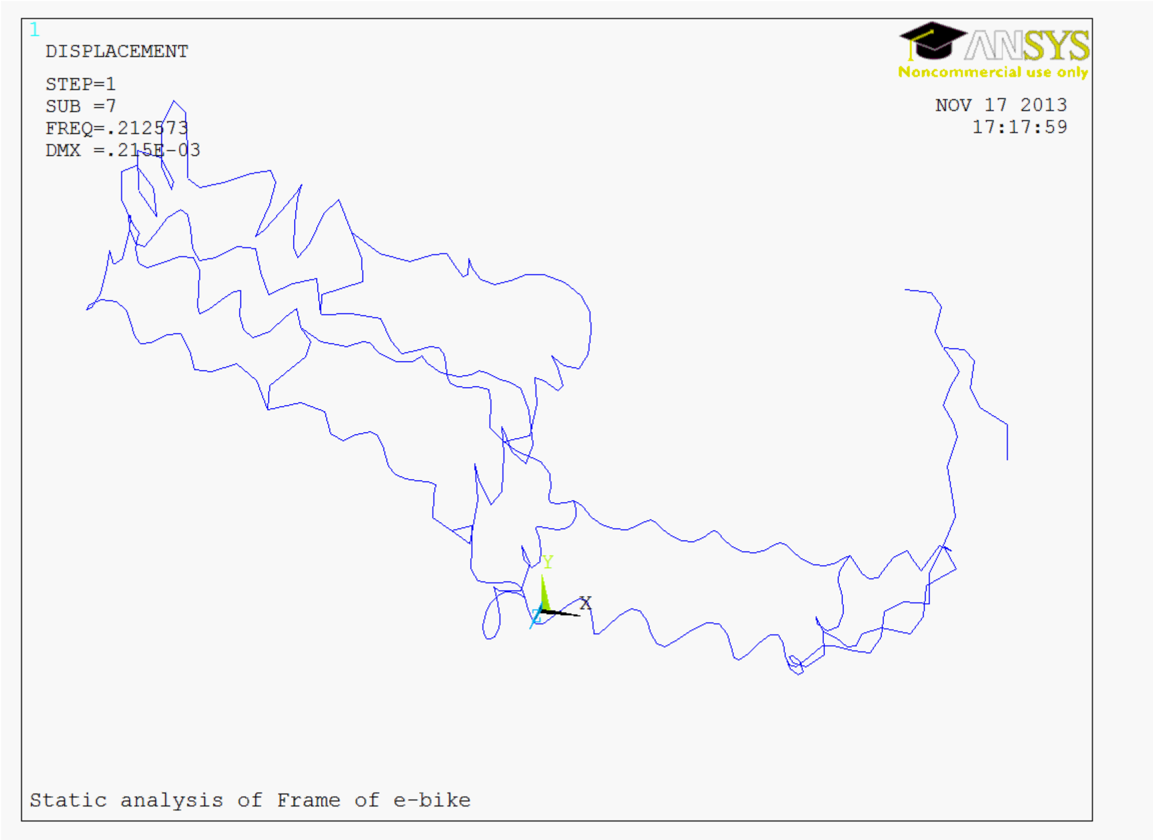


*Figure 5.12 Deforming frame in modal analysis*

Once the geometry of the meshes is modified and the interconnection of the common nodes ensured to allow the model to be retrieved, then, as in Figure 5.12, the gap between the elements cannot be found so that the connection situation between the components can be confirmed. Therefore, the validation of the FE model of the e-bike is implemented according to modal analysis.

## 5.5. Summary

This chapter has reported the original creation of the FE model in ANSYS. It was conducted by the generation of a 3D geometric model and meshes. Two methods of 3D geometric model construction in the ANSYS environment have been considered, the importing model method and the direct modelling method. An overview of formulae of the finite element method (FEM) preceded the meshing of the simplified model by beam and shell elements. The fundamentals of beam and shell element geometry are illustrated by the solid element, which shows the procedure of derivation and the characters of these elements. A mass element is placed in the mass centre, the location of which was determined in Chapter 4.

Even though the FE model has been created, the quality of the model meshes must be checked by performing modal analysis. Before static and dynamic analysis, the derived FE model has been processed into a model verification stage, i.e., modal analysis. The validation stage is imperative as it is essential for the accuracy of further analysis.

Now the corrected FE model is created and will be used in the straight falling test in ANSYS.

# CHAPTER 6. DROP-TEST ANALYSIS IN ANSYS - 3D FRICTIONLESS CONTACT CASE BETWEEN THE STRUCTURE OF THE E-BIKE AND THE GROUND

## 6.1. Introduction

This chapter deals with the 3D frictionless contact simulation process. A penalty method is adopted as the equation for the contact simulation. The key contact pair parameter, introduced in the penalty method, represents the stiffness of the structure during contact. This key parameter is critical for the frictionless contact simulation. Thus, a series of values for the contact stiffness is investigated and analysed by conducting transient simulation, determined by comparison with the theoretical results. The steps in this process are shown in sequence as:

1) Illustration of contact theory – the penalty method is used to understand the basic contact principle which is then used to explain the meaning of the contact parameters referred to in the simulation results;

2) Construction of the model of the ground. This is then applied into the drop testing and the frictionless contact simulation between the existing e-bike model and this ground model;
3) A quick run of a static analysis of the drop testing to verify that the model of the e-bike fits the model of the ground;
4) Transient simulation (dynamic analysis) of the straight falling test and its results allow comparison with theoretical results in order to determine the contact parameters (contact stiffness).

## 6.2. Frictionless Contact Conditions and their Implementations – the Penalty Method

### 6.2.1. Instructions Concerning Frictionless Contact

Contact mechanics is the study of the deformation caused by solid bodies that touch each other at one or more points [159]. Contact interaction can be divided into two components, non-frictional and frictional contact. In the case of frictionless contact, pressures act in the normal direction to the surfaces of the master bodies. In the case of frictional contact, the frictional stresses act in the plane tangential to contact surfaces as well [160]. This research focuses only on contact cases, ignoring the interaction in tangential directions (the frictional stresses), which would be a frictionless contact analysis.

### 6.2.2. Simplest Spring Mass System – Penalty Method

It is necessary to establish the contact simulation prior to contact testing. In general, there are three common algorithms which satisfy contact situations. They are the Lagrange multiplier method, the Penalty method, and the Augmented Lagrange method [161]. The penalty function contact algorithm has been shown to be an efficient method for contact treatment [162], hence, it is employed here.

The penalty method is derived by starting from the simplest idealized model – the spring-mass system. The spring-mass system in contact mechanics is a suspended system consisting of a mass point attached to a spring of which stiffness is *c*, as shown in Figure 6.1 [161].

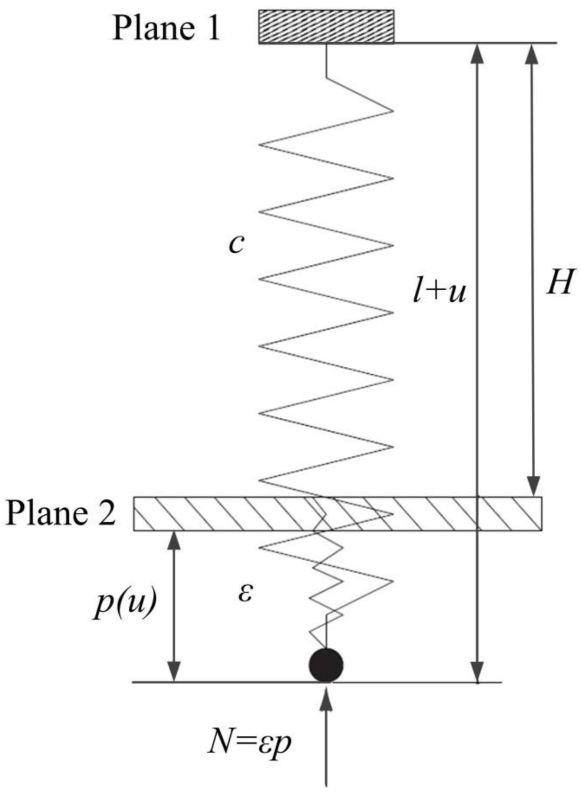


*Figure 6.1 Mechanical interpretation of the penalty method*

$H$ is the height between Planes 1 and 2, $l$ is the stretched length of the spring, and $\varepsilon$ is the penalty parameter which, in this case, is the stiffness of the additional spring attached to the rigid Plane 2. The deformation of the spring is $u$, and function $p(u)$ is the contact penetration in this system [161].

$$p(u) = l + u - H \tag{6.1}$$

The normal contact force, $N$, with the penalty method is expressed as:

$$N = \varepsilon p(u) \tag{6.2}$$

In the numerical method, the penalty parameter $\varepsilon$ for force $N$ should be well determined in order to be suitable for numerical algorithm with sufficient tolerance. This is, in a mathematical sense, regularization of the contact solution.

### 6.2.3. Weak Formula – Regularization with the Penalty Method

Considering the weak formula for contact, the definition of contacting objects "slave" and "master" should be clarified. "Slave" is the observed surface that consists of the arbitrary contact point "$S$". "Master" is the body acting as the observer, the position (convective coordinates on the "master" surface $\xi^1$- $\xi^2$) of which is derived via the closest projection point "$C$", with respect to point "$S$". Before the regularization, the natural convective coordinates "$\xi^1$- $\xi^2$- $\xi^3$" are introduced, see Figures 6.2 and 7.3. The scalar $\xi^3$ is the initial normal distance between points "$S$" and

"$C$", while $\xi^1$ and $\xi^2$ are local convective coordinates defined on the surface coordinate lines. The geometry of a "slave" is given by,

$$\vec{r}(\xi^1, \xi^2, \xi^3) = \vec{\rho}(\xi^1, \xi^2) + \xi^3 \vec{n} \tag{6.3}$$

Where $\vec{\rho}(\xi^1, \xi^2)$ is the vector of the "master" surface and $\xi^3 \vec{n}$ is the normal vector to the "master" surface from point "$C$" to point "$S$".

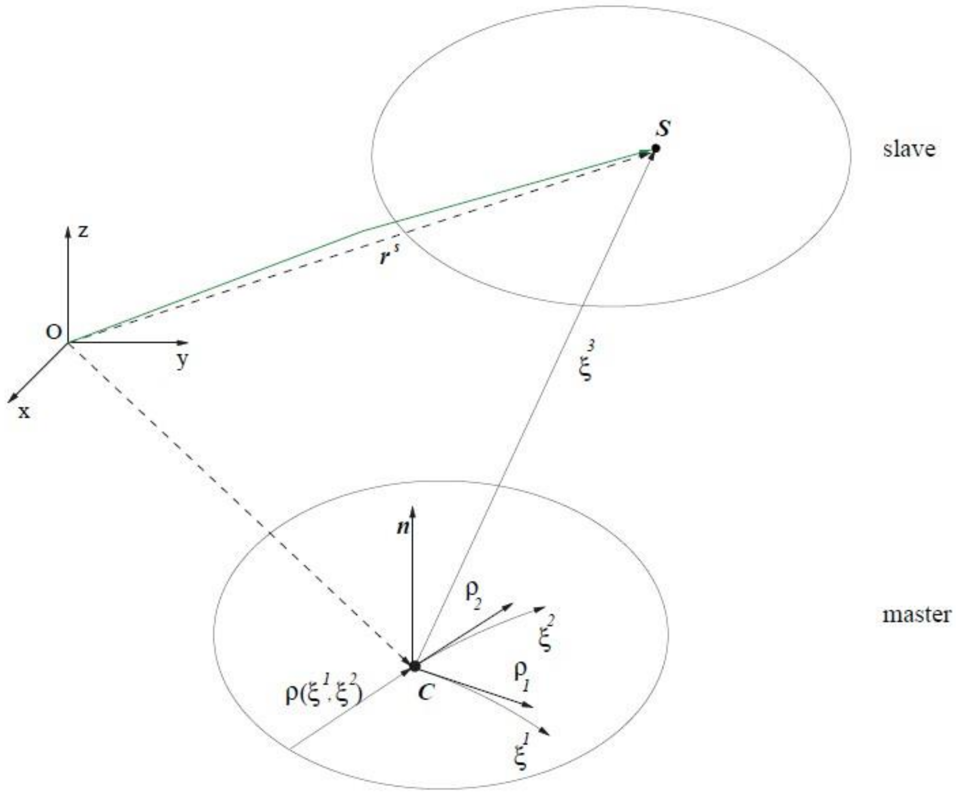


***Figure 6.2 Contact kinematics in 3D case [163]***

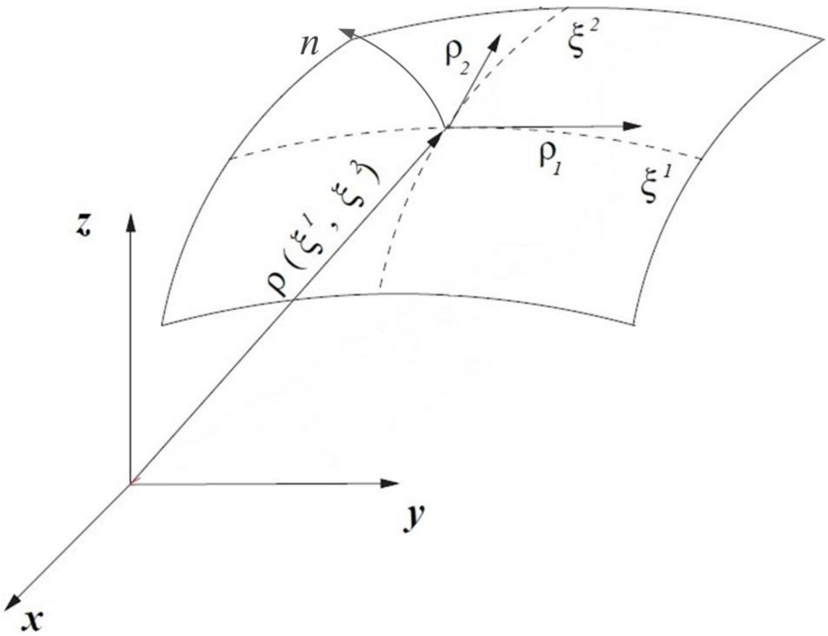


*Figure 6.3 Geometrical magnitudes for the contact formulation*

In the natural coordinates "$\xi^1$- $\xi^2$- $\xi^3$", the virtual work $\delta W$ can be written in the following form [161]:

$$\delta \mathrm{W} = \int_{s} \left( \underbrace{\mathrm{N}\delta\xi^{3}}_{\text{normal part}} + \underbrace{\mathrm{T}^{\mathrm{i}}\left(\rho_{\xi^{\mathrm{i}}} \cdot \rho_{\xi^{\mathrm{j}}}\right)\delta\xi^{\mathrm{j}}}_{\text{frictional part}} \right) \mathrm{ds} \tag{6.4}$$

For the frictionless case, formulated by the Penalty Method, the tangential term (frictional part) is ignored ($T^i$=0) and the normal part of the contact term is a function with the penalized tractions $N$ (normal contact force) [164]. The integral of virtual work is reduced to,

$$\delta W = \int_{s} N\delta\xi^{3}\, ds \tag{6.5}$$

When regularization by the penalty method of frictionless conditions is taken into account in equation (6.5), then the normal force, *N,* is computed as follows,

$$N = \varepsilon H(-\xi^3)\xi^3 \tag{6.6}$$

where $\varepsilon$ is the physical normal penalty parameter (refer to Equation (6.2)) and $H(-\xi^3)$ is the Heaviside function. The evaluation of $H(-\xi^3)$ depends on the value of the normal distance $\xi^3$, therefore, it is computed only for the penetration case as follows [165],

$$H(-\xi^3) = \begin{cases} 0 & \xi^3 > 0 \\ 1 & \xi^3 \leq 0 \end{cases} \tag{6.7}$$

When two bodies are in a condition of contact, scalar penetration $\xi^3$ is non-positive, a normal contact force is computed, and function $H(-\xi^3)$ is equal to "1". In other words, term $H(-\xi^3)\xi^3$ is exactly the penetration *p(u)*, refer to Equation (6.2).

The frictionless contact integral in equation (6.5) is transformed with the penalty regularization as follows,

$$\delta W = \int_s \varepsilon H(-\xi^3)\xi^3 \delta\xi^3 \, ds \tag{6.8}$$

The theory of frictionless contact applying the Penalty Method is used for all following simulations.

## 6.3. Implementation of Modelling and the Penalty Method

### 6.3.1. Modelling of the E-bike and the Ground

The frictionless contact simulation refers to the contact between the e-bike's wheels and the ground, therefore it is necessary to add an FE model of the ground to the FE model of the e-bike. The isometric view of the FE model of the e-bike and a ground plate in ANSYS is shown in Figure 6.4. The ground was discretized by shell elements. The boundary condition in this FE model is that the centre point of the front wheel is fixed by restricting six DOFs. The rear wheel is constrained in all directions except for the translation in Y-direction. The 3D surface to surface contact method was chosen in this simulation. In addition, contacting elements were adopted, CONTA174 contact element and the 3-D target element (TARGE170), as these two types of elements can be perfectly located on shell elements [166].

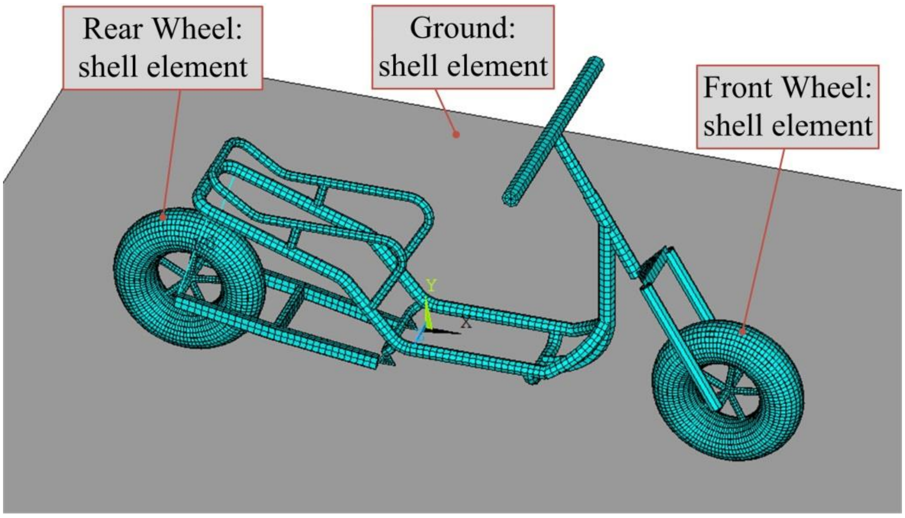


*Figure 6.4 FE model of e-bike and the ground*

### 6.3.2. Implementation of the Penalty Method in the Drop Test Case

The theory of the penalty method has been introduced. During the contact simulation, the whole contacting process can be explained as the motion which is demonstrated in Figure 6.5.

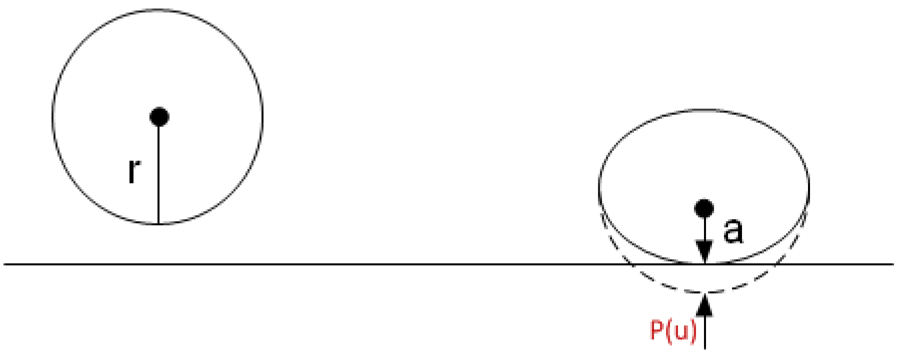


*Figure 6.5 The relationship between the deformation of the tire and penetration*

From Figure 6.5, the penetration $p(u)$, which has been illustrated in the simplest spring-mass system, can be regarded as the deforming part of the wheel during contact with the ground, thus the deformation of the wheel results from contact with the ground. In this case, $p(u)$ is described as,

$$p(u) = r - a \tag{6.9}$$

where, $r$ is radius of the circle which represents the original shape of the wheel. This penetration, $p(u)$, is used to present the results of the drop test (straight falling downwards simulation).

## 6.4. Static Analysis of Drop Testing

Quickly running a static analysis is helpful because it saves time when checking the correction of the FE model, the validity of the boundary conditions, and the convergence property of the model. This section shows the content of the formula of static analysis and the contact simulation using the static solution.

### 6.4.1. The Formula of Static Analysis

Supposing static analysis in terms of a linear elastic system, the equilibrium formula removes the terms concerned with acceleration and velocity and can be expressed in the following general form,

$$[K]\{u\} = \{F\} \tag{6.10}$$

The corresponding solution to Equation (6.10) is,

$$\{u\} = [K]^{-1}\{F\} \tag{6.11}$$

Where, $[K]$ is the total stiffness matrix of the system, $\{F\}$ is the resultant force vector acting on the system, and $\{u\}$ is the node displacement vector. In the element aspect, the stiffness matrix $[K_e]$ presents in different forms, depending on the specific elements.

For the beam element, it is in the form,

$$[K_{beam}] = EA \int_0^l [B]^T [B] dx \tag{6.12}$$

When it turns to the shell element, this is given by,

$$[K_{Shell}] = h \int_{-1}^{1} \int_{-1}^{1} [B]^T [D][B] det[J] d\eta d\xi \tag{6.13}$$

While taking into account this complex e-bike system, the stiffness of the whole system is calculated in ANSYS. Referring to the modelling session, the FE model of the e-bike mainly consists of beam and shell elements. Therefore, the computation for total stiffness, $[K] = \sum_{i=1}^{N} [K_{beam}] + \sum_{i=1}^{M} [K_{Shell}]$ is based on the foundation of beam and shell stiffness. From equation (6.11), the displacement vector $\{u\}$ is solved when the system stiffness is determined, which is used to represent the solution to the static analysis.

## 6.4.2. Solution to Static Analysis

The solution which results from static analysis is carried out after interactive computing, which is shown in Figure 6.6.

Figure 6.6(a) indicates the original position of the e-bike structure. It can be seen that the structure contains two axisymmetric wheels. The front wheel was originally positioned at the perfect point of contact with the ground, and the rear wheel was 76.06 mm vertically above the ground.

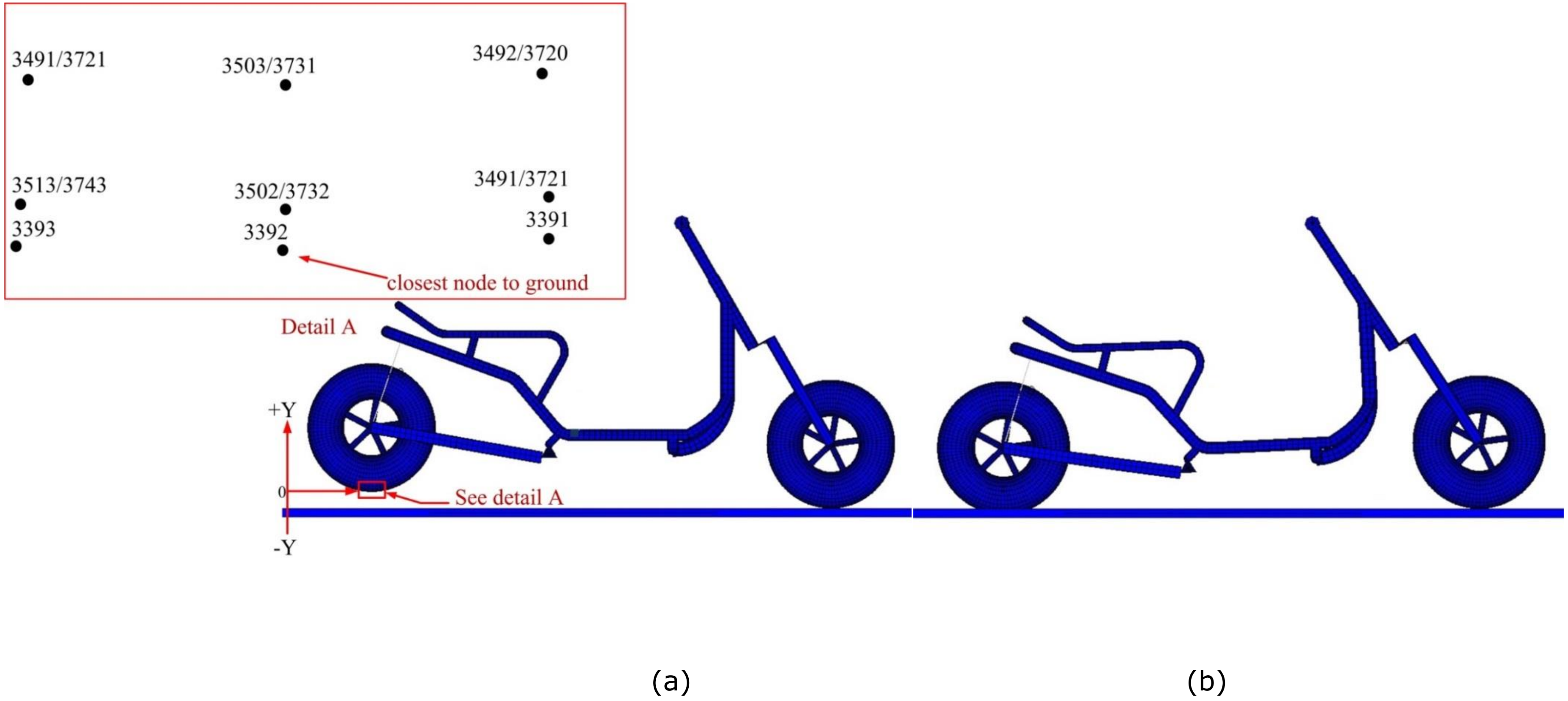


*Figure 6.6 (a) Drop process and (b) contact process of the e-bike*

Figure 6.6(b) shows the corresponding results and makes it clear that the rear wheel successfully touches the ground surface. If it fails to make contact, the slave object (e-bike) will either be impeded by the master body (ground) or simply fly away. In conclusion, the models of the e-bike and the ground, and all the parameters, including the load/constraints and the contact pair, are correct. It is to this exact contact model that the transient analysis is applied.

In addition, from Figure 6.6(b), it can be seen that Node 3392 is the closest node to the ground from the rear wheel. The application of Node 3392 will be discussed in detail in the section on the simulation of the transient analysis.

## 6.5. Dynamic Analysis (Transient Analysis) of Drop Testing

The state of many dynamic systems are undergoing time-dependent changes (transient). Transient analysis, in numerical analysis, is carried out by computing the temporary state of any element in the system. It is varied in terms of time and analysing in the aspect of dynamic definitely.

The principle of transient analysis, as the foundation of simulation, is introduced prior to the calculation of the corresponding solution.

### 6.5.1. Transient Analysis Formula

The ordinary differential expression of the structural dynamic motion equation (5.7) with constant coefficient is written in the form of equation

(6.14). The velocities and the accelerations, in any convenient finite difference equation, can be expressed in terms of displacements as, $\{\dot{u}\} = \frac{1}{dt}\{u\}$ and $\{\ddot{u}\} = \frac{1}{dt^2}\{u\}$.

$$[\mathrm{M}]\{\ddot{\mathrm{u}}\ (\mathrm{t})\} + [\mathrm{C}]\{\dot{\mathrm{u}}(\mathrm{t})\} + [\mathrm{K}]\{\mathrm{u}(\mathrm{t})\} = \{\mathrm{F}(\mathrm{t})\} \qquad (6.14)$$

where, $[K]$ (stiffness matrix) is also called the tangent matrix in the dynamic system. The term $[K]\{u(t)\}$ is the internal load, which, as shown in the expression, is linear and proportional to the node displacement $\{u(t)\}$. $[M]$ is the mass matrix of the global system. The expression of the element mass matrix is,

$$[M_e] = \rho \int_{vol} [N]^T [N] d(vol) \qquad (6.15)$$

Where, $\rho$ is element density, $[N]$ is the matrix of shape function.

In the numerical method, the continuous variable $t$, in the differential equation (6.14), is discretized into certain numbers of small domains. It is solved progressively in time increments, which start from the initial known conditions. The corresponding finite difference form of equation (6.14) is given as,

$$[M]\{\ddot{u}_{n+1}\} + [C]\{\dot{u}_{n+1}\} + [K]\{u_{n+1}\} = \{F_{n+1}\} \qquad (6.16)$$

The parameters, with the subscript *n+1* in Equation (6.16), represent its corresponding state at time $t_{n+1}$. The solution to equation (6.16) is approximate, but the accuracy of the solution can be improved by selecting a suitable time increment.

The e-bike drop testing with transient analysis in ANSYS is discussed in the following section. The corresponding results are represented by the displacement of Node 3392 $u_{N3392}$.

## 6.5.2. Transient Analysis Simulation - Dynamic Problem

As discussed before, stiffness is significant during contact, and this is the only key parameter when applying the penalty method. In ANSYS, parameter FKN (the stiffness in contacting) is linear and proportional to Young's modulus. Thus, it is necessary to implement the determination of the coefficient of proportionality "*c*".

### *Contact Parameter Determination*

In ANSYS, FKN is the critical contact parameter within the penalty method. In this section details of determination of the FKN parameter, based on the results of the transient analysis, are described. Before that, the definition of FKN in ANSYS should be clarified. FKN, referring to the principle of the penalty method, is the contact stiffness ε, FKN=*ε=N/p(u)*. In ANSYS, FKN is proportional to Young's modulus "*E*" of the underlying shell's finite element FKN=*c*E*. Normal contact force "*N*" is associated with the gravity of the e-bike itself. Thus, the ratio of FKN to E is a constant value "*c*". In practical computations, and usually recommended in the ANSYS handbook, the range of "*c*" is changing from 0.1 to 1. From Hooker's Law, specifying a higher value of "*c*" leads to a smaller penetration. In order to obtain the distinct differences of results using the penalty method, the parameter *c* is set to change from 0.001 to 10.

As mentioned in the previous section (Figure 6.6(a)), Node 3392, belongs to the rear wheel and is the closest node to the ground, thus, displacement in the Y axis is chosen to represent the following transient analysis results in ANSYS, shown in Figure 6.7.

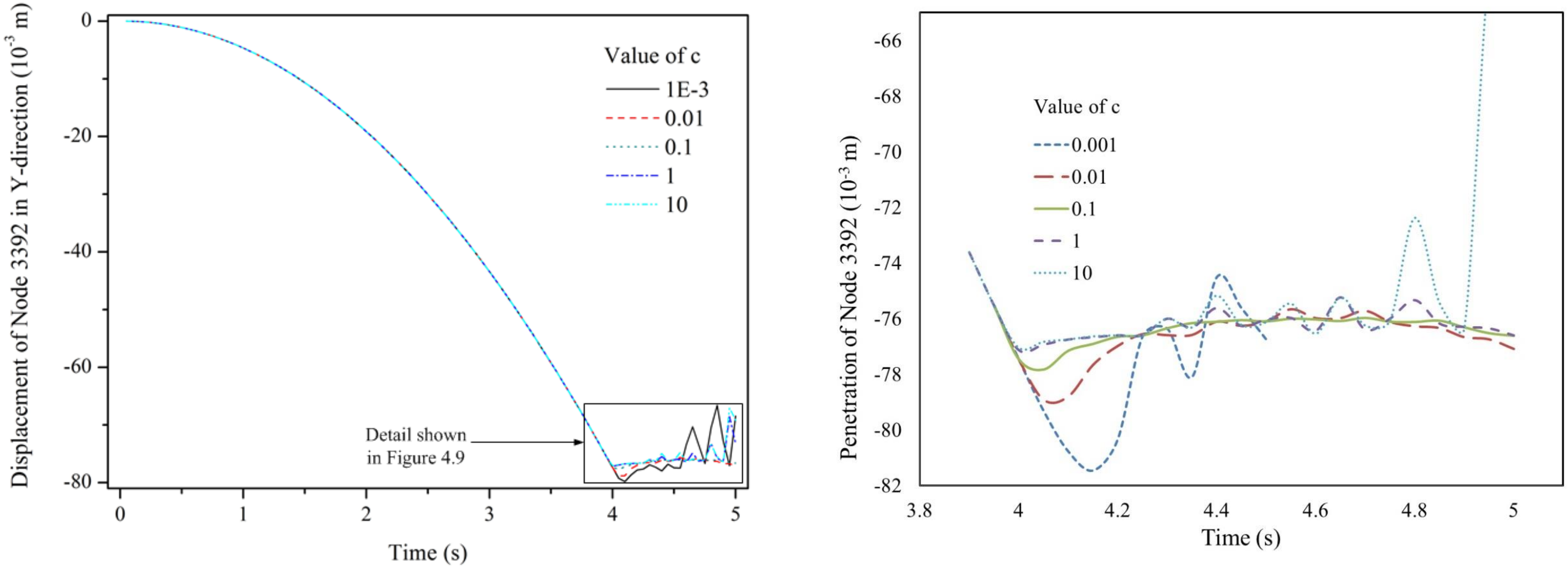


***(a)*** ***(b)***

***Figure 6.7 Displacement of node 3392 in the whole drop process (a) and its detail view where constant c varies from 0.001 to 10 during the contact period (b).***

In Figure 6.7, the result of the displacement of Node 3392 is shown with five different colours of curves. Each curve refers to the specific value of "*c*". Comparing the five results, it is found that the curve with *c=0.1* (FKN=0.1*E) is the most smooth, which demonstrates that the process of contact was most stable at this point. The corresponding simulation shows the best performance of convergence and a reasonable penetration value. Hence, the contact results when *c=0.1* are selected for comparison with the theoretical results.

### *Comparison between the Simulation Results and the Theory Results*

The transient results are shown in Figure 6.8. The resultant curve, which represents the Kinetic Energy (KE) in the post process, is drawn based on equation (6.16). The KE curve is scaled by pre-setting the magnitude of mass as "1".

$$E_k = \frac{1}{2}mv^2 = \frac{1}{2} * 1 * v^2 = 0.5v^2 \tag{6.17}$$

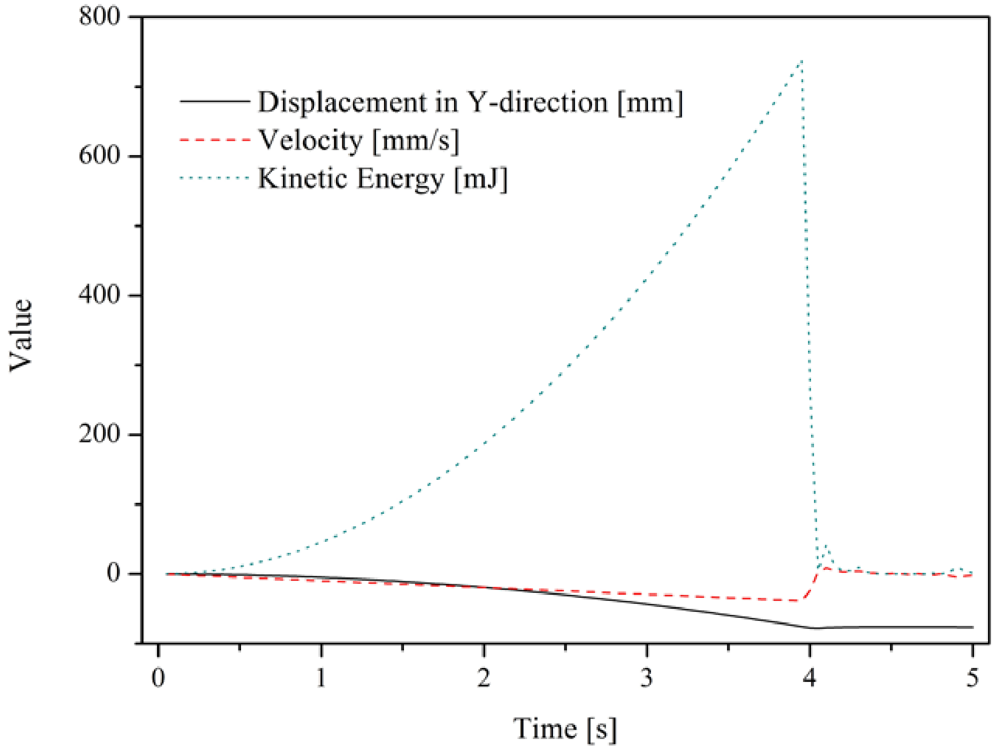


*Figure 6.8 Results of transient analysis*

Figure 6.8 indicates that the energy increases parabolically when there is some distance to fall during the drop process, and decreases sharply when the tire is in contact with the ground. Velocity was found to increase linearly with the falling distance, and also to decrease abruptly after the e-bike interacts with the ground.

*Table 6.1 Comparison Between Results of the Transient Analysis and the Theoretical Analysis*

| Physical quantity | Theoretical results [Rt] [9] | ANSYS results [Ra] | Relative error [Ra/Rt-1 ] 100% |
|---|---|---|---|
| initial contact time ($t_0$) (s) | 3.87 | 3.95 | 2 % |
| displacement at $t_0$ (10-3 m) | -76.06 | -75.53 | -3% |
| velocity at $t_0$ (10-3 m/s) | -37.99 | -38.45 | 1% |
| time of maximum displacement ($t_m$) (10-3 m) | 4.14 | 4.05 | -2% |
| maximum displacement (10-3 m) | -78.56 | -77.83 | -1% |
| Maximum penetration (10-3 m) | 2.50 | 2.30 | -8% |
| velocity at $t_m$ [$10^{-3}$ m /s] | 0 | 3.07 | - |

The comparison of results between the theoretical and the numerical analysis is shown in Table 6.1. For the theoretical result the mass point with the mass of the e-bike was dropped from a certain height – all corresponding values can be obtained with the help of the conservation of mechanical energy theorem. The e-bike starts to drop under gravity acceleration when t=0. The time at which the closest node (Node 3392) of the rear wheel contacts the ground is called the initial contact time (t). Immediately after contact, the e-bike continues to penetrate until the velocity is equal to zero, after which time it will rebound. In terms of the law of conservation of mechanical energy, when v=0, the PE reaches its extremum. This is the maximum penetration displacement [167].

Considering the last row of Table 6.1, the magnitude of velocity corresponds to the value of maximum displacement. Data obtained by the numerical method are only approximate values. In this simulation, data were collected every 0.05s, which results in a small value of velocity "3.07 x10-3 m /s" in maximum penetration.

Small values of the relative error (in the last column of Table 6.1) compared with a relatively rough theoretical model (a mass point) demonstrate that this contact simulation can be regarded as verified and that it is valid. Optimized parameters in this contact model will be used further for "side falling analysis" of the e-bike. Side contact of an e-bike with designed protective shells are also carried out in the next step. The protective shells are designed following the stability criterion, which was discussed in Chapter 3. The protective shells will be assembled and secured to the main frame of the e-bike, which is described in the following side falling test.

## 6.6. Summary

The drop test analysis in a 3D frictionless contact case has been conducted, this was a preliminary and necessary work for further structural design improvement. The analysis for dropping of the e-bike and its contact with the ground was carried out as follows: firstly, the formula of frictionless contact-penalty method was briefly introduced. The principle of contacting with numerical analysis has been shown; secondly, models of the e-bike and the ground have been constructed, and the implementation of the penalty method has been illustrated. Thirdly, static analysis was used to quickly run the model and was applied to validate the FE model and the correction of the contact pair between the e-bike and the ground. Finally, results of the transient analysis in ANSYS were represented by the data of the displacement of Node 3392. The comparison between the results of theoretical method and that of the numerical method was employed to optimize the parameters of the contact pair.

# CHAPTER 7. SIDE FALLING TEST IN LS-DYNA - MODEL WITH DESIGNED PROTECTIVE SHELLS

## 7.1. Introduction

The objective of this chapter is to validate the design criterion by comparing the simulation results of the e-bike with differently designed protective shells. The design criteria for the geometries of the protective shells is employed by the stability theorem which was introduced in Chapter 3. Moreover, side falling tests are an effective approach for optimizing the design of the protective shells. In order to assess the performance of the over-turning-prevention safety feature, the protective shells are attached to the e-bike for simulation of the sideways falling test.

LS-DYNA is selected as the methodology for the sideways falling (including contacting) simulation The reason for this choice is that LS-DYNA, developed by the Livermore Software Technology Corporation (LSTC) [168], has been proven to be a powerful tool which provides a favourable environment within which to conduct various dynamic motion and contact simulations [169, 170]. In general, the formulae in LS-DYNA are solved by explicit time integration, rather than those in ANSYS, which is an implicit scheme [171]. Comparisons between implicit and explicit FEMs are given in the following section.

## 7.2. Comparison of Implicit and Explicit FEMs

The approaches to the solution to the dynamic response of a structural system in FEMs can basically be divided into two categories, the implicit method and the explicit method [172]. The derivation of formulae of implicit and explicit FEMs is discussed in detail in the following sub-sections.

### 7.2.1. Formula for the Implicit Method

The one-step algorithms for the direct integration of the equations of structural dynamics is introduced. The most well-known methods are those of Newmark, Wilson, Houbolt, etc [173, 174], which are used to solve the structural dynamic motion equation in implicit forms [175, 176]. Newmark-$\beta$ method, introduced here, is sufficient to solve this case of e-bike dynamic motion, consequently the Newmark time integration method is used for the implicit approach which will find the solution to the transient analysis.

The fundamental purpose of the implicit method is to solve the differential equation at time "t", when the solution at time "t-1" is determined [177]. A dynamic motion in a linear system without damping is described by satisfying incremental equilibrium over the time step, thus [178],

$$[M]\delta\{\ddot{u}_n\} + [K]\delta\{u_n\} = \delta\{f_n\} \tag{7.1}$$

where, $\delta\{\ddot{u}_n\} = \{\ddot{u}_{n+1}\} - \{\ddot{u}_n\}$, $\delta\{u_n\} = \{u_{n+1}\} - \{u_n\}$ and $\delta\{f_n\} = \{f_{n+1}\} - \{f_n\}$.

With Newmark- $\beta$ method, the relationships, in terms of incremental displacement, are formulated as [179],

$$\begin{aligned} \delta\{\ddot{u}_n\} &= \frac{1}{\beta\Delta t^2}\delta\{u_n\} - \frac{1}{\beta\Delta t}\{\dot{u}_n\} - \frac{1}{2\beta}\{\ddot{u}_n\} \\ \delta\{\dot{u}_n\} &= \frac{\gamma}{\beta\Delta t}\delta\{u_n\} - \frac{\gamma}{\beta}\{\dot{u}_n\} + \Delta t\left(1 - \frac{\gamma}{2\beta}\right)\{\ddot{u}_n\} \end{aligned} \tag{7.2}$$

when, $\beta = \frac{1}{4}, \gamma = \frac{1}{2}$, this method is implicit and unconditionally stable [180]. The implicit procedure is based on the success rate of a full Newton iterative solution method, which was adopted in the e-bike straight falling simulation (refer to Chapter 6). The Newton iterative method is run by an automatic increment strategy [181].

Solving the increments in displacement, equation (7.1) is rewritten as,

$$\left(\frac{4}{dt^2}[M] + [K]\right)(\{u_{n+1}\} - \{u_n\}) = \{f_{n+1}\} - \{f_n\} + \frac{4}{dt}[M]\{\dot{u}_n\} + 2\{\ddot{u}_n\} \tag{7.3}$$

Results of the implicit time integration scheme are unconditionally stable. i.e., it is stable for any time step *dt.* However, the unconditional stable implicit method will result in some difficulties while reduction of the time increment continues [182]. First, as the implicit method requires the matrix, $\frac{4}{\mathrm{dt}^2}[M] + [K]$, and matrix, $[M]$, (as shown in Equation (7.3)) to be inversed, there is a dramatic increase in the computational cost in the matrix inversion. Even more, it may cause divergence of the simulation. Second, it is difficult to achieve force equilibrium due to local instability. In the following sub-section, the explicit method is introduced.

### 7.2.2. Formula for the Explicit Method

The explicit method is a fundamental approach used to predict the solution at time "$t + \Delta t$" by the differential equation at time "t" [183]. The central difference method is one of the most common explicit schemes [184]. With the central time difference integration method, the dynamic motion with zero damping equation is expressed in the time difference scheme as,

$$\frac{1}{dt^2}[M](\{u_{n+1}\} - 2\{u_n\} + \{u_{n-1}\}) + [K]\{u_n\} = \{F_n\} \qquad (7.4)$$

From equation (7.4), only the information about step *n* is used. When using the lumped matrix method (the default in LS-DYNA), this will result in diagonal mass matrix *M* [185, 186]. Thus, calculation by this method is relatively fast as inversion is not involved.

The explicit method is developed to overcome the drawback of the implicit method [187]. The computational cost of using explicit techniques depends on the mesh size of the FE model. However, the explicit operator has its own weakness, i.e., its property of conditional stability and that stability being limited by its maximum time step, which must not be greater than the smallest critical transient time interval $\Delta t_{cr}$ [172], thus,

$$\Delta t \leq \Delta t_{cr} = \frac{\tau_n}{\pi} \qquad (7.5)$$

where $\tau_n$ is the natural period of the system.

Although the explicit technique has its limitations (i.e., the time step must be very small), it is not necessary to calculate a series of linear equations at each step because all the response quantities depend on those in the previous state [188]. In terms  of computational time and memory usage this method is more effective and useful than the implicit method. Therefore, it is selected as the simulation principle for the sideways falling test of the e-bike. The following section describes the implementation of explicit integration in LS-DYNA.

## 7.3. Original Protective Shell Design and Side Falling

As seen in Chapter 3, the strategy of protective shell design is as follows. Firstly, the selection of a typical boundary point on the side structure is necessary, this is defined as "the limit case stability curve". Secondly, the use of criteria proved in Chapter 3 ($r > h$), and the subsequent geometry of the protective shells, are adjusted to the current structure. However, satisfying the criterion, "smooth surface below the limit stability curve", must occur during the complete period of motion. In this case, if the simulation of the sideways falling motion does not result in overturning, it can be used to validate the design criterion. The modelling and simulation process is described in detail in the following sub-section.

### 7.3.1. Modelling in LS-DYNA

In order to test the safety feature, an FE model for a simplified e-bike has been constructed in the LS-DYNA environment and employed in the investigated cases, i.e., contact between a protective side shell and the ground, and the design of such a shell.

The created FE model had to be transferred from ANSYS to LS-DYNA. However, the existing FE model had to be adjusted and partially re-modelled and re-meshed because of the different types of finite elements used for implicit and explicit analysis. The re-meshed model was used to add the safety shell, see Figure 7.1, which will protect the driver during a sideways falling road accident.

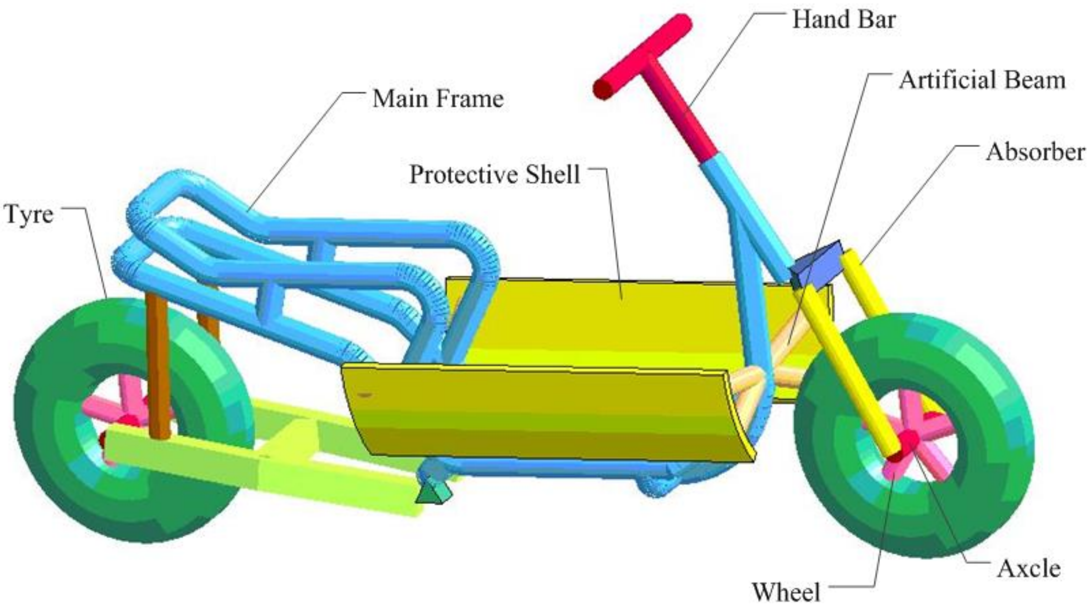


***Figure 7.1 Simplified 3D model of the e-bike in LS-DYNA which consists of tires, axles, main frame, absorbers, and protective shells***

The components of this model were meshed mainly by finite beam elements with the exception of the tires and the protective shells, in which finite shell elements have been used. Different components were connected by simple common nodes. These finite elements and their constitutive laws have been derived in Chapter 5.

Figure 7.1 shows the oblique view of one simple shell which has been designed following the stability criteria, and which satisfies the shape of the e-bike structure. Thus, it is a partial cylindrical shell. For convenience of analysis, its 3D geometry is represented by a 2D curve, see Figure 7.2.

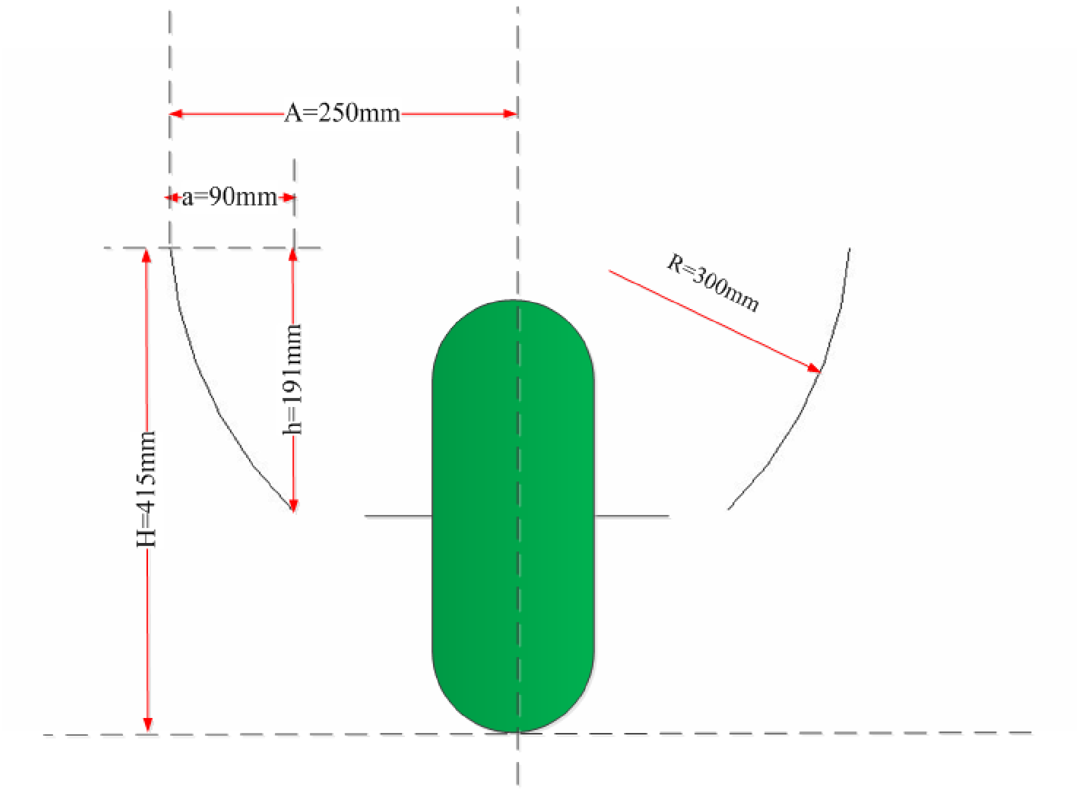


***Figure 7.2 Dimensions of the protective shells***

From Figure 7.2, it can be seen that curves with 300 mm radius are applied to present the two symmetrically cylindrical protective shells, which are placed at the angle denoted by the distance between the top and bottom edges (horizontal distance is 90mm and vertical distance is 191 mm). The displacement of the shell with respect to the main structure of the e-bike is 415 mm. The length from the top edge of the protective shells to the symmetrical centre is 250 mm.

### *Assembly to the main structure of the simplified e-bike model*

When an e-bike falls sideways and makes contact with the ground, the stress and strain on the surface of the protective shells will also influence the other parts of the structure. In order to activate the impact mechanism from the protective shells to the entire model, it is necessary to add "artificial" beams as a connector between the main frame and the protective shells, as shown in Figures 7.3 and 7.4.

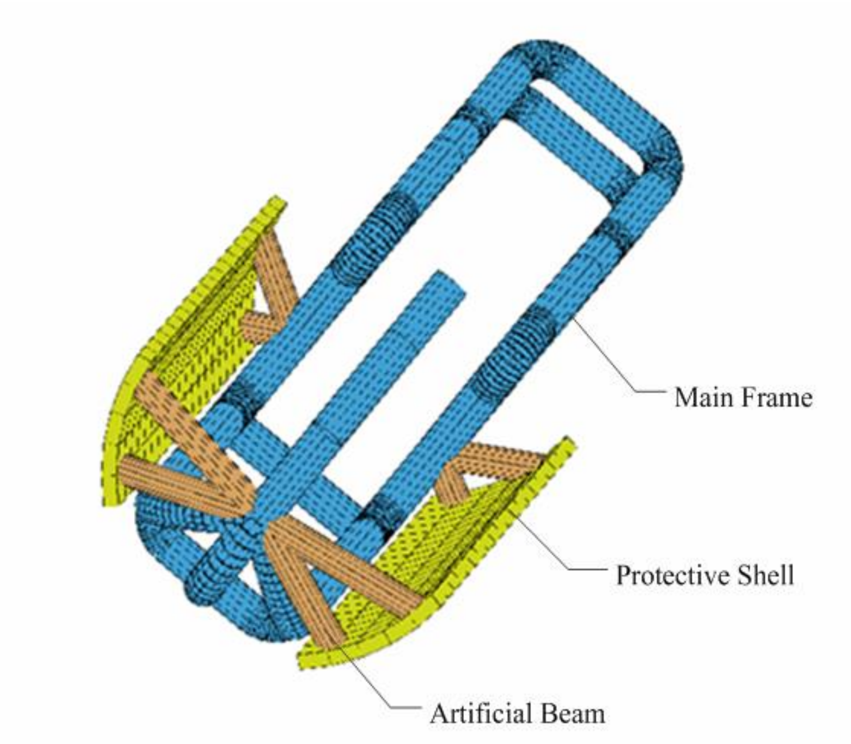


***Figure 7.3 Artificial beams (brown colour) attached to connect the protective shells (yellow) and the main frame of e-bike (blue).***

*Discretization of the protective shells component*

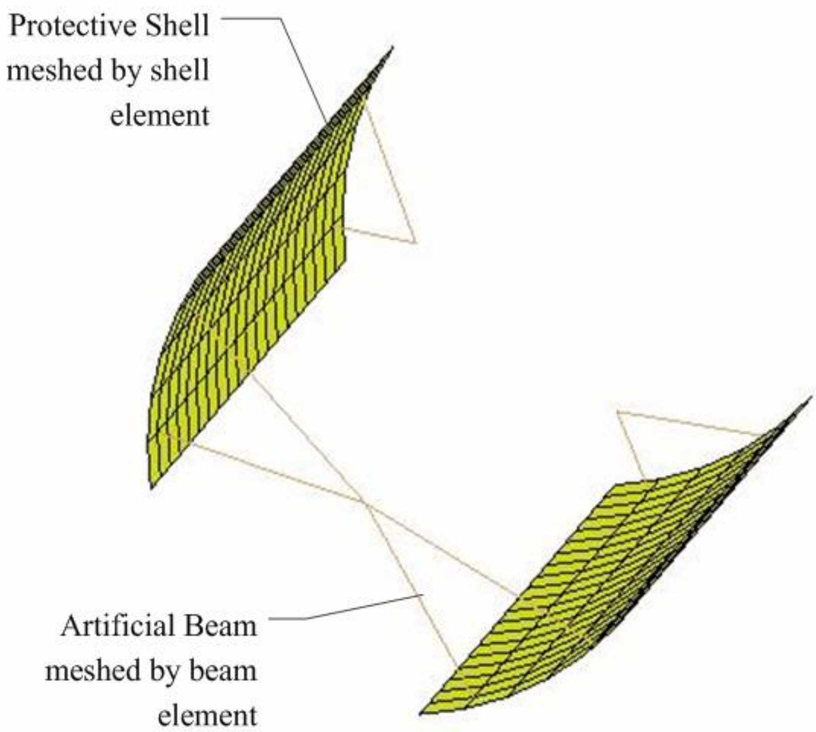


***Figure 7.4 Shell element and beam element.***

In this simulation, the protective shells, attached by artificial beams, are the essential component to be discussed. Figure 7.4 shows the discrete FE model of the shell component. Protective shells were meshed by finite shell elements and artificial supporting beams were meshed by finite beam elements.

### 7.3.2. Simulation and Results

Among these models, the solid bolt model, which is modelled by using 3D solid elements and surface-to-surface contact elements between head/nut and the flange interfaces, provides the best accurate responses in contrast to the experimental results.

Figure 7.5 shows the simulation process and result in LS-DYNA. There are two procedures representing this sideways falling contact simulation – a "before" status and an "after" status. In the "before" status, the whole e-bike model was positioned at an initial angle of five degrees between the global Y-axis and the symmetrical axis of the e-bike structure. Under gravity force, the e-bike started to fall and the protective shells on one side made contact with the ground. After several repeated rebounding and downward contacting events, the whole structure was in a balanced static state. Meanwhile the mechanical energy was fully converted to denote to the heat. That is the exactly the "after" status.

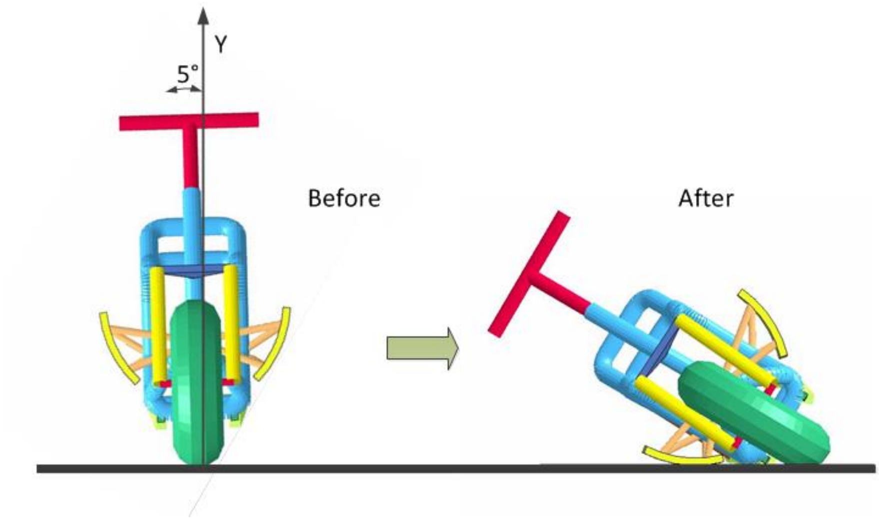


*Figure 7.5 Contact process*

Figure 7.5, demonstrated that there was no over-turning during the whole sideway falling process.

## 7.4. Comparison Between Shells in Different Stability Configurations

A preliminary simulation of the e-bike with protective shells has now been carried out. In order to validate the design criterion, a comparison between three types of protective shells is required. The three protective shells were designed in the three stability configurations, whereby one follows, and the other two do not follow, the static criteria. The safety feature of the protective shells using the design criteria will then be confirmed.

### 7.4.1. Protective Shells Design in LS-DYNA

Recalling the knowledge realised in Chapter 3, there are three stability configurations in terms of static stability. They are neutral, stable, and unstable stabilities. The protective shells were designed within these three stability configurations. According to Roly-Poly stability, the geometry of the protective shells was designed from a partial cylinder with $r$ of 250 mm. Instead of changing $r$, $h$ was varied at 200 mm, 250 mm, and 300 mm to simulate the three cases of stable, neutral, and unstable stabilities respectively. Figure 6.20 denotes the schematic diagram of protective shells designed according to the three stabilities, and Table 8.1 provides the detailed information of these designs.

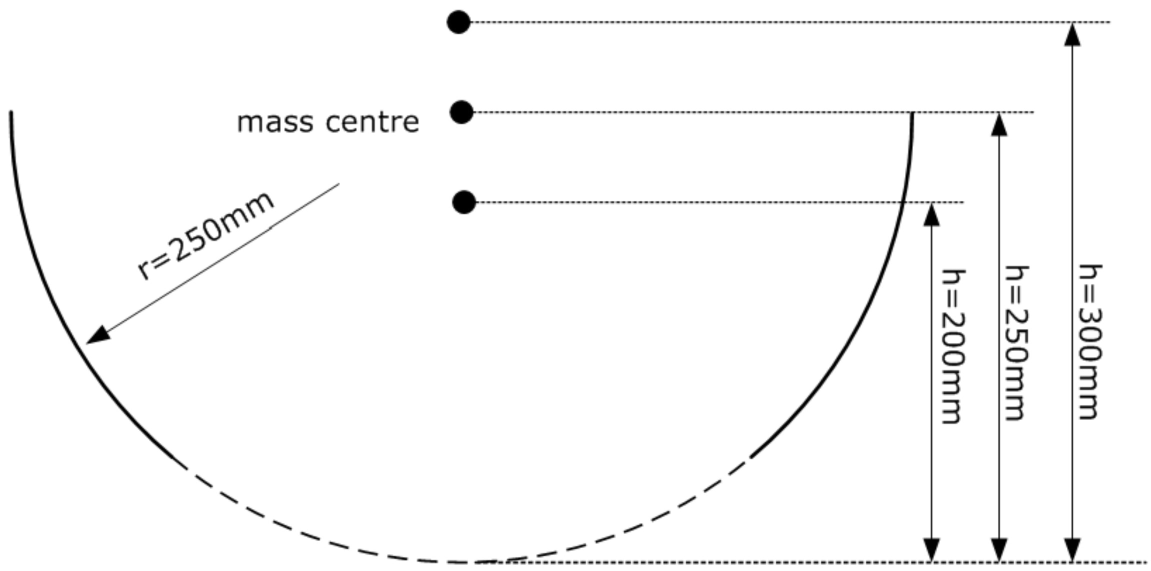


***Figure 7.6 Schematic diagram of protective shells designed according to three stabilities***

From Figure 7.6, it can be seen that, in this design, the mass properties of the driver and the e-bike were implemented using one mass point of each e-bike system. This is because mass distribution, in simulation, is only in control of the change in time iteration, rather than in the geometry of the protective shells. Hence, two masses, that of the driver and that of the e-bike, are combined as one mass point.

***Table 7.1 Design of three types of protective shells***

| Type | *r* (mm) | *h* (mm) | Conditions | Stability configurations | Following the design criterion |
|---|---|---|---|---|---|
| Type 1 | 250 | 200 | $r > h$ | Stable stability | Yes |
| Type 2 | 250 | 250 | $r = h$ | Neutral stability | No |

| | | | | | |
|---|---|---|---|---|---|
| Type 3 | 250 | 300 | $r < h$ | Unstable stability | No |

Type 1 is the design based on the stable stability criterion where *r* > *h*. Type 2 is the protective shells in the condition of neutral stability where *r* = *h*. Type 3, is based on unstable stability where $r < h$.

## 7.4.2. Simulation and Results

The middle surface of the ground plate is placed at -200 mm in the global Y-axis. The coordinate of the ground was taken as the reference point during contact. A five degree angle was initially given between the global Y-axis and the symmetrical axis of the e-bike structure. The e-bike started to fall sideways under the force of gravity and stopped when the mechanical energy was fully converted through several rounds of collision and rebounding.

Node 34852, which belongs at one point at the right-hand end of the handlebar, is selected and its path along the Y-axis used for the simulation results. The results of the simulations are presented in Figures 7.7, 7.8, and 7.9.

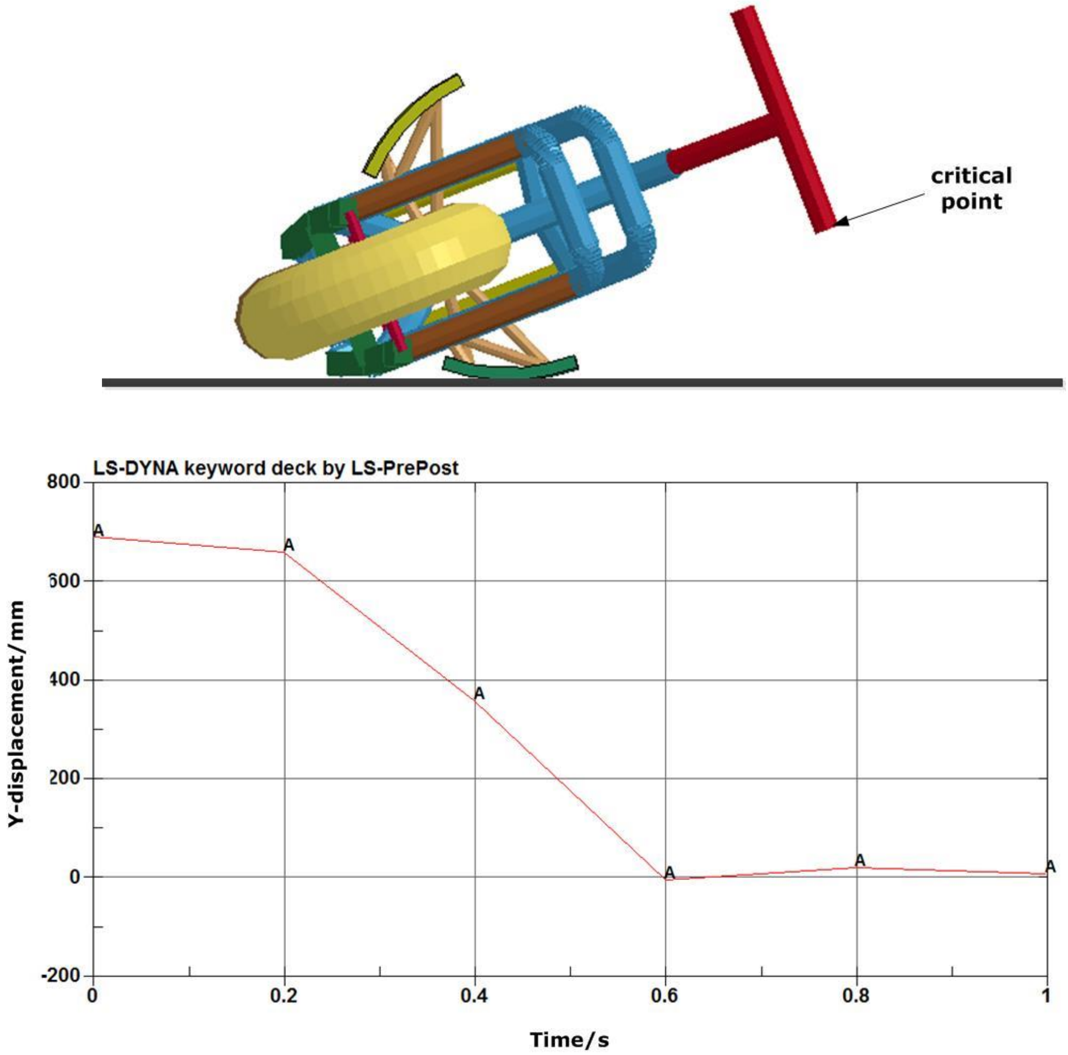


*Figure 7.7 Simulation results for the protective shells designed following the stable stability simulation.*

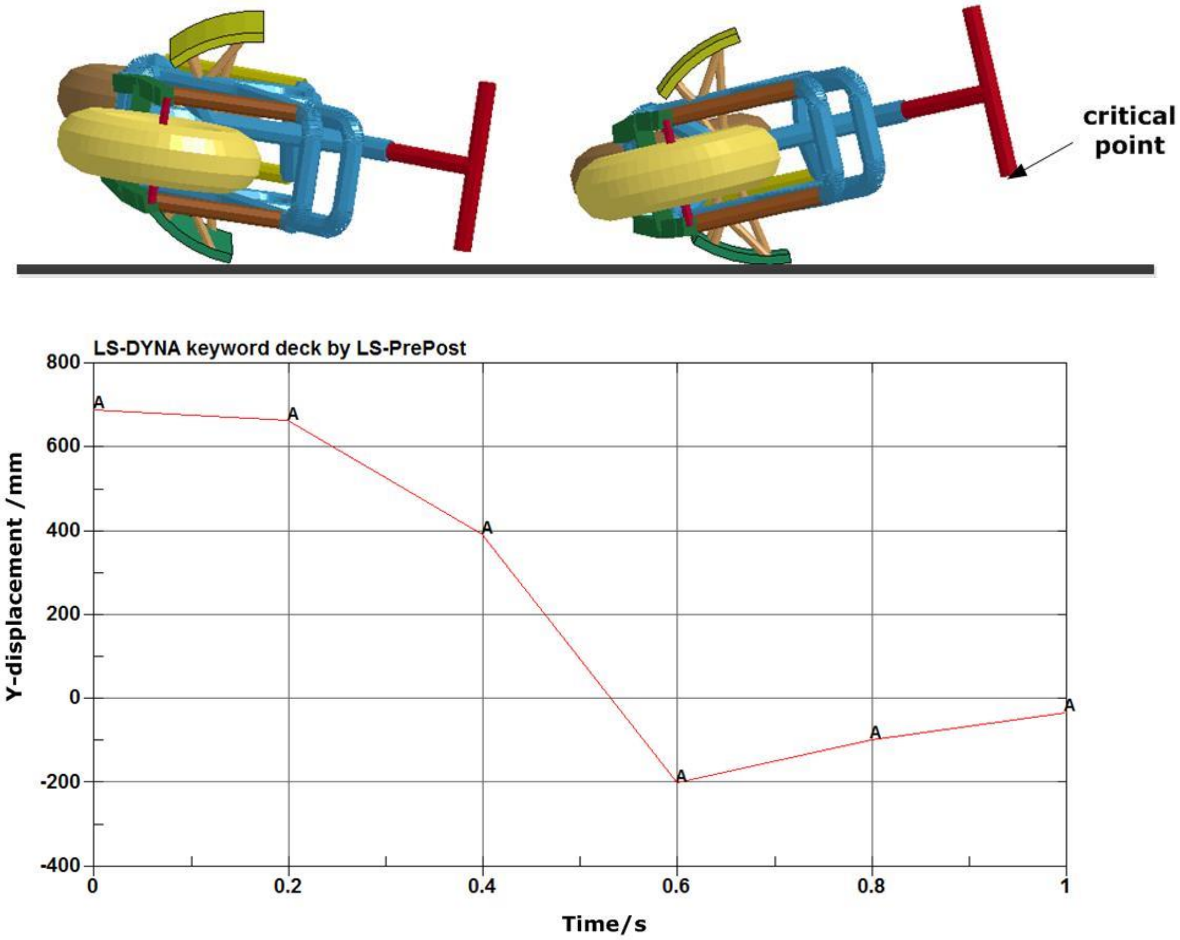


*Figure 7.8 Simulation results for the protective shells designed following the neutral stability simulation.*

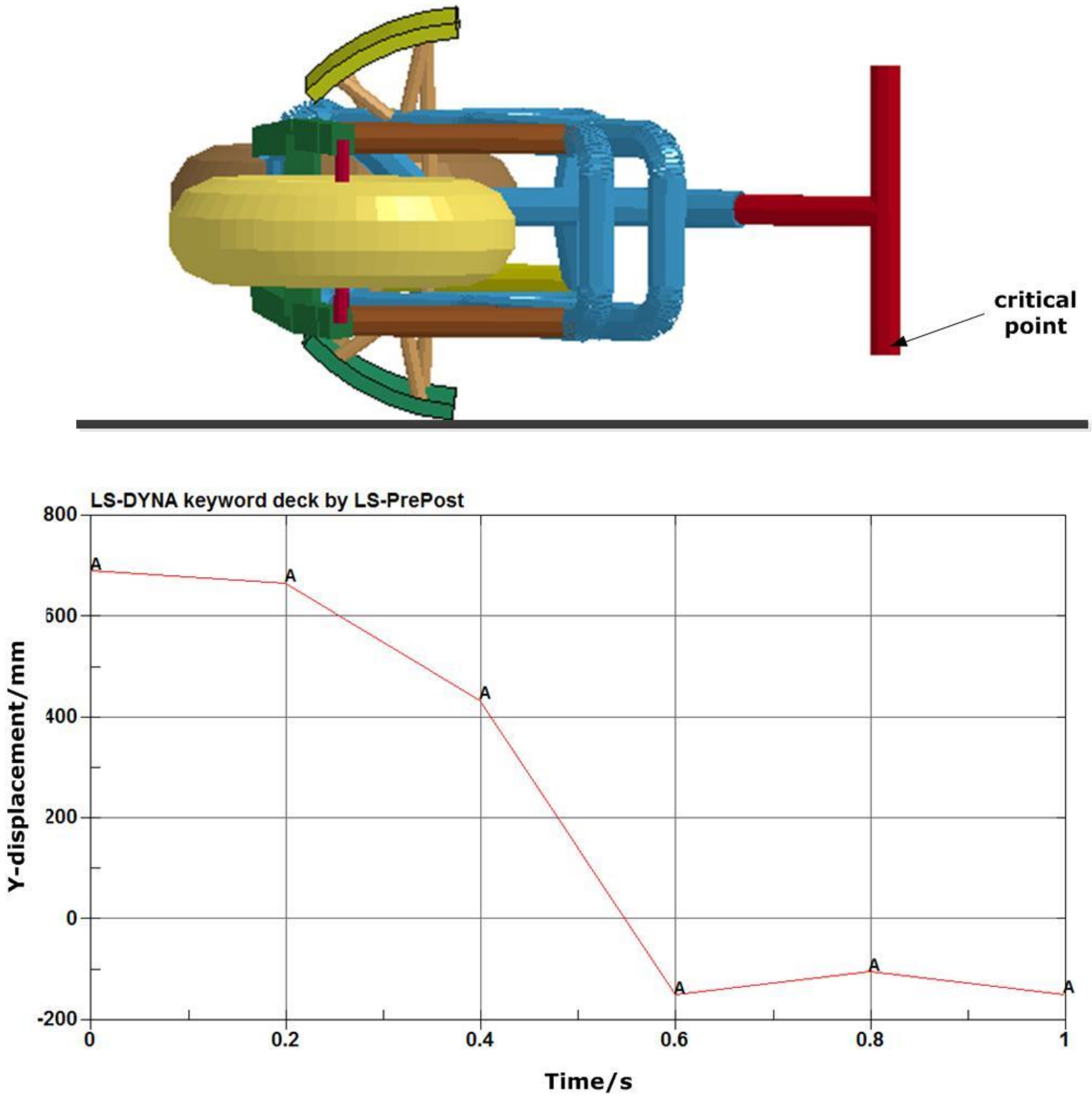


***Figure 7.9 Simulation results for the protective shells designed following the unstable stability simulation.***

Figure 7.7 shows the sideways falling results of the e-bike with the protective shells produced following the stable design criterion. It shows that there is safety space between the handlebar and the ground (more than 200 mm) and the e-bike will not overturn.

Figure 7.8 shows the simulation results of the e-bike with protective shells designed with the theory of neutral stability. It can be seen that the handlebar touched the ground and rebounded during the test.

Figure 7.9 displays the process and the results of sideways falling with protective shells designed under the condition of unstable stability. It was found that the right-hand-side of the structure remained permanently in contact with the ground after the collision and in a state of rest. The e-bike in this case can be regarded as having over-turned.

Sideways falling simulations show that protective shells which are designed on the basis of the stability criterion ($r > h$) will protect the driver during an accident.

## 7.5. Summary

The outcome of the modelling of the protective shells has been discussed in relation to its design. The results from the sideways falling simulation presented in this thesis prove to be informative and thus are employed to guide the subsequent design and analysis.

It is necessary to compare the effects of protective shells designed to satisfy the static stability criteria with those that do not in order to demonstrate the validity of this design criterion.

This chapter has focused on the sideways falling contact simulation process which has been established to test the validity of the protective shells, to optimize the geometry of the protective shells, and to develop the static stability criteria. In order to implement the contact simulation, the process of the FE modelling in LS-DYNA, the design and optimization of the protective shells has been detailed. The sequence of the procedure for the proposed safety design approach is as follows. Utilization of the simplified CAD e-bike model with key components to present the physical size in 3D. This was applied to create the FE model in ANSYS. During modal analysis, the quality of the meshed model was checked. By implicit simulation in ANSYS, including static and transient analysis, penalty parameters were determined. For cost saving, explicit analysis was selected and its application to the sideways falling test conducted in LS-DYNA. The sideways falling simulation has been conducted with the protective shells designed with respect to the developed static stability criteria in LS-DYNA. During design of the shells, changing the relative distances between the CoMs and the curves of the protective shells led to the designed systems being in certain conditions of stability. The results of the sideways falling test were thus obtained and compared with the protective shells designed on the basis of three equilibrium conditions. In this way, the design criterion ($r > h$) derived from Roly-Poly stability was verified. The geometry of the protective shells met the static stability criteria and therefore fulfil the safety goal.

# CHAPTER 8. CONCLUSIONS AND FUTURE WORK

The China e-bike market occupies the largest portion of the world e-bike market and this is accompanied by a huge number of injuries and deaths. As more attention is paid by the public to the issue of e-bike accidents, improvements to their safety features is increasingly demanded. To this end, this PhD project has focused on the design of protective shells for e-bikes. The protective shells, as a passive road safety component, allow the driver to avoid fatal injuries during severe crashes [52]. The basic idea is to develop the famous Roly-Poly design criterion which will not allow the e-bike to overturn during a sideways falling accident, thus: "DESIGN CRITERION FOR STABILITY DURING SIDEWAYS FALLING". These developments include not only consistent implementations of the geometrical criteria, but also contact analysis during a sideways falling event. This has allowed the development of consistent steps for both the geometry designer and the computational engineer about how to construct and validate the geometry of an e-bike which includes a safety shell, such that the e-bike will not overturn in the event of a sideways falling accident. Conclusions and future work are discussed in the following sections.

## 8.1. Conclusions

So far, all the stated research aims and objectives for this project have been accomplished. This thesis focuses on the numerical verification of e-bike protective shell design criterion and the development of design criteria for the protective safety shell. The stability criterion was formulated for the case of severe road accidents causing sideways falling of an e-bike. It has been developed based on principles of passive road safety applied to e-bikes. The idea of formulating the design criterion originated in the Roly-Poly stability criterion. The main goal such as "no over-turning" during the sideways falling accident was realized in the simulation analysis. The key-points for this research are listed as follows:

### 8.1.1. Roly-Poly Stability

First, a simple criterion for the design of protective shells for e-bikes was developed. The design criterion was derived based on the "Roly-Poly" stability criterion. The final formula was derived as $r > h$. This indicates that the radius of curvature *r* for the protective shell should be larger than the distance between the centres of mass for e-bike *h* and each contact point *P* of the curve during its contact with the ground when it is rolling to the side. This is the first time such a criterion has been established for a TWV. The principle of the Roly-Poly stability fulfils the condition of static stable equilibrium; however, it can also be directly employed for dynamic contact analysis.

### 8.1.2. Static Stability

The basic knowledge of static stability can be illustrated by the simple case of a mass point on a curve. Three configurations of equilibriums were derived by the analysis of the PE. In all systems, there are three equilibriums: unstable equilibrium points, reflecting the maximum of the PE; stable equilibrium points, reflecting the minimum of the PE; and neutral equilibrium points, reflecting the constant PE. Correspondingly, these are unstable, stable, and neutral stability systems. The "Roly-Poly" system is a more advanced example of the stable stability systems, including the rolling type of contact of the protective shell with the road.

### 8.1.3. Contact Parameters Verification

Determination of the contact parameters is the preliminary work of the contact case between the protective shells and the ground. The penalty method was chosen as a numerical approach for the contact simulation. The penalty enforcement formula has been simplified for the frictionless conditions. The only key parameter, in the circumstance of a frictionless case, is a contact stiffness, which is influenced by the material property and the convergence during numerical analysis for impact situations. By comparing the theoretical and the numerical results, which were conducted by "straight falling down testing", with a series of values in ANSYS, the value of a contact stiffness was determined as 0.1*E.

### 8.1.4. Design of the Protective Shells

The Zuma e-scooter was selected as the prototype for the modelling and for the attachment of the designed shells. Zuma is a type of heavy e-bike with a total weight of 114kg, a speed limited to 60km/h, and an e-motor power of more than 1000W. The protective shells have been designed in the three stability configurations. According to the Roly-Poly Stability criterion, the geometry of the protective shells was designed as a partial cylinder with a radius of 250mm. By adjusting the position of the protective shells in the vertical Y axis, the distance between the CoM and the contact point for the computation was varied at 200mm, 250mm, and 300mm. This makes it possible to locate the protective shell for a sideways falling situation in stable and in unstable equilibrium positions.

### 8.1.5. Setting up the Model

A 3D geometrical model was constructed in Creo software. The frame of the model was created based on the real Zuma e-scooter and used for parameter presentation. In the pre-processing, an FE model of an e-bike was built using ANSYS and LS-DYNA software. The tires and the shells were meshed with finite shell elements, and the other key components were discretized as finite beam elements. The mass of the whole e-bike, and that of the driver, were modelled with mass elements with corresponding masses and moments of inertia. During the post processing, static analysis was conducted in ANSYS. In this static simulation, contact formulation and parameters were validated. LS-DYNA was chosen for implementing the sideways falling dynamic test with different protective shells.

### 8.1.6. Simulation Results

The simulation results for the sideways falling tests with the designed protective shells have successfully shown that if $r > h$, then the e-bike is found in a stable stability situation and hence no overturning occurs in the event of a sideways fall. In the other two cases ($r = h$ and $r < h$), a collision occurred between the handlebar and the ground, resulting in the overturning of the e-bike. Summarizing the results, those protective shells which do not obey the stability criterion cannot protect the driver during a sideways falling accident and, therefore, only the shells satisfying the DESIGN CRITERIA FOR STABILITY DURING SIDEWAYS FALLING should be realized.

## 8.2. Future Work

This work provides a theoretical foundation for many future research developments. This section is presented in order to recommend prospective research areas based on this stage of the project. Such research would build on the current understanding of this design criterion and its applications. The related topics in future work are listed in the following sub-section.

### 8.2.1. Development of the Design Criterion - Double Curved Surfaces

The analysis assumes that the e-bike is moving forward with a constant velocity before a sideways fall – this allows the investigation to use a static formulation, as the e-bike would be standing still in the coordinate system attached to CoM, and the coordinate system is moving parallel with constant velocity. Prior investigations can be seen as sideways falling in a moving coordinate system. This gives the effect of an e-bike standing still in a coordinate system moving with a constant velocity .

However, arbitrary motion is, of course, 3D motion. The development, in the current thesis, of a safe cylindrical surface is enough to show stability in a 3D situation. Nevertheless, the cylindrical surface has a pure design, and a double-curved surface is required. The general stability criteria for an arbitrary double-curved surface is much more complicated and requires the sophisticated apparatus of differential geometry. However, simplified cases are possible – e.g., the case of an elliptical surface. Combinations of the stability criteria developed in the thesis, with the standard stability criteria for the ellipsoid, allow the stability criteria for the double curved surface overlapped by the elliptical surface to be obtained.

#### *Derivation of A Double Curved Surface – Ellipsoid Case*

In this project, cylindrical geometry has been taken into consideration. The cylinder has only one radius of curvature (the second is infinity), and is represented only in 2D geometry ($K_1 = \frac{1}{r}, K_2 = 0,$ where $K_1$ and $K_2$ are the maximum and minimum values of the curvature of cylinder respectively) [189, 190]. This case is suitable when assuming the e-bike is still. However, when the e-bike is moving forward and backward, the cylindrical protective shells are no longer applicable. Hence, a double curved surface design should be taken into account.

In general, in a double curved case, the rolling is extremely complicated, while in a particular case， for example an ellipsoid， the rolling is a simplified case with axes "a", "b", and "c". Figure 8.1 shows the general ellipsoid system centred at the original point of the coordinate and its three aligned axes.

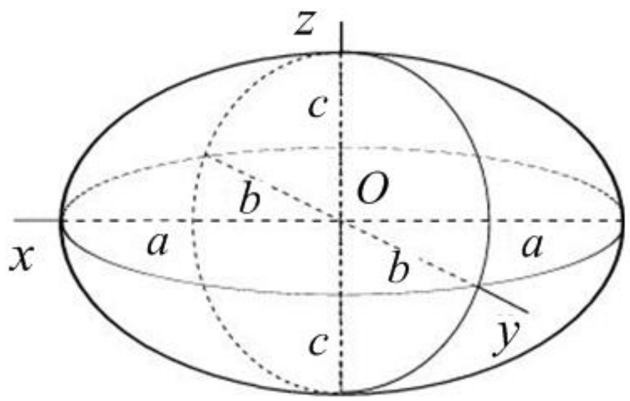


***Figure 8.1 A general ellipsoid system***

The formula of an ellipsoid is expressed in the canonical form as [191],

$$\frac{x^2}{a^2} + \frac{y^2}{b^2} + \frac{z^2}{c^2} = 1 \tag{8.1}$$

Figure 8.2 indicates the axes x and y are parallel to the ground and z is vertical.

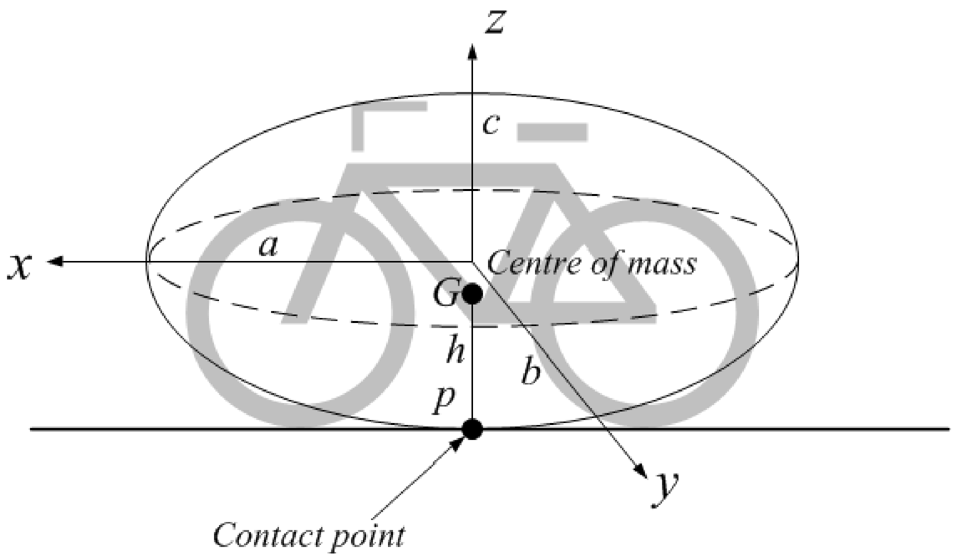


*Figure 8.2 Ellipsoid and e-bike*

Considering only this particular case, the protective shells are taken as a surface from the ellipsoid. The distance from contact point "*p*", to CoM "*G*", and the distance from CoM to the forward point and the back point will determine the first two axes of the ellipsoid — "*x*", "*y*". Let x be the moving axis and use y to determine the side motion. The third axis is going in the left-right direction from the driver and is not important for stability. The stability criteria have to be taken via "r", for the curvature to align with one axis, and "h" for the distance from the CoM, and applied twice: firstly, for the side stability, take "b" instead of "r"; and then secondly, for the forward-back stability, take "a" instead of "r". This ensures that x=a, y=b will be a stable point.

That is, if the lowest point is the stable one, and a point (0,0,0) is a CoM, then the following criteria should be satisfied.

Predefining:

x - forward-back axis

y - side axis - left-right to the driver

z - vertical axis

The criteria for "*a*", as previously for "*r*" (*r*>*h*), is a criterion for the forward-backward motion. It should be noted that the forward-backward-directional curvature "a" will be constructively larger than "b" (a>b) due to the dimensions of the e-bike, and the previous stability criteria applied for c instead of r: c> h. Then the result is solved as: c>h; a>c>h; b>c>h. This is a shortest and fastest solution to have a double curved surface.

This will be a stable and safe ellipsoidal surface as it was a stable and safe cylindrical surface previously. An ellipse is the simplest example of a double curved surface, and allows better understanding of the rolling and the stability point. However, this is only a particular case for a double curved surface. General surface rolling is quite complex.

### 8.2.2. Experimental Validation of the Protective Shells Design.

Future experiments could be carried out by fitting the actual e-bike with the designed protective shells. Results of the sideways falling can then be compared with the simulated results. This would demonstrate that the protective shells which have been designed based on the stability criterion have the safety feature required in order to avoid fatal injury to the driver in the event of sideways falling.

### *One example for the experimental validation*

To test whether overturning of the e-bike would occur with differently designed protective shells during lateral falling and contact with the ground, the following experimental data will be used to validate the design criterion.

Experiment devices:

- A high-speed camera
- An e-bike prototype
- Supporter and cable

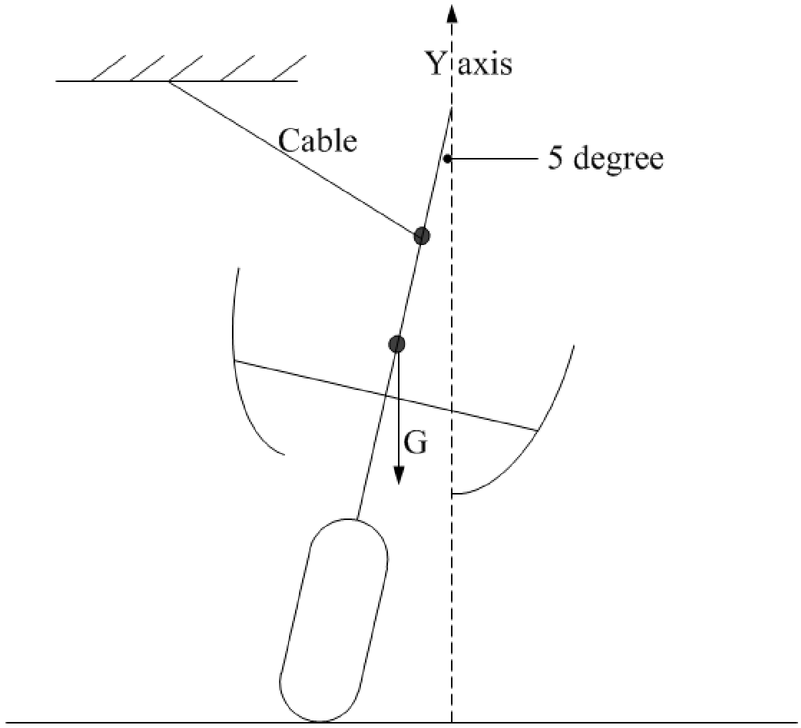


*Figure 8.3 Experimental validation process design*

The e-bike, attached with differently designed protective shells following different theories will be fitted with a simple support and lifted by a cable, as shown in Figure 8.3. The e-bike is not standing strictly perpendicular to the ground. It is positioned with a small angle between its axis and the vertical axis. When releasing the cable, the e-bike will start to fall laterally due to the force of gravity. The distance between one end of the handlebar and the ground will change and be detected by the high-speed camera during the whole falling and contacting period. Experimental results will be used and compared with the results obtained from the numerical simulation to verify the applicability of the design criterion.

### 8.2.3. Expanding Application of the Criterion

Statistics resulting from many investigations reveal that crashes involving other TWVs with internal combustion engines, such as mopeds, motorcycles, and scooters, are also significant [192-194], and the probability of an injury or fatality to a rider is much higher in comparison to that of the driver of a passenger car [195, 196]. The safety features of these powered two-wheelers (PTWs), because of their similar axial structure, can be improved by utilizing this e-bike protective shell design criterion. However, the implementation of this criterion to a moped, motorcycle, or scooter must be further developed due to factors which cannot be ignored, such as their high speed [197] (see Table 8.1 – data from PTWs crash factor investigations in Queensland, Australia) and their larger engine size [198, 199] (see Table 8.2 – data from PTWs crash frequency and severity investigations in Greece).

***Table 8.1 Investigation of characteristics of PTW crashes in Queensland [200]***

| Crash characteristic | PTW Type | | |
|---|---|---|---|
| Speed zone | Moped units (%) | Scooter units (%) | Motorcycle units (%) |
| 0–50 km/h | 136 (25.1) | 17 (17.9) | 1034 (15.4) |
| 60 km/h | 349 (64.5) | 67 (70.5) | 3632 (54.1) |
| 70 km/h | 21 (3.9) | 5 (5.3) | 389 (5.8) |

| | | | |
|---|---|---|---|
| 80–90 km/h | 21 (3.9) | 4 (4.2) | 720 (10.7) |

Powered scooters and mopeds, however, are less capable of excessive speeds when compared with motorcycles. Therefore, there are relatively fewer opportunities for risk taking [201].

***Table 8.2 PTWs driver fatalities frequencies and accident severity rates for the period 1998–2001 in Greece [199].***

| Groups | Engine Size | | | | |
|---|---|---|---|---|---|
| | <49 cc | 50–115 cc | 116–269 cc | 270–730 cc | >730 cc |
| Drivers killed | 184 | 238 | 83 | 43 | 34 |
| Drivers not killed | 6.212 | 19.687 | 9.060 | 5.897 | 2.083 |
| Drivers killed per 1000 drivers involved | 52 | 33 | 39 | 46 | 66 |

### 8.2.4. Design for Integration with the Real Product.

This research focused only on the theoretical derivation and validation of the criterion for the design of protective shells for an e-bike. The realistic geometry of the protective shell product will be taken into account in the future. One example of a real protective shell design is shown in Figure 8.4.

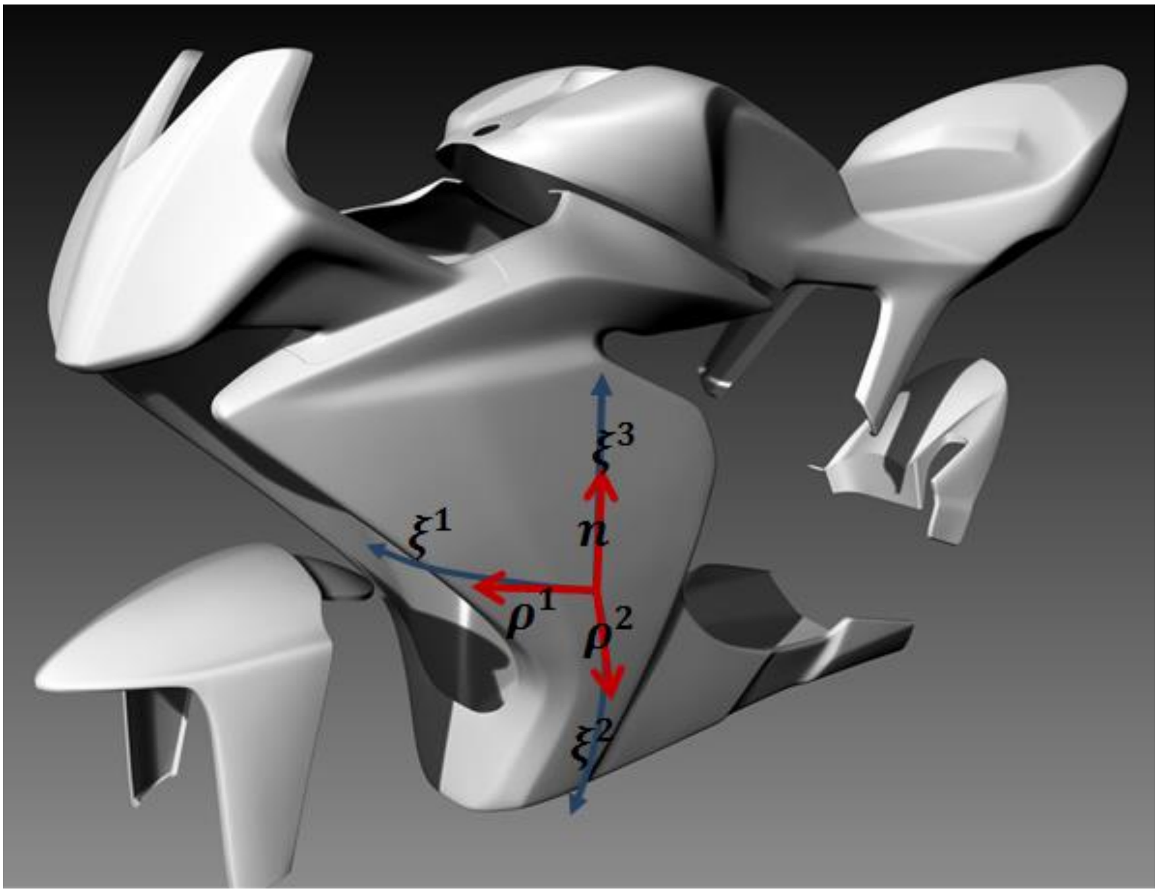


*Figure 8.4 One example of a real protective shell for a motorcycle [202]*

Due to the limited scope governing the work in this thesis, other aspects, such as material selection, aesthetic appearance, user-friendliness, and comfort in real product design were inevitably excluded. However, each of these areas are worthy of further study. This is especially important because the challenges of real world behaviour are comparatively more complex and often tentatively explored in experimental research.

# REFERENCES

1. Fyhri, A. and N. Fearnley, *Effects of e-bikes on bicycle use and mode share.* Transportation Research Part D: Transport and Environment, 2015. **36**: p. 45-52.

2. Cappelle, J., P. Lataire, and J.-M. Timmermans. *Personalized testing method for E-PACs*. in *Proceedings of the 21th international battery, hybrid and fuel cell Electric Vehicle Symposium and Exhibition*. 2005. World Electric Vehicle Association.

3. Dave, S., *Life cycle assessment of transportation options for commuters.* Massachusetts Institute of Technology (MIT), Boston, 2010.

4. Thaler, R., P. Wiederkehr, and R. Krutak, *Promoting e-mobility in Austria.* ECOMM Frankfurt, Frankfurt, 2012: p. 1-23.

5. Cappelle, J., et al., *Characterisation of Electric Bicycles Performances.* Blood, 2002. **200**: p. 220.

6. Cappelle, J., et al. *Electrically assisted cycling around the world*. in *Proceedings of the 20th international battery, hybrid and fuel cell Electric Vehicle Symposium*. 2003. World Electric Vehicle Association.

7. Cherry, C. and R. Cervero, *Use characteristics and mode choice behavior of electric bike users in China.* Transport Policy, 2007. **14**(3): p. 247-257.

8. Weinert, J.X., A.F. Burke, and X. Wei, *Lead-acid and lithium-ion batteries for the Chinese electric bike market and implications on future technology advancement.* Journal of Power Sources, 2007. **172**(2): p. 938-945.

9. Mendoza, J.-M.F., et al., *Development of urban solar infrastructure to support low-carbon mobility.* Energy Policy, 2015. **85**: p. 102-114.

10. Bertoluzzo, M. and G. Buja, *Development of Electric Propulsion Systems for Light Electric Vehicles.* Industrial Informatics, IEEE Transactions on, 2011. **7**(3): p. 428-435.

11. Larminie, J. and J. Lowry, *Elecric Vehicle Technology Explained*. 2003, New York: Wiley.

12. Jamerson, F. and E. Benjamin, *Electric Bike Worldwide Reports*. 2009.

13. Rose, G., *E-bikes and urban transportation: emerging issues and unresolved questions.* Transportation, 2011. **39**(1): p. 81-96.

14. Times, T.N.Y. *An Electric Boost for Bicyclists*. 2010; Available from: http://www.nytimes.com/2010/02/01/business/global/01ebike.html?_r=0.

15. Weinert, J., et al., *The future of electric two-wheelers and electric vehicles in China.* Energy Policy, 2008. **36**(7): p. 2544-2555.

16. Fairley, P., *China's cyclists take charge: electric bicycles are selling by the millions despite efforts to ban them.* IEEE Spectrum, 2005. **42**(6): p. 54-59.

17. Daily, C. *Chinese expected to get back on their (electric) bikes.* 2006; Available from: www.chinadaily.com.cn/cndy/2006-05/16/content_590600.htm.

18. Beijing, G.o., *An Action Plan for Green Transport, Hi-tech Transport and Humanity Transport in Beijing (2009–2015). .* 2009.

19. Ramzy, A. *On the Streets of China, Electric Bikes Are Swarming.* 2009 June 14, 2009; Available from: http://content.time.com/time/world/article/0,8599,1904334,00.html.

20. Bae, A. *Regulations Slow E-Bike Adoption in China*. 2011 November 22, 2011; Available from: http://www.navigantresearch.com/blog/regulations-slow-e-bike-adoption-in-china.

21. News, X. *Electric bike ownership in China was over 120 million*. 2010 February 2010; Available from: http://www.bj.xinhuanet.com/bjpd_sdzx/2010-02/03/content_18946567.htm.

22. Woodford, C. *Electric bicycles*. 2015 October 16, 2015; Available from: http://www.explainthatstuff.com/electricbikes.html.

23. Benjamin, E. *US E-Bike Market Upgrades*. 2016 5 Apr 2016; Available from: http://www.bike-eu.com/.

24. Muetze, A. and Y.C. Tan, *Electric bicycles - A performance evaluation.* IEEE Industry Applications Magazine, 2007. **13**(4): p. 12-21.

25. Stewart, C., *The Global E-bike Market.* INSG, 2014.

26. Wu, C., L. Yao, and K. Zhang, *The red-light running behavior of electric bike riders and cyclists at urban intersections in China: An observational study.* Accident Analysis & Prevention, 2012. **49**: p. 186-192.

27. Aarts, L. and I. van Schagen, *Driving speed and the risk of road crashes: A review.* Accident Analysis & Prevention, 2006. **38**(2): p. 215-224.

28. Zhang, G., K.K.W. Yau, and G. Chen, *Risk factors associated with traffic violations and accident severity in China.* Accident Analysis & Prevention, 2013. **59**: p. 18-25.

29. Eichenberg, D.J., *Baseline testing of the EV Global E-Bike SX*. 2001: [Cleveland, Ohio] : National Aeronautics and Space Administration, Glenn Research Center ; Hanover, MD : Available from NASA Center for Aerospace Information, [2001].

30. CRTASR, *China Road Traffic Accidents Statistics Report*, T.M.R.I.o.t.M.o.P. Security, Editor. 2005-2013: Wuxi, Jangsu.

31. Hu, F., et al., *Related risk factors for injury severity of e-bike and bicycle crashes in Hefei.* Traffic Injury Prevention, 2014. **15**(3): p. 319-323.

32. Dittel, T. and H.-J. Aryus, *How to "Survive" a safety case according to ISO 26262*. 2010: Springer.

33. FMVSS, N., *108,".* Lamps, reflective devices, and associated equipment, 2004.

34. Sayer, J.R., *Just noticeable differences for low-beam headlamp intensities.* 1997.

35. Weinert, J., C. Ma, and C. Cherry, *The transition to electric bikes in China: history and key reasons for rapid growth.* Transportation, 2007. **34**(3): p. 301-318.

36. Jarašūniene, A. and G. Jakubauskas, *Improvement of road safety using passive and active intelligent vehicle safety systems.* Transport, 2007. **22**(4): p. 284-289.

37. Falcone, P., et al., *Predictive active steering control for autonomous vehicle systems.* IEEE Transactions on control systems technology, 2007. **15**(3): p. 566-580.

38. Coelingh, E., et al. *Collision warning with auto brake*. in *FISITA 2006 World Automotive Congress: 22/10/2006-27/10/2006*. 2006. JSAE.

39. Seiffert, U. and L. Wech, *Automotive safety handbook*. 2003.

40. Mashaw, J.L. and D.L. Harfst, *Regulation and legal culture: the case of motor vehicle safety.* Yale J. on Reg., 1986. **4**: p. 257.

41. De Filippi, P., et al., *Enhancing active safety of two-wheeled vehicles via electronic stability control.* IFAC Proceedings Volumes, 2011. **44**(1): p. 638-643.

42. Evangelou, S., D.J. Limebeer, and M.T. Rodriguez, *Influence of road camber on motorcycle stability.* Journal of Applied Mechanics, 2008. **75**(6): p. 061020.

43. Abumi, T. and T. Murakami. *Slip ratio control considering road condition for Two-Wheel drive electric motorcycle*. in *Mecatronics (MECATRONICS), 2014 10th France-Japan/ 8th Europe-Asia Congress on*. 2014.

44. Minh, C.C. and K. Sano, *Analysis of motorcycle effects to saturation flow rate at signalized intersection in developing countries.* Journal of the Eastern Asia Society for Transportation Studies, 2003. **5**: p. 1211-1222.

45. Nakatsuji, T., et al., *Effects of motorcycle on capacity of signalized intersections.* Journal of Infrastructure Planning Review, 2001. **18**(5): p. 935-942.

46. Hamid, H., S.F. Faezi, and S.R. Davoodi, *Predicting speed model of horizontal curves on exclusive motorcycle lane.* Australian journal of basic and applied sciences, 2011. **5**(5): p. 590-598.

47. Berg, F.A., et al. *Motorcycle impacts into roadside barriers-Real-world accident studies, crash tests and simulations carried out in Germany and Australia*. in *Proceedings of the Nineteenth International Conference on Enhanced Safety of Vehicles", Washington, DC*. 2005.

48. Quddus, M., H. Chin, and J. Wang, *Motorcycle crash prediction model for signalised intersections.* 2001.

49. Haque, M.M., H.C. Chin, and H. Huang, *Applying Bayesian hierarchical models to examine motorcycle crashes at signalized intersections.* Accident Analysis & Prevention, 2010. **42**(1): p. 203-212.

50. Schneider IV, W., P. Savolainen, and D. Moore, *Effects of horizontal curvature on single-vehicle motorcycle crashes along rural two-lane highways.* Transportation Research Record: Journal of the Transportation Research Board, 2010(2194): p. 91-98.

51. Seiniger, P., K. Schröter, and J. Gail, *Perspectives for motorcycle stability control systems.* Accident Analysis & Prevention, 2012. **44**(1): p. 74-81.

52. Green, D. *A comparison of stopping distance performance for motorcycles equipped with ABS, CBS and conventional hydraulic brake systems*. in *International Motorcycle Safety Conference*. 2006.

53. Rizzi, M., et al., *Effectiveness of motorcycle antilock braking systems (ABS) in reducing crashes, the first cross-national study.* Traffic injury prevention, 2015. **16**(2): p. 177-183.

54. Huang, C.-K. and M.-C. Shih, *Design of a hydraulic anti-lock braking system (ABS) for a motorcycle.* Journal of Mechanical Science and Technology, 2010. **24**(5): p. 1141-1149.

55. Vavryn, K. and M. Winkelbauer. *Braking performance of experienced and novice motorcycle riders–results of a field study*. in *International Conference on Transport and Traffic Psychology*. 2004.

56. Rizzi, M., A. Kullgren, and C. Tingvall, *The combined benefits of motorcycle antilock braking systems (ABS) in preventing crashes and reducing crash severity.* Traffic injury prevention, 2015(just-accepted): p. 00-00.

57. Teoh, E.R., *Effectiveness of antilock braking systems in reducing motorcycle fatal crash rates.* Traffic Injury Prevention, 2011. **12**(2): p. 169-173.

58. Wood, D.P., et al., *Physical and empirical models for motorcycle speed estimation from crush.* International Journal of Crashworthiness, 2014. **19**(5): p. 540-554.

59. Slimi, H., et al. *Motorcycle maximal safe speed in cornering situation*. in *Networking, Sensing and Control (ICNSC), 2013 10th IEEE International Conference on*. 2013. IEEE.

60. Slimi, H., et al. *Motorcycle speed profile in cornering situation*. in *Proceedings of the 2010 American Control Conference*. 2010.

61. Rose, G., *E-bikes and urban transportation: emerging issues and unresolved questions.* Transportation, 2012. **39**(1): p. 81-96.

62. Zaidel, D., A. Hakkert, and A. Pistiner, *The use of road humps for moderating speeds on urban streets.* Accident Analysis & Prevention, 1992. **24**(1): p. 45-56.

63. Afukaar, F.K., *Speed control in developing countries: issues, challenges and opportunities in reducing road traffic injuries.* Injury control and safety promotion, 2003. **10**(1-2): p. 77-81.

64. Osendorfer, H. and S. Rauscher. *The development of a new class of two-wheeler vehicles*.

65. Daswick, A.C. and A.C. Landry, *Lightweight two-wheeled vehicle*. 1981, Google Patents.

66. Berg, F., P. Rücker, and J. König, *Motorcycle crash tests—an overview.* International Journal of Crashworthiness, 2005. **10**(4): p. 327-339.

67. Yamazaki, T., S. Iijima, and T. Yamamoto. *Exploratory study of an airbag concept for a large touring motorcycle: Further research*. in *17 th International Technical Conference on the Enhanced Safety of Vehicles*. 2001.

68. Nayak, R., et al., *Airbags.* Textile Progress, 2013. **45**(4): p. 209-301.

69. Aikyo, Y., et al., *Feasibility study of airbag concept applicable to motorcycles without sufficient reaction structure.* Traffic injury prevention, 2015. **16**(sup1): p. S148-S152.

70. Lin, M.-R. and J.F. Kraus, *A review of risk factors and patterns of motorcycle injuries.* Accident Analysis & Prevention, 2009. **41**(4): p. 710-722.

71. Keng, S.-H., *Helmet use and motorcycle fatalities in Taiwan.* Accident Analysis & Prevention, 2005. **37**(2): p. 349-355.

72. Nakahara, S., et al., *Temporal distribution of motorcyclist injuries and risk of fatalities in relation to age, helmet use, and riding while intoxicated in Khon Kaen, Thailand.* Accident Analysis & Prevention, 2005. **37**(5): p. 833-842.

73. DeMarco, A.L., et al., *The impact response of motorcycle helmets at different impact severities.* Accident Analysis & Prevention, 2010. **42**(6): p. 1778-1784.

74. Branas, C.C. and M.M. Knudson, *Helmet laws and motorcycle rider death rates.* Accident Analysis & Prevention, 2001. **33**(5): p. 641-648.

75. Ichikawa, M., W. Chadbunchachai, and E. Marui, *Effect of the helmet act for motorcyclists in Thailand.* Accident Analysis & Prevention, 2003. **35**(2): p. 183-189.

76. Coben, J.H., C.A. Steiner, and T.R. Miller, *Characteristics of motorcycle-related hospitalizations: comparing states with different helmet laws.* Accident Analysis & Prevention, 2007. **39**(1): p. 190-196.

77. Houston, D.J., *Are helmet laws protecting young motorcyclists?* Journal of safety research, 2007. **38**(3): p. 329-336.

78. Houston, D.J. and L.E. Richardson, *Motorcyclist fatality rates and mandatory helmet-use laws.* Accident Analysis & Prevention, 2008. **40**(1): p. 200-208.

79. Mayrose, J., *The effects of a mandatory motorcycle helmet law on helmet use and injury patterns among motorcyclist fatalities.* Journal of Safety Research, 2008. **39**(4): p. 429-432.

80. Hill, P.S., et al., *Mandatory helmet legislation and the print media in Viet Nam.* Accident Analysis & Prevention, 2009. **41**(4): p. 789-797.

81. Ranney, M.L., et al., *Correlates of motorcycle helmet use among recent graduates of a motorcycle training course.* Accident Analysis & Prevention, 2010. **42**(6): p. 2057-2062.

82. Robinson, D.L., *Head injuries and bicycle helmet laws.* Accident Analysis & Prevention, 1996. **28**(4): p. 463-475.

83. Rane, S.S., A. Srividya, and A.K. Verma, *Taguchi methods and finite element methods in reliability based crashworthiness and risk analysis of motorcycle frame.* International Journal of System Assurance Engineering and Management, 2012. **2**(4): p. 319-324.

84. Ross, D.J., *The prevention of leg injuries in motorcycle accidents.* Injury, 1983. **15**(2): p. 75-77.

85. Seabury, J.J., W.C. Adams, and M.R. Ramey, *Influence of pedalling rate and power output on energy expenditure during bicycle ergometry.* Ergonomics, 1977. **20**(5): p. 491-498.

86. Lin, H.-L., et al., *Neck collar used in treatment of victims of urban motorcycle accidents: over-or underprotection?* The American journal of emergency medicine, 2011. **29**(9): p. 1028-1033.

87. ZHU, M.-t., et al., *FEA and Lightweight Design for ATV Frame Structure [J].* Tractor & Farm Transporter, 2008. **3**: p. 021.

88. Rodríguez, J.E., A.L. Medaglia, and J.P. Casas. *Approximation to the optimum design of a motorcycle frame using finite element analysis and evolutionary algorithms*. in *Systems and Information Engineering Design Symposium, 2005 IEEE*. 2005. IEEE.

89. Hsiao, S.-W., R.-Q. Chen, and W.-L. Leng, *Applying riding-posture optimization on bicycle frame design.* Applied Ergonomics, 2015. **51**: p. 69-79.

90. Chih-Jer, L., et al. *Optimization of suspension design based on evolution algorithm for a novel E-bike*. in *Intelligent Control and Automation (WCICA), 2011 9th World Congress on*. 2011.

91. Mitra, A., M. Patil, and N. Banerjee, *Optimization of Vehicle Suspension Parameters for Ride Comfort Based on RSM.* Journal of The Institution of Engineers (India): Series C, 2015. **96**(2): p. 165-173.

92. Barone, S. and G. Lo Iacono, *Robust Dynamic Comfort Modeling for Motorcycle Riding.* Human Factors and Ergonomics in Manufacturing & Service Industries, 2015. **25**(2): p. 239-250.

93. Gaspar, P., et al., *Towards global chassis control by integrating the brake and suspension systems.* IFAC Proceedings Volumes, 2007. **40**(10): p. 563-570.

94. Poussot-Vassal, C., et al., *Vehicle dynamic stability improvements through gain-scheduled steering and braking control.* Vehicle System Dynamics, 2011. **49**(10): p. 1597-1621.

95. Barnard, R.H., *Road vehicle aerodynamic design-an introduction*. 2001.

96. Kim, J., et al., *Active control of turbulent flow over a model vehicle for drag reduction.* Journal of Turbulence, 2004. **5**(019): p. 1-12.

97. Cooper, K. *The effects of aerodynamics on the performance and stability of high speed motorcycles*. in *Proc. 2nd AIAA Symp. Aerodynamics Sport Competition Automobiles*. 1974.

98. Mohamed-Kassim, Z. and A. Filippone, *Fuel savings on a heavy vehicle via aerodynamic drag reduction.* Transportation Research Part D: Transport and Environment, 2010. **15**(5): p. 275-284.

99. Gupta, S. and M. Patil. *A hybrid approach to optimal electric drive train design*. in *Power Electronics Systems and Applications, 2009. PESA 2009. 3rd International Conference on*. 2009.

100. Sharp, R.S., *The stability and control of motorcycles.* Journal of mechanical engineering science, 1971. **13**(5): p. 316-329.

101. Lot, R., V. Cossalter, and M. Massaro. *The significance of frame compliance and rider mobility on the motorcycle stability*. in *Proceedings of Multibody Dynamics 2005, International Conference on Advances in Computational Multibody Dynamics-ECCOMAS Thematic Conference*. 2005.

102. Roland, R., *Simulation study of motorcycle stability at high speed*. 1973.

103. Cossalter, V., et al., *The effect of rider's passive steering impedance on motorcycle stability: identification and analysis.* Meccanica, 2011. **46**(2): p. 279-292.

104. Cossalter, V., et al., *Experimental and numerical investigation on the motorcycle front frame flexibility and its effect on stability.* Mechanical Systems and Signal Processing, 2015. **60–61**: p. 452-471.

105. Hof, A.L., M.G.J. Gazendam, and W.E. Sinke, *The condition for dynamic stability.* Journal of Biomechanics, 2005. **38**(1): p. 1-8.

106. Chow, T.L., *Classical mechanics*. 2013: CRC Press.

107. Rajasekaran, S. and G. Sankarasubramanian, *COMPUTATIONAL STRUCTURAL MECHANICS: WITH CD ROM*. 2006: PHI Learning Pvt. Ltd.

108. Chen, W.-F. and T. Atsuta, *In-plane behavior and design*. 2008: J. Ross Pub.

109. Luebkeman, C.H., *Structures I Topics*, in *Lectures*. 1998, MIT. p. 40.

110. Chart, S., *Principles of mechanics: by John L. Synge and Byron A. Griffith. 530 pages, 15 X 23 cm., illustrations. New York, McGraw-Hill Book Co., 1949. Price, $5.00*. 1949, Pergamon. p. 45-46.

111. Corben, H.C. and P. Stehle, *Classical mechanics*. 1994: Courier Corporation.

112. Feller, W., *An introduction to probability theory and its applications: volume I*. Vol. 3. 1968: John Wiley & Sons London-New York-Sydney-Toronto.

113. Hille, E. and R.S. Phillips, *Functional analysis and semi-groups*. Vol. 31. 1996: American Mathematical Soc.

114. Langhaar, H.L., *Energy methods in applied mechanics*. 1962: John Wiley & Sons Inc.

115. Tauchert, T.R., *Energy principles in structural mechanics*. 1974: McGraw-Hill Companies.

116. Reddy, J.N., *Theory and analysis of elastic plates and shells*. 2006: CRC press.

117. Shevell, R.S. and R.S. Shevell, *Fundamentals of flight*. Vol. 2. 1989: Prentice Hall Englewood Cliffs, New Jersey.

118. Anderson Jr, J.D., *Fundamentals of aerodynamics*. 2010: Tata McGraw-Hill Education.

119. Stengel, R.F., *Flight dynamics*. 2015: Princeton University Press.

120. /AE1110x, I.o. *Dynamic stability*. Available from: http://pepe.vacau.com/AE1110x/Dynamic%20stability.jpg.

121. Glocker, C., *Formulatin of spatial contact situations in rigid multibody systems.* Computer Methods in Applied Mechanics and Engineering, 1999. **177**(3–4): p. 199-214.

122. Baron, M.E., *The origins of the infinitesimal calculus*. 1969: Courier Corporation.

123. Liu, W. and B.M. Nigg, *A mechanical model to determine the influence of masses and mass distribution on the impact force during running.* Journal of Biomechanics, 2000. **33**(2): p. 219-224.

124. Toepker, T.P., *Center of mass of a suspended slinky: an experiment.* The Physics Teacher, 2004. **42**(1): p. 16-17.

125. Serna, J.D. and A. Joshi, *The Center of Mass of a Soft Spring.* The College Mathematics Journal, 2011. **42**(5): p. 389-394.

126. Cholewiak, S.A., R.W. Fleming, and M. Singh, *Perception of physical stability and center of mass of 3-D objects.* Journal of vision, 2015. **15**(2): p. 13-13.

127. Feynman, R.P., R.B. Leighton, and M. Sands, *Lecture on physics.* Narosa book disributirs ltd, 1963. **1**.

128. Kleppner, D. and R. Kolenkow, *An introduction to mechanics*. 2013: Cambridge University Press.

129. Dhatt, G., E. Lefrançois, and G. Touzot, *Finite element method*. 2012: John Wiley & Sons.

130. Bathe, K.J., *Finite element method*. 2008: Wiley Online Library.

131. Hughes, T.J., *The finite element method: linear static and dynamic finite element analysis*. 2012: Courier Corporation.

132. Terzopoulos, D. and A. Witkin, *Physically based models with rigid and deformable components.* IEEE Computer Graphics and Applications, 1988. **8**(6): p. 41-51.

133. Wördenweber, B., *Finite element mesh generation.* Computer-Aided Design, 1984. **16**(5): p. 285-291.

134. Ho-Le, K., *Finite element mesh generation methods: a review and classification.* Computer-Aided Design, 1988. **20**(1): p. 27-38.

135. Campbell, D., *Finite Element Mesh Generation.* New Zealand Engineering, 1996. **51**(4): p. 12.

136. Sarcar, M., K.M. Rao, and K.L. Narayan, *Computer aided design and manufacturing*. 2008: PHI Learning Pvt. Ltd.

137. Horgan, J., *EDA & PLM?* 2004.

138. M, M., et al., *Challenges in feature-based manufacturing research.* Commun. ACM, 1996. **39**(2): p. 77-85.

139. LaCourse, D.E., *Handbook of solid modeling*. 1995: McGraw-Hill, Inc.

140. Reddy, J.N., *An introduction to the finite element method*. Vol. 2. 1993: McGraw-Hill New York.

141. Liu, G.-R., *Meshfree methods: moving beyond the finite element method*. 2009: Taylor & Francis.

142. Šarler, B. and R. Vertnik, *Meshfree explicit local radial basis function collocation method for diffusion problems.* Computers & Mathematics with applications, 2006. **51**(8): p. 1269-1282.

143. Edelsbrunner, H., *Geometry and topology for mesh generation*. 2001: Cambridge University Press.

144. Bathe, K.-J., *Finite element procedures*. 2006: Klaus-Jurgen Bathe.

145. Liu, H. and R. Setiono. *Chi2: Feature selection and discretization of numeric attributes*. in *ICTAI*. 1995.

146. Misner, C.W., K.S. Thorne, and J.A. Wheeler, *Gravitation*. 1973: Macmillan.

147. 16, C. *Introduction to Finite Element Methods (ASEN 5007)* 2015; Available from: http://www.colorado.edu/engineering/CAS/courses.d/IFEM.d/Home.html.

148. Xie, Y.M. and G.P. Steven, *Basic evolutionary structural optimization*. 1997: Springer.

149. Ahmad, S., B.M. Irons, and O. Zienkiewicz, *Analysis of thick and thin shell structures by curved finite elements.* International Journal for Numerical Methods in Engineering, 1970. **2**(3): p. 419-451.

150. Hallquist, J.O. and L.-D.T. Manual, *Livermore Software Technology Corporation.* Livermore, Ca, 1998.

151. Li, S., *Reflection on 'finite rotation problem'in plate and shell theories and in finite element formulation–Back to basics.* International Journal of Mechanical Sciences, 2015. **91**: p. 12-17.

152. Hallquist, J., *LS-DYNA Theory manual, Livermore software technology corporation, 2006.* Reproduced with permission of the copyright owner. Further reproduction prohibited without permission.

153. Hearn, G. and R.B. Testa, *Modal analysis for damage detection in structures.* Journal of Structural Engineering, 1991. **117**(10): p. 3042-3063.

154. Cossalter, V., R. Lot, and F. Maggio, *The modal analysis of a motorcycle in straight running and on a curve.* Meccanica, 2004. **39**(1): p. 1-16.

155. Sharp, R., S. Evangelou, and D.J. Limebeer, *Advances in the modelling of motorcycle dynamics.* Multibody system dynamics, 2004. **12**(3): p. 251-283.

156. Clough, R.W. and J. Penzien, *Dynamics of structures. 1993.* Copyright of Applied Mechanics & Materials, 1993: p. 173-201.

157. Riley, K.F., M.P. Hobson, and S.J. Bence, *Mathematical methods for physics and engineering: a comprehensive guide*. 2006: Cambridge University Press.

158. Jurgen, B.K., *Finite element procedures*. 1996, Prentice Hall India: New Jersey. p. 786.

159. Popov, V., *Contact mechanics and friction: physical principles and applications*. 2010: Springer Science & Business Media.

160. Yu, M.M.-H. and B. Bhushan, *Contact analysis of three-dimensional rough surfaces under frictionless and frictional contact.* Wear, 1996. **200**(1): p. 265-280.

161. Konyukhov, A. and R. Izi, *Introduction to computational contact mechanics: a geometrical approach*. 2015: John Wiley & Sons.

162. Shimizu, T. and T. Sano, *An application of a penalty method contact and friction algorithm to a 3-dimensional tool surface expressed by a B-spline patch.* Journal of Materials Processing Technology, 1995. **48**(1): p. 207-213.

163. Konyukhov, A. and K. Schweizerhof, *Computational Contact Mechanics: geometrically exact theory for arbitrary shaped bodies*. Vol. 67. 2012: Springer Science & Business Media.

164. Weyler, R., et al., *On the contact domain method: A comparison of penalty and Lagrange multiplier implementations.* Computer Methods in Applied Mechanics and Engineering, 2012. **205**: p. 68-82.

165. Smith, A.E. and D.W. Coit, *Penalty functions.* Handbook on Evolutionary Computation, pages C, 1997. **5**: p. 1-6.

166. Al-Tabey, W., *Finite element analysis in mechanical design using ANSYS: Finite element analysis (FEA) hand book for mechanical engineers with ANSYS tutorials*. 2012: LAP LAMBERT Academic Publishing.

167. Lele Zhang and A. Konyukhov, *Annual Review "Finite Element Modeling of Electric-BIKE"*. 2013, Mechanical Enginnering, University of Nottingham Ningbo China.

168. Benson, D.D.J., *The History of LS-DYNA*. 2009, University Of California, San Diego.

169. Mehrasa, H., G. Liaghat, and D. Javabvar, *Experimental analysis and simulation of effective factors on explosive forming of spherical vessel using prefabricated four cones vessel structures.* Central European Journal of Engineering, 2012. **2**(4): p. 656-664.

170. Nimmala, S., *A comparison of DYNA3D, NIKE3D and LS-DYNA*. 2012, Oregon State University.

171. Rust, W. and K. Schweizerhof, *Finite element limit load analysis of thin-walled structures by ANSYS (implicit), LS-DYNA (explicit) and in combination.* Thin-Walled Structures, 2003. **41**(2–3): p. 227-244.

172. Hughes, T. and W. Liu, *Implicit-explicit finite elements in transient analysis: stability theory.* Journal of applied Mechanics, 1978. **45**(2): p. 371-374.

173. Gladwell, I. and R. Thomas, *Stability properties of the Newmark, Houbolt and Wilson θ methods.* International Journal for Numerical and Analytical Methods in Geomechanics, 1980. **4**(2): p. 143-158.

174. Katona, M.C. and O. Zienkiewicz, *A unified set of single step algorithms part 3: The beta-m method, a generalization of the Newmark scheme.* International Journal for Numerical Methods in Engineering, 1985. **21**(7): p. 1345-1359.

175. Chung, J. and G. Hulbert, *A time integration algorithm for structural dynamics with improved numerical dissipation: the generalized-α method.* Journal of applied mechanics, 1993. **60**(2): p. 371-375.

176. Hilber, H.M., T.J. Hughes, and R.L. Taylor, *Improved numerical dissipation for time integration algorithms in structural dynamics.* Earthquake Engineering & Structural Dynamics, 1977. **5**(3): p. 283-292.

177. Subbaraj, K. and M. Dokainish, *A survey of direct time-integration methods in computational structural dynamics—II. Implicit methods.* Computers & Structures, 1989. **32**(6): p. 1387-1401.

178. Gavin, H.P., *Numerical Integration in Structural Dynamics*, in *CEE 541. Structural Dynamics*. Department of Civil & Environmental Engineering, Duke University.

179. Newmark, N.M. *A method of computation for structural dynamics*. in *Proc. ASCE*. 1959.

180. Nickel, R.E., *On the stability of approximation operators in problems of structural dynamics.* International Journal of Solids and Structures, 1971. **7**(3): p. 301-319.

181. Hilber, H.M. and T.J. Hughes, *Collocation, dissipation and [overshoot] for time integration schemes in structural dynamics.* Earthquake Engineering & Structural Dynamics, 1978. **6**(1): p. 99-117.

182. Rebelo, N., et al. *Comparison of implicit and explicit finite element methods in the simulation of metal forming processes*. in *ABAQUS Users Conf., Newport, RI*. 1992.

183. Chang, S.-Y., *Improved explicit method for structural dynamics.* Journal of Engineering Mechanics, 2007. **133**(7): p. 748-760.

184. Wu, B., et al., *Stability and accuracy analysis of the central difference method for real‐time substructure testing.* Earthquake engineering & structural dynamics, 2005. **34**(7): p. 705-718.

185. Kuhlemeyer, R.L. and J. Lysmer, *Finite element method accuracy for wave propagation problems.* Journal of Soil Mechanics & Foundations Div, 1973. **99**(Tech Rpt).

186. Benhassine, S., L. Pichon, and W. Tabbara, *An efficient finite-element time-domain method for the analysis of the coupling between wave and shielded enclosure.* IEEE transactions on magnetics, 2002. **38**(2): p. 709-712.

187. Prior, A., *Applications of implicit and explicit finite element techniques to metal forming.* Journal of Materials Processing Technology, 1994. **45**(1): p. 649-656.

188. Dokainish, M.A. and K. Subbaraj, *A survey of direct time-integration methods in computational structural dynamics—I. Explicit methods.* Computers & Structures, 1989. **32**(6): p. 1371-1386.

189. Asnafi, N., *On springback of double-curved autobody panels.* International Journal of Mechanical Sciences, 2001. **43**(1): p. 5-37.

190. Linkwitz, K., *About formfinding of double-curved structures.* Engineering Structures, 1999. **21**(8): p. 709-718.

191. Bowman, F., *Introduction to elliptic functions with applications*. 1961.

192. Cesari, D. *Motorcycle Accident Investigations: OECD RS9*. in *The 78th Annual Meeting of Transportation Research Board, Washington, DC*. 1999.

193. Hurt, H., J. Ouellet, and D. Thom, *Motorcycle accident cause factors and identification of countermeasures Volume I: Technical Report.* Traffic Safety Center, University of Southern California, Contract No. DOT HS-5-01160, 1981.

194. Vlahogianni, E.I., G. Yannis, and J.C. Golias, *Overview of critical risk factors in Power-Two-Wheeler safety.* Accident Analysis & Prevention, 2012. **49**: p. 12-22.

195. Wells, S., et al., *Motorcycle rider conspicuity and crash related injury: case-control study.* Bmj, 2004. **328**(7444): p. 857.

196. Keall, M.D. and S. Newstead, *Analysis of factors that increase motorcycle rider risk compared to car driver risk.* Accident Analysis & Prevention, 2012. **49**: p. 23-29.

197. Harnen, S., et al., *MOTORCYCLE CRASH PREDICTION MODEL FOR NON-SIGNALIZED INTERSECTIONS.* IATSS Research, 2003. **27**(2): p. 58-65.

198. Langley, J., et al., *Motorcycle engine size and risk of moderate to fatal injury from a motorcycle crash.* Accident Analysis & Prevention, 2000. **32**(5): p. 659-663.

199. Yannis, G., J. Golias, and E. Papadimitriou, *Driver age and vehicle engine size effects on fault and severity in young motorcyclists accidents.* Accident Analysis & Prevention, 2005. **37**(2): p. 327-333.

200. Blackman, R.A. and N.L. Haworth, *Comparison of moped, scooter and motorcycle crash risk and crash severity.* Accident Analysis & Prevention, 2013. **57**: p. 1-9.

201. Haworth, N., K. Greig, and A. Nielson, *Comparison of risk taking in moped and motorcycle crashes.* Transportation Research Record: Journal of the Transportation Research Board, 2009(2140): p. 182-187.

202. ENGINEERING, R. *Motorcycle – Full Body Shell*. 2013; Available from: http://eurocompositi.it/en/portfolio/reverse-engineering-of-a-motorcycle-body-shell/.

# APPENDIX I. Modal Analysis

```
!* Modal analysis to check the quality of mesh
/SOLU
ANTYPE,2
!*
!MODOPT,SUBSP,10 ! 10 modes
!EQSLV,FRONT ! solver'type
!MXPAND,10, , ,0 ! write 10 modes
!*
MODOPT,LANB,10
EQSLV,SPAR
MXPAND,10, , ,1
LUMPM,0
PSTRES,0
MODOPT,LANB,10,0,0, ,OFF
!*
/STATUS,SOLU
SOLVE
FINISH
!*
/POST1
SET,FIRST  !right and left
PLDISP,1
PLDI, ,
ANMODE,10,0.5, ,0
!*
SET,NEXT !up and down
PLDISP,1
PLDI, ,
ANMODE,10,0.5, ,0
```

# APPENDIX II. Static Analysis

```
!*set up the contact parameters
/COM, CONTACT PAIR CREATION - START
CM,_NODECM,NODE
CM,_ELEMCM,ELEM
CM,_KPCM,KP
CM,_LINECM,LINE
CM,_AREACM,AREA
CM,_VOLUCM,VOLU
/GSAV,cwz,gsav,,temp
MP,MU,1,0
MAT,1
MP,EMIS,1,7.88860905221e-031
R,5
REAL,5
ET,8,170
ET,9,174
R,5,,,10,0.1,0,
RMORE,,,1.0E20,0.0,1.0,
RMORE,0.0,0,1.0,,1.0,0.5
RMORE,0,1.0,1.0,0.0,,1.0
KEYOPT,9,4,0
KEYOPT,9,5,0
KEYOPT,9,7,0
KEYOPT,9,8,0
KEYOPT,9,9,0
KEYOPT,9,10,2
KEYOPT,9,11,0
KEYOPT,9,12,0
KEYOPT,9,2,0
KEYOPT,8,1,0
KEYOPT,8,2,0
```

```
KEYOPT,8,3,0
KEYOPT,8,5,0
! Generate the target surface
ASEL,S,,,24
CM,_TARGET,AREA
AATT,-1,5,8,-1
TYPE,8
AMESH,ALL
! Generate the contact surface
ASEL,S,,,4
ASEL,A,,,5
ASEL,A,,,6
ASEL,A,,,7
ASEL,A,,,8
ASEL,A,,,9
ASEL,A,,,10
ASEL,A,,,11
ASEL,A,,,12
ASEL,A,,,13
ASEL,A,,,14
ASEL,A,,,15
ASEL,A,,,16
ASEL,A,,,17
ASEL,A,,,18
ASEL,A,,,19
ASEL,A,,,20
ASEL,A,,,21
ASEL,A,,,22
ASEL,A,,,23
CM,_CONTACT,AREA
TYPE,9
NSLA,S,1
ESLN,S,0
NSLE,A,CT2 ! CZMESH patch (fsk qt-40109 8/2008)
```

```
ESURF
*SET,_REALID,5
ALLSEL
ESEL,ALL
ESEL,S,TYPE,,8
ESEL,A,TYPE,,9
ESEL,R,REAL,,5
ASEL,S,REAL,,5
/PSYMB,ESYS,1
/PNUM,TYPE,1
/NUM,1
EPLOT
! Reverse target normals
CM,_Y,AREA
ASEL, , , ,      24
CM,_YLN,LINE
CM,_YEL,ELEM
CM,_YND,NODE
LSLA,S,1
NSLA,S,1
ESLN,S,1
ESEL,R,REAL,,_REALID
ESURF,,REVERSE
CMSEL,S,_Y
CMSEL,S,_YLN
CMSEL,S,_YEL
CMSEL,S,_YND
CMDELE,_Y
CMDELE,_YLN
CMDELE,_YEL
CMDELE,_YND
/REPLOT
!*
ESEL,ALL
```

```
ESEL,S,TYPE,,8
ESEL,A,TYPE,,9
ESEL,R,REAL,,5
ASEL,S,REAL,,5
/PSYMB,ESYS,1
/PNUM,TYPE,1
/NUM,1
EPLOT
ESEL,ALL
ESEL,S,TYPE,,8
ESEL,A,TYPE,,9
ESEL,R,REAL,,5
ASEL,S,REAL,,5
CMSEL,A,_NODECM
CMDEL,_NODECM
CMSEL,A,_ELEMCM
CMDEL,_ELEMCM
CMSEL,S,_KPCM
CMDEL,_KPCM
CMSEL,S,_LINECM
CMDEL,_LINECM
CMSEL,S,_AREACM
CMDEL,_AREACM
CMSEL,S,_VOLUCM
CMDEL,_VOLUCM
/GRES,cwz,gsav
CMDEL,_TARGET
CMDEL,_CONTACT
/COM, CONTACT PAIR CREATION - END
/MREP,EPLOT

Fini

/solu
```

```
ANTYPE,0
NLGEOM,ON
NSUBST,1
acel,,9.81
SOLVE
```

# APPENDIX III. Transient Analysis

```
! Solution
/SOLU
ANTYPE,4 ! Transient

NLGEOM,ON
SOLC,ON
!* All substeps
OUTPR,BASIC,ALL,
!* Print result
OUTRES,ALL,ALL,
TIME, 5 ! The final time
AUTOTS,0 ! Automatic time step for numerical integration is disabled
! Time steps is T/100
DELTIM,0.05, , ,1
KBC,1 ! Load is changing step by step from zero to the full load
! Initial condition
IC,all,all,0,0,! to all nodes (ALL), to all DOF (ALL) ¨C! initial displacements
u0 = 0,! initial velocity v0 = 0
acel,,9.81
SOLVE
FINISH

/POST26
FILE,'file','rst','.'
/UI,COLL,1
NUMVAR,200
SOLU,191,NCMIT
STORE,MERGE
FILLDATA,191,,,,1,1
REALVAR,191,191
```

```
!*
NSOL,2,3392,U,Y, UY_3392
DERIV,3,2, 1,,VY_3392
PROD,4,3,3,,K.E.,,,0.5
DERIV,5,3,1,,AY_3392
*GET,t0,VARI,4,EXTREM,TMAX
PLVAR,2,3,4,5
PRVAR,2,3,4,5

C***
*GET,UY_0,VARI,2,RTIME,t0
*GET,VY_0,VARI,3,RTIME,t0
*GET,ENG_0,VARI,4,RTIME,t0
*GET,UY_MAX,VARI,2,EXTREM,VMIN
*GET,T_MAX,VARI,2,EXTREM,TMIN
*GET,VY_MAX,VARI,3,RTIME,T_MAX
*GET,ENG_MAX,VARI,4,RTIME,T_MAX
*status
  /page,99999,132,99999,240
/header,on,on,on,on,on,on
/format,7,g,17,9,99999
```

# APPENDIX IV. Side Falling Test in LS-DYNA

```
*KEYWORD
*TITLE
$# title
LS-DYNA keyword deck by LS-PrePost
*CONTROL_CONTACT
$#   slsfac    rwpnal    islchk    shlthk    penopt    thkchg     orien
enmass
     0.000     0.000         2         0         0         0         1         0
$#   usrstr    usrfrc     nsbcs    interm     xpene     ssthk      ecdt   tiedprj
         0         0         0         0     0.000         0         0         0
$#    sfric     dfric       edc       vfc        th     th_sf    pen_sf
     0.000     0.000     0.000     0.000     0.000     0.000     0.000
$#   ignore    frceng   skiprwg    outseg   spotstp   spotdel   spothin
         0         0         0         0         0         0     0.000
$#     isym    nserod    rwgaps    rwgdth     rwksf      icov    swradf    ithoff
         0         0         0     0.000  1.000000         0     0.000         0
$#   shledg
         0
*CONTROL_ENERGY
$#     hgen      rwen    slnten     rylen
         2         2         2         1
*CONTROL_SHELL
$#   wrpang     esort     irnxx    istupd    theory       bwc     miter      proj
 20.000000         0        -1         0         2         1         1         1
$# rotascl    intgrd    lamsht    cstyp6    tshell    nfail1    nfail4   psnfail
  1.000000         0         0         1         0         0         0         0
$# psstupd    irquad     cntco
         0         0         0
*CONTROL_TERMINATION
```

```
$#   endtim    endcyc     dtmin    endeng    endmas
  1.000000         0     0.000     0.000     0.000
*CONTROL_TIMESTEP
$#   dtinit    tssfac      isdo    tslimt     dt2ms      lctm     erode     ms1st
  0.100000  0.800000         0     0.000     0.000         0         0         0
$#  dt2msf   dt2mslc     imscl
     0.000         0         0
*DATABASE_GLSTAT
$#       dt    binary      lcur     ioopt
     0.000         3         0         1
*DATABASE_MATSUM
$#       dt    binary      lcur     ioopt
     0.000         3         0         1
*DATABASE_NCFORC
$#       dt    binary      lcur     ioopt
     0.000         3         0         1
*DATABASE_NODFOR
$#       dt    binary      lcur     ioopt
  0.500000         3         0         1
*DATABASE_NODOUT
$#       dt    binary      lcur     ioopt      dthf     binhf
     0.000         3         0         1     0.000         0
*DATABASE_SLEOUT
$#       dt    binary      lcur     ioopt
     0.000         3         0         1
*DATABASE_BINARY_D3PLOT
$#       dt      lcdt      beam     npltc    psetid
  0.200000         0         0         0         0
$#    ioopt
         0
*DATABASE_HISTORY_NODE
$#      id1       id2       id3       id4       id5       id6       id7       id8
     34996     34993     35104     35101         0         0         0         0
*BOUNDARY_SPC_SET
```

```
$#     nsid       cid      dofx      dofy      dofz     dofrx     dofry     dofrz
         1         0         1         1         1         0         0         0
*SET_NODE_LIST
$#      sid       da1       da2       da3       da4    solver
         1     0.000     0.000     0.000     0.000MECH
$#     nid1      nid2      nid3      nid4      nid5      nid6      nid7      nid8
     35179     35181     35183     35185     35187     35189     35191
35193
     35195     35197     35199     35176     35155     35132     35133
35220
     35243     35241     35239     35237     35235     35233     35231
35229
     35227     35225     35223     35200     35113     35112     35135
35156
*LOAD_BODY_Y
$#     lcid        sf    lciddr        xc        yc        zc       cid
         1 9800.0000         0     0.000     0.000     0.000         0
*CONTACT_AUTOMATIC_ONE_WAY_SURFACE_TO_SURFACE_ID
$#      cid                                                                 title
         1one way contact
$#     ssid      msid     sstyp     mstyp    sboxid    mboxid       spr       mpr
         2         3         2         2         0         0         1         1
$#       fs        fd        dc        vc       vdc    penchk        bt        dt
     0.000          0.000          0.000          0.000          0.000                0
0.0001.0000E+20
$#      sfs       sfm       sst       mst      sfst      sfmt       fsf       vsf
  1.000000  1.000000     0.000     0.000  1.000000  1.000000  1.000000
1.000000
*SET_PART_LIST_TITLE
ebike
$#      sid       da1       da2       da3       da4    solver
         2     0.000     0.000     0.000     0.000MECH
$#     pid1      pid2      pid3      pid4      pid5      pid6      pid7      pid8
         1         2         3         4         5         6         9        10
        12        14        15         0         0         0         0         0
```

```
*SET_PART_LIST_TITLE
plate
$#     sid       da1       da2       da3       da4    solver
         3     0.000     0.000     0.000     0.000MECH
$#    pid1      pid2      pid3      pid4      pid5      pid6      pid7      pid8
        11         0         0         0         0         0         0         0
*PART
$# title
hand bar
$#     pid     secid       mid     eosid      hgid      grav    adpopt      tmid
         1         1         1         0         0         0         0         0
*SECTION_BEAM_TITLE
bar
$#   secid    elform      shrf   qr/irid       cst     scoor       nsm
         1         1  1.000000         2         1     0.000     0.000
$#     ts1       ts2       tt1       tt2     nsloc     ntloc
 40.000000 40.000000     0.000     0.000     0.000     0.000
*MAT_PIECEWISE_LINEAR_PLASTICITY_TITLE
main frame
$#     mid        ro         e        pr      sigy      etan      fail      tdel
         1       7.0800E-9       2.1000E+5            0.300000       220.00000
0.0001.0000E+21     0.000
$#       c         p      lcss      lcsr        vp
     0.000     0.000         0         0     0.000
$#    eps1      eps2      eps3      eps4      eps5      eps6      eps7      eps8
     0.000     0.000     0.000     0.000     0.000     0.000     0.000     0.000
$#     es1       es2       es3       es4       es5       es6       es7       es8
     0.000     0.000     0.000     0.000     0.000     0.000     0.000     0.000
*PART
$# title
main frame
$#     pid     secid       mid     eosid      hgid      grav    adpopt      tmid
         2         2         5         0         0         0         0         0
*SECTION_BEAM_TITLE
```

```
main frame
$#   secid    elform      shrf   qr/irid       cst     scoor       nsm
         2         1  1.000000         2         1     0.000     0.000
$#     ts1       ts2       tt1       tt2     nsloc     ntloc
 50.000000 50.000000 40.000000 40.000000     0.000     0.000
*MAT_RIGID_TITLE
frame rigid
$#     mid        ro         e        pr         n    couple         m     alias
         5 7.0800E-9 2.1000E+5  0.300000     0.000     0.000     0.000
$#     cmo      con1      con2
     0.000         0         0
$# lco or a1      a2        a3        v1        v2        v3
     0.000     0.000     0.000     0.000     0.000     0.000
*PART
$# title
sheet_metal
$#     pid     secid       mid     eosid      hgid      grav    adpopt      tmid
         3         3         1         0         0         0         0         0
*SECTION_BEAM_TITLE
sheet metal
$#   secid    elform      shrf   qr/irid       cst     scoor       nsm
         3         1  1.000000         2         0  3.000000     0.000
$#     ts1       ts2       tt1       tt2     nsloc     ntloc
 40.000000 40.000000 30.000000 30.000000     0.000     0.000
*PART
$# title
front_fork
$#     pid     secid       mid     eosid      hgid      grav    adpopt      tmid
         4         1         1         0         0         0         0         0
*PART
$# title
shock_absorber
$#     pid     secid       mid     eosid      hgid      grav    adpopt      tmid
         5         1         1         0         0         0         0         0
```

```
*PART
$# title
shaft
$#     pid     secid       mid     eosid      hgid      grav    adpopt      tmid
         6         9         1         0         0         0         0         0
*SECTION_BEAM_TITLE
axcle
$#   secid    elform      shrf   qr/irid       cst     scoor       nsm
         9         1  1.000000         2         1     0.000     0.000
$#     ts1       ts2       tt1       tt2     nsloc     ntloc
 20.000000 20.000000     0.000     0.000     0.000     0.000
*PART
$# title
rear-wheel
$#     pid     secid       mid     eosid      hgid      grav    adpopt      tmid
         9         6         2         0         0         0         0         0
*SECTION_SHELL_TITLE
tire
$#   secid    elform      shrf       nip     propt   qr/irid     icomp     setyp
         6         2  1.000000         2         1         0         0         1
$#      t1        t2        t3        t4      nloc     marea      idof    edgset
 20.000000 20.000000 20.000000 20.000000     0.000     0.000     0.000
0
*MAT_ELASTIC_TITLE
rubber
$#     mid        ro         e        pr        da        db  not used
         25.0000E-10 2.1000E+5  0.490000     0.000     0.000         0
*PART
$# title
front-wheel
$#     pid     secid       mid     eosid      hgid      grav    adpopt      tmid
        10         6         2         0         0         0         0         0
*PART
$# title
```

```
plate
$#     pid     secid       mid     eosid      hgid      grav    adpopt      tmid
        11         7         3         0         0         0         0         0
*SECTION_SHELL_TITLE
plate
$#   secid    elform      shrf       nip     propt   qr/irid     icomp     setyp
         7         2  1.000000         2         1         0         0         1
$#      t1        t2        t3        t4      nloc     marea      idof    edgset
 20.000000 20.000000 20.000000 20.000000     0.000     0.000     0.000
0
*MAT_RIGID_TITLE
rigid
$#     mid        ro         e        pr         n    couple         m     alias
         3 7.0800E-9 2.0700E+5  0.300000     0.000     0.000     0.000
$#     cmo      con1      con2
  1.000000         7         7
$# lco or a1      a2        a3        v1        v2        v3
     0.000     0.000     0.000     0.000     0.000     0.000
*PART
$# title
spork
$#     pid     secid       mid     eosid      hgid      grav    adpopt      tmid
        12         1         1         0         0         0         0         0
*PART
$# title
shell left
$#     pid     secid       mid     eosid      hgid      grav    adpopt      tmid
        13         6         1         0         0         0         0         0
*PART
$# title
shell right
$#     pid     secid       mid     eosid      hgid      grav    adpopt      tmid
        14         6         1         0         0         0         0         0
*PART
```

```
$# title
artificial_beam
$#     pid     secid       mid     eosid      hgid      grav    adpopt      tmid
       15         9         1         0         0         0         0         0
*HOURGLASS_TITLE
Hourglass control
$#    hgid       ihq        qm       ibq        q1        q2    qb/vdc        qw
        1          3   0.100000            0   1.500000   0.060000   0.100000
0.100000
*MAT_ELASTIC_TITLE
structure
$#     mid        ro         e        pr        da        db   not used
        4 7.0800E-9 2.1000E+5  0.300000     0.000     0.000         0
*DEFINE_COORDINATE_NODES_TITLE
local coordinate
$#     cid        n1        n2        n3      flag       dir
        1     35130     35128     33414         0X
*DEFINE_CURVE
$#    lcid      sidr       sfa       sfo      offa      offo    dattyp
        1         0  1.000000  1.000000     0.000     0.000         0
$#                a1                  o1
             0.000           1.0000000
       1000.0000000           1.0000000
*AIRBAG_SIMPLE_PRESSURE_VOLUME
$#     sid    sidtyp      rbid      vsca      psca      vini       mwd      spsf
        1         1         0     0.000     0.000     0.000 15.000000     0.000
$#      cn      beta      lcid    lciddr
  0.320000  1.000000         0         0
```